Final Report
(01 Oct 1996- 31 May 2000)

ONR GRANT / CONTRACT INFORMATION

Grant/Contract Title: Analysis of Electromagnetic Interaction with Ships on the Ocean Surface

Performing Organization: Massachusetts Institute of Technology

Principal Investigator: Dr. Jin Au Kong, Professor of Electrical Engineering

Contract Number: N00014-97-1-0172

PR Number:

ONR Scientific Officer: Dr. Ronald Radlinski

OSP 65364

REPORT DOCUMENTATION PAGE

Form Approved
OMB No. 0704-0188

1. AGENCY USE ONLY (Leave blank)	2. REPORT DATE 6/20/2000	3. REPORT TYPE AND DATES COVERED Final 12/1/96 – 5/31/2000

4. TITLE AND SUBTITLE
Analysis of Electromagnetic Interaction with Ships on the Ocean Surface

5. FUNDING NUMBERS
N00014-97-1-0172

6. AUTHOR(S)
Prof. Jin-Au Kong

7. PERFORMING ORGANIZATION NAME(S) AND ADDRESS(ES)
Research Laboratory of Electronics
Massachusetts Institute of Technology
77 Massachusetts Avenue
Cambridge, MA 02139

8. PERFORMING ORGANIZATION REPORT NUMBER

9. SPONSORING/MONITORING AGENCY NAME(S) AND ADDRESS(ES)
Office of Naval Research
Ballston Center Tower One
800 North Quincy Street
Arlington, VA 22217-5660

10. SPONSORING/MONITORING AGENCY REPORT NUMBER
97PR02851-00

11. SUPPLEMENTARY NOTES
The view, opinions and/or findings contained in this report are those of the author(s) and should not be construed as an official Department of the Army position, policy, or decision, unless so designated by other documentation.

12a. DISTRIBUTION/AVAILABILITY STATEMENT
Approved for public release; distribution unlimited.

12b. DISTRIBUTION CODE

13. ABSTRACT (Maximum 200 words)

The objective of this research project has been to develop electromagnetic models for three-dimensional (3-D) objects above a rough surface, analyze and predict their scattering responses, determine dominant wave interaction mechanisms, investigate the origins of these scattering features, and provide physical interpretation for both analysis and synthesis of the response.

14. SUBJECT TERMS

15. NUMBER OF PAGES

16. PRICE CODE

17. SECURITY CLASSIFICATION OF REPORT	18. SECURITY CLASSIFICATION OF THIS PAGE	19. SECURITY CLASSIFICATION OF ABSTRACT	20. LIMITATION OF ABSTRACT
UNCLASSIFIED	UNCLASSIFIED	UNCLASSIFIED	UL

List of Publications / Reports / Presentations

1. Papers Published in Refereed Journals

Y. Zhang, Y. E. Yang, H. Braunisch, and J. A. Kong, "Electromagnetic wave interaction of conducting object with rough surface by hybrid SPM/MoM technique- Abstract", *J. Electromagn. Waves Appl.*, vol.13, no. 7, pp.983-984.

Y. Zhang, Y. Eric Yang, and J. A. Kong, "A spatial-domain equivalent source formulation for electromagnetic wave scattering from a rough surface", *IEEE Trans. Antennas Propagat.*, submitted, September 1999.

H. Braunisch, Y. Zhang, C. O. Ao, S.-E, Shih, Y. Eric Yang, K.-H. Ding, J. A. Kong, and L. Tsang, "Tapered wave with dominant polarization state for all angles of incidence", *IEEE Trans. Antennas Propagat.*, to be published, September 2000.

2. Non-Refereed Publications and Published Technical Reports

Y. Zhang, "Forward and inverse problems in microwave remote sensing of objects in complex media", Ph.D. Thesis, Department of Electrical and Computer Engineering, Massachusetts Institute of Technology, November, 1999

3. Presentations

a. Invited

(blank)

b. Contributed

C. O. Ao, Y. Zhang, and J. A. Kong, "Backscattering of Electromagnetic Waves from a Cylinder on a Rough Surface," in *1997 Progress In Electromagnetics Research Symposium (PIERS)*, Cambridge, MA, July 7-11, 1997.

Y. Zhang, Y. E. Yang, H. Braunisch, and J. A. Kong, "Electromagnetic wave scattering from conducting objects above a randomly rough surface", *1999 National Radio Science Meeting (URSI)*, Boulder, CO, January, 1999.

Y. E. Yang, Y. Zhang, H. Braunisch, and J. A. Kong, "Electromagnetic wave scattering from conducting objects partially buried under a randomly rough surface", *in 1999 Progress In Electromagnetics Research Symposium (PIERS)*, vol. 1, p. 540, Taiwan, March 22-26, 1999.

H. Braunisch, Y. Zhang, C. O. Ao, S.-E.Shih, Y. E. Yang, K.-H. Ding, J. A. Kong, and L. Tsang, "A modified tapered wave for the simulation of rough surface scattering", in *2000 Progress In Electromagnetics Research Symposium (PIERS)*, p. 835, Cambridge, MA, July 5-14, 2000, to be presented.

4. Books (and sections thereof)

Y. Zhang, Y. E. Yang, H. Braunisch, and J. A. Kong, "Electromagnetic wave interaction of conducting object with rough surface by hybrid SPM/MoM technique", *Progress in Electromagnetics Research Monograph Series, PIER 22*, pp. 315-335, EMW Publishing, Cambridge, MA, 1999.

J. A. Kong, Electromagnetic Wave Theory, EMW Publishing, Cambridge, MA, 1999.

L. Tsang, J. A. Kong, and K. H. Ding, *Scattering of Electromagnetic Waves Vol.1: Theories and Applications*, John Wiley & Sons, New York, NY, to be published, 2000.

L. Tsang, J. A. Kong, K. H. Ding, and C. O. Ao, *Scattering of Electromagnetic Waves Vol.2: Numerical Simulations*, John Wiley & Sons, New York, NY, to be published, 2000.

L. Tsang and J. A. Kong, *Scattering of Electromagnetic Waves Vol.3: Advanced Topics*, John Wiley & Sons, New York, NY, to be published, 2000.

List of Honors / Awards

Name of Person Receiving Award	Recipient's Institution	Name, Sponsor and Purpose of Award
Jin Au Kong	Massachusetts Institute of Technology	Outstanding Researcher Award by Pan-Wen Yuan Memorial Foundation for Outstanding contribution in scientific research

Summary

Publications/ Patents/ Presentations/ Honors/ Participants
(Number Only)

	ONR Supported	Non ONR
a. Number of Papers Submitted to Refereed Journals but not yet published:	2	4
b. Number of Papers Published in Refereed Journals:	1	5
c. Number of Books or Chapters Submitted but not yet Published:	3	0
d. Number of Books or Chapters Published:	2	0
e. Number of Printed Technical Reports & Non-Refereed Papers:	1	2
f. Number of Patents Filed	0	0
g. Number of Patents Granted:	0	0
h. Number of Invited Presentations at Workshops or Prof Society Meetings:	0	0
i. Number of Contributed Presentations at Workshops or Prof. Society Meetings:	4	18
j. Honors /Awards / Prizes for Contract / Grant Employees: (selected list attached)	1	0
k. Number of Graduate Students and Post-Docs Supported at least 25% this year on contract grant:	2	6

			ONR Supported	Non ONR
Grad Students:		TOTAL	2	6
		Female	0	0
		Minority	0	0
Post Doc:	TOTAL		0	0
	Female		0	0
	Minority		0	0

i. Number of Female or Minority PIs or CO-PIs

	ONR Supported	Non ONR
New Female	0	0
Continuing Female	0	0
New Minority	0	0
Continuing Minority	0	0

Analysis of Electromagnetic Interaction with Ships on the Ocean Surface

Jin Au Kong
Massachusetts Institute of Technology
Cambridge, MA 02139

1. Research Objective

The objective of this research project has been to develop electromagnetic models for three-dimensional (3-D) objects above a rough surface, analyze and predict their scattering responses, determine dominant wave interaction mechanisms, investigate the origins of these scattering features, and provide physical interpretation for both analysis and synthesis of the response.

2. Background

Electromagnetic scattering from surface ships is an important subject of study for the Navy. For all practical purposes, the main concerns are the identification from radar signatures and reduction of radar signatures by better designs. Both of these require fundamental understanding of how electromagnetic wave interacts with the ship body in the presence of ocean surface.

In the past, progress in this area has been hampered by the complexity of the problem. A real ship is composed of large number of different parts, each with distinctive response in the time and the frequency domains. Moreover, the presence of rough and highly reflective ocean surface creates huge amount of multiple electromagnetic interactions with the ship body. This is especially true at low elevation angles, where most practical applications are concerned. Although recent advances in computational electromagnetics and increasing capability of digital computers have made large scale electromagnetic scattering problem more manageable [1-3], analytical methods [4-6] are still needed to facilitate the interpretation of numerical solution. Furthermore, analytical methods can also be efficiently combined with numerical techniques to increase the overall computational efficiency. This research emphasizes the use of hybrid analytical/numerical techniques for the analysis of electromagnetic interaction with surface ships.

3. Research Achievements

Numerical simulation techniques for electromagnetic wave scattering by arbitrary shaped objects in free space are well developed using wire and surface-patch models. The theory and numerical approaches associated with objects near flat interfaces of layered media have also been studied extensively by many researchers. However, in the case of a ship on

the ocean surface, the interface is inherently rough (sea surface) and relatively little work has been reported. In principle, the standard Method of Moments (MoM) can be used to solve for the unknowns (surface currents) both on the object and on the rough surface. However, the need to discretize the rough surface significantly increases the computational resource requirements compared to the case of scattering from the object alone.

The main effort in our work has been the development of iterative techniques that perform perturbational expansion to the extended boundary condition (EBC) integral equations. After separating the equations into different orders, they are then solved using the MoM technique. The layered dyadic Green's function formulation is applied to all orders to allow only unknown current distribution on the discrete conducting object but not that on the rough surface to be solved, thus saving significant amount of computer memory and CPU time. This hybrid SPM/MoM overcomes the difficulties of having to deal with a large randomly rough surface that the standard MoM encounters when it is applied to full three-dimensional problem. The zeroth order response in the hybrid SPM/MoM technique has been found to be equivalent to scattering in the presence of a flat interface, and the first and higher order responses can be solved from the same set of (impedance) matrix equations with different equivalent sources derived at the ocean-air interface.

3.1 Phase I

In the first phase, we have focused on the development of far-field interaction models for flat plates and circular cylindrical shapes. An iterative solution for scattering from a conducting object above a randomly rough dielectric surface has been formulated using Huygens' principle. This model incorporates analytical techniques, Small Perturbation Method (SPM) and Kirchhoff Approximation (KA) for rough surface scattering and Physical Optics (PO) for scattering from the conducting body, to examine the direct and multiple scattering mechanisms for the coupled configuration.

We first considered scattered field from the conducting body and from the rough surface alone. The secondary scattering components were evaluated by projecting the primary scattering fields to the discrete object and rough surface as additional sources. Using the iterative technique, we can evaluate the spread of scattering energy associated with different surface roughness. The main lobe in bistatic return was seen to decrease with increasing roughness, whereas some sidelobes pick up strengths. This spread is expected, as the scattered energy is directed away from the specular direction.

A numerical technique based on the Method of Moments (MoM) solution of surface integral equations was developed to validate the iterative solution. Monte Carlo simulations over about 50 realizations of surface profiles were used to evaluate the statistical average return in the combined rough surface/discrete object environment. The surface roughness statistics and the incident waveform were assumed to be the same as in the iterative method. Both models were applied to investigate the effects of radar parameters (incidence and observation angles, polarization and frequency), and target

parameters (size and location of the object, roughness of ocean surface) on the scattered fields. It was observed that the interactions strongly depend on the frequency, location of object, and the ocean roughness. Discrepancies were observed between the iterative technique using Kirchhoff approximation and MoM when the object is slightly above the rough surface or partially submerged (practical case of interest), which suggest that multiple interactions, beyond the secondary scattering covered by the iterative method, need to be included. The use of the hybrid technique outlined in the next sections improves the approximation significantly. As a by-product of this study, we also examined angular correlation function of scattered waves based on the results of MoM. It was observed that the detection of discrete object in the presence of rough interface would be easier if angular correlation is taken along certain directions.

3.2 Phase II

In this phase of research [7,8], we have developed a spatial-domain formulation for electromagnetic scattering from a rough surface for an arbitrarily shaped incident wave using the extinction theorem. By expanding the Green's function and surface variables in terms of the rough surface height function, the electric field integral equations (EFIE) has been decomposed into different orders. It has been found that the higher order equations are of the same form as the zeroth order equations, except for the source terms. Therefore, for each order, the scattered field from the rough surface can be formulated as the radiation fields from equivalent sources on the (flat) mean surface. In other words, we only need to solve the zeroth order equations with different sources successively. Moreover, the problem at each order corresponds to a flat surface problem, which can be solved without discretizing the surface. Up to the first order, we have shown that the total field of the equivalent source on a PEC rough surface is the field scattered by the rough surface.

The advantage of using the spatial-domain formulation instead of the frequency-domain formulation as in the conventional SPM technique is that there is no need to integrate over the spatial frequency . Furthermore, using the spatial-domain formulation, the non-averaged scattered fields are well defined. However, the derivation of the total scattered field of higher order ($n \geq 2$) or the field scattered from a dielectric rough surface requires more analytical effort since Sommerfeld integrals are involved. In the case of a PEC rough surface, this extra analytical effort is avoided because the Green's function can be obtained by image theory and does not involve Sommerfeld integrals. By considering a plane incident wave, we have shown that the total field of the equivalent source is the same as the field scattered by a rough surface obtained by using the conventional SPM technique.

Particularly for a rough PEC surface, the proposed spatial-domain technique is more powerful than the conventional SPM for the calculation of the scattered field because:

(a) The incident wave is not restricted to be a plane incident wave as in the conventional SPM, thereby allowing lower grazing angles in numerical simulations.
(b) The spatial domain formulation can be used to calculate the near field, which is particularly important to account for near field interactions.

(c) The non-averaged complex scattered field in the spatial-domain formulation does not requires the evaluation of a Fourier integral over the rough surface, therefore is a well-defined quantity.

(d) The spatial-domain formulation is more computationally efficient, since there is no integration over the spatial frequency as in the conventional SPM.

More detailed research results of Phase II are presented in the Appendix A [8].

3.3 Phase III

In this phase of research [7,9], we developed a hybrid spatial-domain SPM/MoM technique to calculate the EM scattering from arbitrary 3-D conducting objects above a rough surface based on the results of Phase II.

In this hybrid technique, the Green's function and surface variables are expanded (using a Taylor's expansion) in terms of the surface height functions on the (flat) mean surface. The electric field integral equations based on the extinction theorem and the surface boundary conditions are then decomposed into the different orders. Each order represents an equivalent flat-surface scattering problem with the same geometry but different equivalent sources. As a result, the problems of electromagnetic scattering from an object above a rough surface can be solved efficiently by using the MoM incorporating the dyadic Green's function for layered media. More importantly, only the surface currents on the object need to be found numerically by the MoM.

A nice picture emerges because the separation of the solution into different orders helps the identification and characterization of the individual interaction terms between the object and the rough surface. The separation of the return field into the sum of individual interaction terms allow us to identify the coherent and incoherent return field, and thus better characterize the rough surface effects quantitatively.

We have also analyzed the case of an object partially buried in a PEC rough surface. In comparison to the case of an object above a rough surface, we have found the following differences [7]:

(a) The integration area of the equivalent sources on the mean surface is changed to accommodate the fact that part of the (infinite) flat surface is covered by the interacting object.

(b) The are extra terms in the expression for the equivalent sources on the mean surface. These terms are related to the correction of the equivalent source due to the change on the exposed area on the object (part of it being buried) and to the modification of the equivalent source due to the projected area of the rough surface on the mean surface.

Several numerical results have been obtained. In particular, we have investigated the interaction of horizontal conducting cylinders above a rough surface with Gaussian power spectrum and validated the results against standard MoM results. Monte Carlo results

have also been generated using 100 rough surface realizations. The number of unknowns for typical cases considered has been reduced by roughly 20 times. Moreover, a full Monte Carlo monostatic RCS calculation which would require 3 months in a our 500 MHz Digital Alpha 21164A processor using the standard MoM, was reduced to approximately 17 hours using the hybrid MoM/SMP technique.

More detailed research results of Phase III are presented in the Appendix B [9].

3.4 Phase IV

A basic limitation of usual numerical techniques to analyze the problem of electromagnetic scattering from rough surfaces is the need to truncate the rough surface because of limited computational resources. This leads to erroneous results due to artificial edge truncation when ideal plane waves are used to excite the configuration. The tapered wave concept is based on providing an illumination for the numerical simulation which resembles the plane wave case to be modeled closely to the center of the scattering scenario (including the choice of a particular polarization) while its intensity becomes negligibly small upon approaching the artificially introduced edges of the rough surface. Therefore, unwanted edge effects due to the primary incident wave are minimized and a proper normalization of the computed scattering coefficients allows a meaningful comparison with the ideal plane wave case. Moreover, near field quantities such as current distributions induced near the center of the tapered wave are also expected to be similar.

The tapered wave should be constructed in such a way that it satisfies the Maxwell's equations. This helps to increase the confidence in the results obtained from numerical simulations. Furthermore, it should also be possible to substitute it for a plane wave of arbitrary polar and azymuthal angles of incidence without loss of polarization or degradation of tapering.

In this research phase [10], we have considered the problem of constructing a 3-D tapered wave with dominant polarization state for all angles of incidence as a superposition of plane waves, taking into account both propagating and evanescent waves. The use of the simple Gaussian plane wave spectrum was considered in order to avoid problems near grazing incidence. Moreover, we have proposed a choice of unit vectors which leads to integrand which are continuous at normal incidence. As a result, a clean footprint (no degradation of tapering) with clear polarization (no loss of dominant polarization state) has been obtained for all angles of incidence. Besides removing the singularity at the origin of the wavenumber space, the proposed special choice of polarization vectors has lead to a least square error property of the wave. The choice of polarization vectors was shown to lead to an exact solution of the Maxwell's equations which is an optimal approximation of an ideal but non-Maxwellian tapered field that is constructed by multiplying a scalar tapered wave with a constant polarization vector. Approximate 3-D scalar and vector tapered waves, which can be evaluated without any numerical integrations, has also been derived.

More detailed research results of Phase IV are presented in the Appendix C [10].

4. General Conclusions and Future Directions

4.1 General Remarks

In our approach we successfully combined an analytical preprocessing (perturbational expansion) of the problem of electromagnetic scattering from an object in presence of rough surface to be used in a numerical solution by the MoM. This combination of analytical and numerical treatment lead not only an improvement on the overall computational efficiency of the resultant (hybrid) scheme, but also permits a better physical interpretation of the results given by the computer (i.e., separation of the object-rough surface interaction into different orders) which is much difficult using a strictly numerical procedure.

The development of theoretical framework needs to be coupled with experiments, both for validation, and for evaluating new measurement techniques. In essence, one can perform theoretical simulations that take into account the measurement setup and assess the impact of testing probes. One of the long-term goals of our research is to provide recommendation on experimental schemes.

However, many important issues are unresolved still. For instance, being a perturbational expansion, the hybrid scheme can become very involved for non-slightly rough surfaces. Hybridization with other techniques and use of composite surface models need to be investigated in connection with more general rough surface conditions. Moreover, in the course of our research we have dealt only with the forward problem. For the identification of radar signatures and reduction of radar signatures the forward techniques need to be coupled to inverse scattering techniques. These and other issues are discussed below.

4.2 Future Work

One immediate future goal is to extend the applicable range of our hybrid technique. Major technical issues to be addressed include the extension of the hybrid technique to composite rough surface model with impedance boundary condition, which will be used to characterize different sea states, and the integration with standard high-frequency techniques, such as ray-optical methods, for large objects.

4.2.1 Impedance boundary condition.
To obtain a closed-form Green's function, thus avoiding the need of extra integrations, we have assumed that the ocean surface behaves like a perfectly conductor. In reality, the behavior of highly conducting interface is quite different for low-grazing incidence angles. Major difference is exhibited in the angular variation of reflection coefficient for the vertical polarized waves. The reflection coefficient converges to minus one (-1) at near grazing incidence even at the limit of conductivity reaching the infinity. On the other hand, the reflection coefficient at a perfectly conducting interface is always plus one (+1). This non-uniform convergence property can conceivably contribute to differences

between the perturbational series expansion for the perfect-conducting interface case and that for the high-conductivity interface (real sea water) case. Because of this concern, we propose to extend our formulation to incorporate impedance boundary conditions for highly (non-perfect) conducting interfaces. Doing so should represent the sea surface property better and avoid the non-uniform convergence problem.

4.2.2 Composite rough surface model.

Based on practical experience, the effect of rough ocean surface on scattering from ship objects becomes non-negligible only at high frequencies. In such cases, it is necessary to consider a two-scale composite rough surface representation of the ocean surface [11]. The perturbational formulation developed here can be easily generalized to deal with the two-scale model. With the two-scale model, the large scale underlying surface structure is sufficiently smooth to apply high-frequency scattering techniques such as physical optics or ray-optical techniques. The ship objects can also be facetized and included in the computational domain with the large-scale rough surface. The hybrid technique developed here may then be used in parts of the object and surface where there strong multiple interactions are expected to improve the accuracy, with the perturbational formulation being introduced to account for the effect of small-scale roughness.

4.2.3 Finite-distance source synthesis.

At low grazing incidence, it is important to observe that the scattered field from the rough ocean surface will interfere and merge with the incident field that is propagating near the surface. The net result is that the actual incident field reaching ship objects is modified; likewise the return field to the sensor will be modified owing to scattering from the rough surface. To deal with this practical problem, we propose to include a source term at a finite distance into the iterative formulation instead of a synthesized wave beam that may not represent the true incident field near the ship objects. The source term should be constructed to emulate the transmitting antenna properties. Taking into consideration the statistical properties of rough ocean surface and the antenna beam pattern, we can calculate the surface current distribution for near-field illumination as well as the dispersion characteristics. The calculated results can then be compared against experiments that involve objects on a real ocean surface.

4.2.4 Inverse problem.

The essence of identifing radar signatures can be considered an inverse scattering problem. The work here begin with the forward scattering model developed and proceed to the inverse model. The link between the two is established through optimization techniques. In the optimization approach, the developed forward model and observed measurements are used to retrieve unknown source parameters. This is usually the most appropriate inversion method when the direct scattering theory is very complicated. In addition, this method offers a great flexibility in the choice of direct scattering models, the parameters to be inverted, and data to be employed. We have previously applied the optimization technique to the inversion of ground truth information from satellite remote sensing data, such as inversion of sea ice parameters from the CRRELX experiment [12]. One drawback of the optimization technique is the amount of computational resources required, since multiple forward scattering solutions are needed. One way to overcome this problem is to extract reduced-order models from the complete forward scattering

solution and use them at intermediate stages of the optimization procedure. An example of reduce-order modeling consists in the replacement of the scattering object by scattering centers [13].

Aside from the optimization techniques, direct time-domain inversion techniques [14,15] can also be considered. For example, in the singularity expansion method (SEM) [16] feature extraction is achieved by studying the natural frequencies contained in the time-domain response. This technique might well be suitable for identifying local dispersion characteristics of substructure components.

For the inverse scattering problem, non-uniqueness and inversion stability issues usually arises with noisy data. It is possible to reduce the effects of these uncertainties by using multi-dimensional data like multi-frequency, multi-angle, and polarimetric data. For instance, electromagnetic wave polarization returns are particularly sensitive to the geometry and the degree of heterogeneity of scattering objects. Using polarimetry, the copolarized and depolarized returns for an arbitrary polarized incident wave can be measured and exploited for the classification and identification of targets [17].

5. References

[1] R.F. Harrington, *Field Computation by Moment Methods*, MacMillan, New York, 1968.

[2] K.S. Yee, "Numerical solution of initial boundary value problems involving Maxwell's equations in isotropic media," *IEEE Trans. Antennas Propagat.*, Vol. AP-17, pp. 585-589, 1966.

[3] M.E. Veysoglu, R.T. Shin, and J.A. Kong, "A finite-difference time-domain analysis of wave scattering from periodic surfaces: oblique incidence case," *J. Electromagn. Waves Applicat.*, Vol. 7, pp. 1595-1607, 1993.

[4] J.A. Kong, *Electromagnetic Wave Theory*, Wiley, New York, 1990.

[5] P. Beckmann, and A. Spizzichino, The Scattering of Electromagnetic Waves form Rough Surfaces, MacMillan, New York, 1963.

[6] L. Tsang, J.A. Kong, and R.T. Shin, *Theory of Microwave Remote Sensing*, Wiley-Interscience, New York, 1985

[7] Y. Zhang, "Forward and inverse problems in microwave remote sensing of objects in complex media", Ph.D. Thesis, Department of Electrical and Computer Engineering, Massachusetts Institute of Technology, November, 1999

[8] Y. Zhang, Y. Eric Yang, and J. A. Kong, "A spatial-domain equivalent source formulation for electromagnetic wave scattering from a rough surface", *IEEE Trans. Antennas Propagat.*, submitted, September 1999.

[9] Y. Zhang, Y. E. Yang, H. Braunisch, and J. A. Kong, "Electromagnetic wave interaction of conducting object with rough surface by hybrid SPM/MoM technique-Abstract", *J. Electromagn. Waves Appl.*, vol.13, no. 7, pp. 983-984, 1999.

[10] H. Braunisch, Y. Zhang, C. O. Ao, S.-E, Shih, Y. Eric Yang, K.-H. Ding, J. A. Kong, and L. Tsang, "Tapered wave with dominant polarization state for all angles of incidence", *IEEE Trans. Antennas Propagat.*, to be published, September 2000.

[11] Johnson JT, Shin RT, Kong JA, Tsang L, Pak K, "A numerical study of the composite surface model for ocean scattering," *1996 International Geoscience and Remote Sensing Symposium (IGARSS'96) Digest*, vol.2, 1996, pp.1401-1403, 1996.

[12] Shih SE, Ding KH, Nghiem SV, Hsu CC, Kong JA, Jordan AK, "Thickness retrieval using time series electromagnetic measurements of laboratory grown saline ice*," 1996 International Geoscience and Remote Sensing Symposium (IGARSS '96) Digest,* vol.2, pp.1208-1210, 1996.

[13] R. Bhalla, J. Moore, and H. Ling, "A global scattering center representation of complex targets using the SBR technique", IEEE Trans. Antennas Propagat., Vol. 45, no. 12, pp. 1850-1856, 1997

[14] D. Lesselier, "Optimization techniques and inverse problems: reconstruction of conductivity profiles in the time domain," *IEEE Trans. Antennas Propagat.*, Vol. AP-30, pp. 59-65, 1982.

[15] A. G. Tijhuis, "Iterative determination of permittivity and conductivity profiles of a dielectric slab in the time domain," *IEEE Trans. Antennas Propagat.*, Vol. AP-29, pp. 239-245, 1981.

[16] A. S. Leveckis, "Application of Singularity Expansion to Electromagnetic Pulse Response Waveforms," M.S. Thesis, Massachusetts Institute of Technology, 1977.

[17] J. A. Kong (ed.), *Polarimetric Remote Sensing*, Elsevier, New York, 1990.

Appendix A

A Spatial-Domain Equivalent Source Formulation for Electromagnetic
Wave Scattering from a Rough Surface

Abstract

We present a derivation of a spatial-domain formulation for electromagnetic wave scattering from a rough surface for an arbitrary-shaped incident wave using the extinction theorem. By expanding the Green's function and surface variables in terms of the rough surface height function, the electric field integral equations (EFIE) are decomposed into different orders. For each order, the scattered field of rough surface is formulated as the radiation of equivalent sources on the mean surface. The spatial-domain formulation is simpler and not restricted to use a plane incident wave as conventional small perturbation method (SPM) does. The spatial-domain formulation can also provides a non-averaged scattered field without using the Fourier transform of the rough surface. The numerical result for a non-planar incident wave is verified using the method of moments (MoM).

Keywords

Rough surface, electromagnetic wave scattering, spatial domain, equivalent source, small perturbation method.

I. Introduction

The electromagnetic wave scattering from a slightly rough surface has been studied extensively using (1) the Rayleigh hypothesis [1], [2], and (2) the extinction theorem [3], [4]. In all of these methods, a plane incident wave has been assumed so that the scattered fields can be obtained by expansion in terms of plane waves. Therefore the scattered fields are the superposition of plane waves. The averaged scattered fields are calculated by ensemble average over the rough surface, thus the expression after the average is the integral over the wavenumber for a function of the power spectrum density of the rough surface. The limitation of the conventional SPM is obvious: (1) a plane incident wave must be assumed, which may arise the difficulty when a incident wave with a grazing angle is considered, (2) a Fourier integral of a rough surface appears in the non-averaged scattered field, and (3) it is time consuming to evaluate the integration over the wavenumber when the closed form of the scattered field could not be obtained.

In this paper, we derive the formulation in spatial domain for the field scattered by a slightly rough surface. In Section II, based on the extinction theorem, we formulate the equivalent sources on the mean surface for a dielectric rough surface. Then we introduce the iterative scheme to calculate the total scattered field. In Section III, in order to calculate the reflected and transmitted fields of the equivalent sources on the mean surface,

we expanded the Green's function as the integral in frequency domain. The closed form in spatial domain of the first-order field scattered by a perfectly conducting (PEC) rough surface is derived in the end of this section. In Section IV, we show that the first-order scattered field in spatial domain from a PEC rough surface is the same as the conventional SPM by assuming a plane incident wave. For arbitrary-shaped incident wave such as Gaussian-tapered wave, the spatial-domain formulation provides accurate result which is verified using the method of moments (MoM) in Section V.

II. ELECTROMAGNETIC FIELD INTEGRAL EQUATIONS

In the recent investigation on the electromagnetic wave interaction between a perfectly electric conducting (PEC) object and a rough surface, it was found that the problem can be solved by replacing the rough surface with a flat one and placing an equivalent surface on the flat mean surface [5], [6]. It immediately arise the question that if the equivalent source method can be applied to calculate the electromagnetic wave scattered by a plain rough surface.

Consider an electromagnetic wave $\overline{E}_i(\bar{r})$ incident upon a rough surface S_r with surface height function $z = f(\bar{r}'_\perp)$ and mean surface S_o coincident with the xy-plane as illustrated in Fig. 1. The upper and lower spaces V_1 and V_2 are homogeneous, isotropic media characterized by (ϵ_1, μ_1) and (ϵ_2, μ_2), respectively. By applying the extinction theorem, the electric field integral equations are written as, respectively, for the observation point at $\bar{r} \in V_2$

$$\overline{E}_i(\bar{r}) + \int_{S_r} dS' \left\{ i\omega\mu_1 \overline{\overline{G}}_1(\bar{r}, \bar{r}') \cdot \left[\hat{n}_1(\bar{r}') \times \overline{H}_1(\bar{r}') \right] \right.$$
$$\left. + \nabla \times \overline{\overline{G}}_1(\bar{r}, \bar{r}') \cdot \left[\hat{n}_1(\bar{r}') \times \overline{E}_1(\bar{r}') \right] \right\} = 0 \tag{1}$$

and for $\bar{r} \in V_2$

$$\int_{S_r} dS' \left\{ i\omega\mu_2 \overline{\overline{G}}_2(\bar{r}, \bar{r}') \cdot \left[\hat{n}_2(\bar{r}') \times \overline{H}_2(\bar{r}') \right] \right.$$
$$\left. + \nabla \times \overline{\overline{G}}_2(\bar{r}, \bar{r}') \cdot \left[\hat{n}_2(\bar{r}') \times \overline{E}_2(\bar{r}') \right] \right\} = 0 \tag{2}$$

where $\overline{\overline{G}}_1$ and $\overline{\overline{G}}_2$ are dyadic Green's functions for unbounded regions V_1 and V_2, respectively. $\hat{n}_1(\bar{r}')$ denotes the local normal vector pointing from the rough surface S_r to the
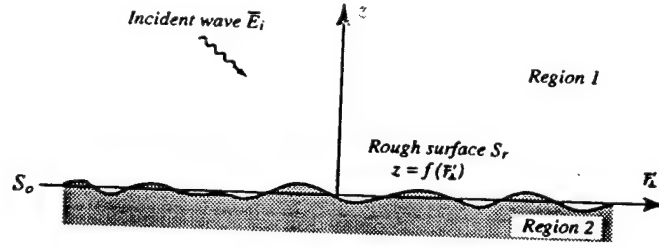
Fig. 1. Electromagnetic wave scattering by a rough surface.

upper region V_1. The normal vector $\hat{n}_2(\bar{r}')$ is anti-parallel to $\hat{n}_1(\bar{r}')$, i.e., $\hat{n}_2(\bar{r}') = -\hat{n}_1(\bar{r}')$. $\overline{E}_1(\bar{r}')$ and $\overline{H}_1(\bar{r}')$ are electric and magnetic fields on the rough surface in region V_1, while $\overline{E}_2(\bar{r}')$ and $\overline{H}_2(\bar{r}')$ are surface fields on S_r in region V_2. If the region V_2 is dielectric, then the tangential fields are continuous, thus

$$\hat{n}_1(\bar{r}') \times \overline{H}_1(\bar{r}') = \hat{n}_1(\bar{r}') \times \overline{H}_2(\bar{r}') \equiv \frac{1}{\eta_1} \frac{d\bar{r}'_\perp}{dS'} \bar{a}(\bar{r}'_\perp) \tag{3}$$

$$\hat{n}_1(\bar{r}') \times \overline{E}_1(\bar{r}') = \hat{n}_1(\bar{r}') \times \overline{E}_2(\bar{r}') \equiv \frac{d\bar{r}'_\perp}{dS'} \bar{b}(\bar{r}'_\perp) \tag{4}$$

where $\bar{a}(\bar{r}'_\perp)$ and $\bar{b}(\bar{r}'_\perp)$ are two new surface variables defined on the mean surface S_o, η_1 is the intrinsic impedance of the upper region V_1, i.e., $\eta_1 = \sqrt{\mu_1/\epsilon_1}$, and $d\bar{r}'_\perp$ is the projection of the infinitesimal area dS' on the mean surface S_o. With the new surface variables, the integral equations are rewritten as

$$\overline{E}_i(\bar{r}) + \int_{S_o} d\bar{r}'_\perp \left\{ ik_1 \overline{\overline{G}}_1(\bar{r}, \bar{r}') \cdot \bar{a}(\bar{r}'_\perp) \right.$$
$$\left. + \nabla \times \overline{\overline{G}}_1(\bar{r}, \bar{r}') \cdot \bar{b}(\bar{r}'_\perp) \right\} = 0 \qquad \text{for } \bar{r} \in V_2 \tag{5}$$

$$\int_{S_o} d\bar{r}'_\perp \left\{ ik_2 \frac{\eta_2}{\eta_1} \overline{\overline{G}}_2(\bar{r}, \bar{r}') \cdot \bar{a}(\bar{r}'_\perp) \right.$$
$$\left. + \nabla \times \overline{\overline{G}}_2(\bar{r}, \bar{r}') \cdot \bar{b}(\bar{r}'_\perp) \right\} = 0 \qquad \text{for } \bar{r} \in V_1 . \tag{6}$$

Theoretically, given a deterministic rough surface profile S_r, the unknown surface variables $\bar{a}(\bar{r}'_\perp)$ and $\bar{b}(\bar{r}'_\perp)$ can be solved from Eqs. (5) and (6). For the special case in which the surface is flat, the surface variables $\bar{a}(\bar{r}'_\perp)$ and $\bar{b}(\bar{r}'_\perp)$ have only the horizontal components, and the local coordinate $\bar{r}'$ in the dyadic Green's functions can be replaced by $\bar{r}'_\perp$.

A. Expansion of Green's Function and Surface Variables

As illustrated in Fig. 2, the local position vector $\bar{r}'$ on the rough surface can be expressed as the sum of the horizontal vector $\bar{r}'_\perp$ and the vertical vector $\hat{z}f(\bar{r}'_\perp)$. Therefore the scalar Green's function g_α in region V_α (where $\alpha = 1$ or 2) can be expanded in terms of the surface height function $f(\bar{r}'_\perp)$ on the mean surface S_o,
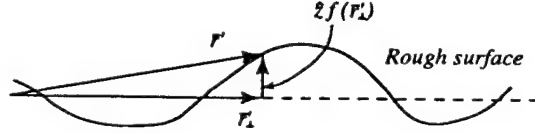

Fig. 2. The local position vector $\bar{r}'$ on a rough surface is the sum of the horizontal and vertical components.

$$
\begin{aligned}
g_\alpha(\bar{r}, \bar{r}') &= g_\alpha(\bar{r}, \bar{r}'_\perp + \hat{z}f(\bar{r}'_\perp)) \\
&= \sum_{m=0}^{\infty} \frac{1}{m!} \frac{\partial^m}{\partial z^m} g_\alpha(\bar{r}, \bar{r}'_\perp) \left[-f(\bar{r}'_\perp)\right]^m
\end{aligned}
\tag{7}
$$

where the following property of the scalar Green's function has been used:

$$
\frac{\partial^m}{\partial z'^m} g_\alpha(\bar{r}, \bar{r}') = (-1)^m \frac{\partial^m}{\partial z^m} g_\alpha(\bar{r}, \bar{r}').
\tag{8}
$$

Thus the dyadic Green's function can be expressed as

$$
\begin{aligned}
\overline{\overline{G}}_\alpha(\bar{r}, \bar{r}') &= \left(\overline{\overline{I}} + \frac{1}{k_\alpha^2} \nabla\nabla\right) g_\alpha(\bar{r}, \bar{r}') \\
&= \sum_{m=0}^{\infty} \frac{1}{m!} \left[-f(\bar{r}'_\perp)\right]^m \frac{\partial^m}{\partial z^m} \overline{\overline{G}}_\alpha(\bar{r}, \bar{r}'_\perp).
\end{aligned}
\tag{9}
$$

The surface variables are also written as the series expansion as follows:

$$
\bar{a}(\bar{r}'_\perp) = \sum_{m=0}^{\infty} \left[\bar{a}_\perp^{(m)}(\bar{r}'_\perp) + \hat{z}\bar{a}_z^{(m)}(\bar{r}'_\perp)\right]
\tag{10}
$$

$$
\bar{b}(\bar{r}'_\perp) = \sum_{m=0}^{\infty} \left[\bar{b}_\perp^{(m)}(\bar{r}'_\perp) + \hat{z}\bar{b}_z^{(m)}(\bar{r}'_\perp)\right].
\tag{11}
$$

In Eqs. (10) and (11), the separation of the z-components allows the only unknown surface variables to be the tangential component since the z-components of the m-th order can be expressed in terms of the tangential components of order $(m-1)$, as we will see below. For the definition of $\bar{a}$ and $\bar{b}$ as in Eqs. (3) and (4), the following identities hold:

$$
\hat{n}_1(\bar{r}'_\perp) \cdot \bar{a}(\bar{r}'_\perp) = 0
\tag{12}
$$

$$
\hat{n}_1(\bar{r}'_\perp) \cdot \bar{b}(\bar{r}'_\perp) = 0
\tag{13}
$$

where the normal vector is related to the surface height function by

$$\hat{n}_1(\bar{r}'_\perp) = \frac{-\nabla'_\perp f(\bar{r}'_\perp) + \hat{z}}{|-\nabla'_\perp f(\bar{r}'_\perp) + \hat{z}|}. \tag{14}$$

Substituting the series expansion of $\bar{a}$ and $\bar{b}$ as in Eqs. (10) and (11) into Eqs. (12) and (13), respectively, and assuming that the derivatives $\partial f(\bar{r}'_\perp)/\partial x'$ and $\partial f(\bar{r}'_\perp)/\partial y'$ are of the same order as $k_1 f(\bar{r}'_\perp)$, we then get the m-th order z-components of the surface variables $\bar{a}$ and $\bar{b}$ in terms of their $(m-1)$-th order tangential components as follows:

$$\bar{a}_z^{(m)}(\bar{r}'_\perp) = \nabla'_\perp f(\bar{r}'_\perp) \cdot \bar{a}_\perp^{(m-1)}(\bar{r}'_\perp) \tag{15}$$

$$\bar{b}_z^{(m)}(\bar{r}'_\perp) = \nabla'_\perp f(\bar{r}'_\perp) \cdot \bar{b}_\perp^{(m-1)}(\bar{r}'_\perp). \tag{16}$$

B. The n-th Order Equation and Equivalent Sources

Substituting the series expansion of the dyadic Green's function [Eq. (9)] and the surface variables [Eqs. (10) and (11)] into the integral Eqs. (5) and (6), and re-grouping the terms with the same order of the surface height function $f(\bar{r}'_\perp)$, we obtain the following n-th order equations:

$$\overline{E}_i^{(n)}(\bar{r}) + \int_{S_o} d\bar{r}'_\perp \left\{ ik_1 \overline{\overline{G}}_1(\bar{r}, \bar{r}'_\perp) \cdot \bar{a}_\perp^{(n)}(\bar{r}'_\perp) \right.$$
$$\left. + \nabla \times \overline{\overline{G}}_1(\bar{r}, \bar{r}'_\perp) \cdot \bar{b}_\perp^{(n)}(\bar{r}'_\perp) \right\} = 0 \quad \text{for } \bar{r} \in V_2 \tag{17}$$

$$\overline{E}_{i2}^{(n)}(\bar{r}) + \int_{S_o} d\bar{r}'_\perp \left\{ ik_2 \frac{\eta_2}{\eta_1} \overline{\overline{G}}_2(\bar{r}, \bar{r}'_\perp) \cdot \bar{a}_\perp^{(n)}(\bar{r}'_\perp) \right.$$
$$\left. + \nabla \times \overline{\overline{G}}_2(\bar{r}, \bar{r}'_\perp) \cdot \bar{b}_\perp^{(n)}(\bar{r}'_\perp) \right\} = 0 \quad \text{for } \bar{r} \in V_1 \tag{18}$$

where for the zero-th order ($n = 0$), $\overline{E}_i^{(0)}(\bar{r}) = \overline{E}_i(\bar{r})$ and $\overline{E}_{i2}^{(0)}(\bar{r}) = 0$. For higher orders ($n \geq 1$), the first terms in the equations above are written as

$$\overline{E}_i^{(n)}(\bar{r}) = \sum_{m=1}^{n} \frac{1}{m!} \int d\bar{r}'_\perp [-f(\bar{r}'_\perp)]^m$$
$$\frac{\partial^m}{\partial z^m} \left\{ ik_1 \overline{\overline{G}}_1(\bar{r}, \bar{r}'_\perp) \cdot \bar{a}_\perp^{(n-m)}(\bar{r}'_\perp) \right.$$
$$\left. + \nabla \times \overline{\overline{G}}_1(\bar{r}, \bar{r}'_\perp) \cdot \bar{b}_\perp^{(n-m)}(\bar{r}'_\perp) \right\}$$
$$+ \sum_{m=1}^{n} \frac{1}{(m-1)!} \int d\bar{r}'_\perp [-f(\bar{r}'_\perp)]^{m-1}$$
$$\frac{\partial^{m-1}}{\partial z^{m-1}} \left\{ ik_1 \overline{\overline{G}}_1(\bar{r}, \bar{r}'_\perp) \cdot \hat{z} \left[\nabla'_\perp f(\bar{r}'_\perp) \cdot \bar{a}_\perp^{(n-m)}(\bar{r}'_\perp) \right] \right.$$
$$\left. + \nabla \times \overline{\overline{G}}_1(\bar{r}, \bar{r}'_\perp) \cdot \hat{z} \left[\nabla'_\perp f(\bar{r}'_\perp) \cdot \bar{b}_\perp^{(n-m)}(\bar{r}'_\perp) \right] \right\} \tag{19}$$

and

$$\overline{E}_{i2}^{(n)}(\bar{r}) = \sum_{m=1}^{n} \frac{1}{m!} \int d\bar{r}_{\perp}' \, [-f(\bar{r}_{\perp}')]^m$$

$$\frac{\partial^m}{\partial z^m} \left\{ ik_2 \frac{\eta_2}{\eta_1} \overline{\overline{G}}_2(\bar{r}, \bar{r}_{\perp}') \cdot \bar{a}_{\perp}^{(n-m)}(\bar{r}_{\perp}') \right.$$

$$+ \nabla \times \overline{\overline{G}}_2(\bar{r}, \bar{r}_{\perp}') \cdot \bar{b}_{\perp}^{(n-m)}(\bar{r}_{\perp}') \Big\}$$

$$+ \sum_{m=1}^{n} \frac{1}{(m-1)!} \int d\bar{r}_{\perp}' \, [-f(\bar{r}_{\perp}')]^{m-1}$$

$$\frac{\partial^{m-1}}{\partial z^{m-1}} \left\{ ik_2 \frac{\eta_2}{\eta_1} \overline{\overline{G}}_2(\bar{r}, \bar{r}_{\perp}') \cdot \hat{z} \left[\nabla_{\perp}' f(\bar{r}_{\perp}') \cdot \bar{a}_{\perp}^{(n-m)}(\bar{r}_{\perp}') \right] \right.$$

$$+ \nabla \times \overline{\overline{G}}_2(\bar{r}, \bar{r}_{\perp}') \cdot \hat{z} \left[\nabla_{\perp}' f(\bar{r}_{\perp}') \cdot \bar{b}_{\perp}^{(n-m)}(\bar{r}_{\perp}') \right] \Big\}. \tag{20}$$

Comparing the zero-th order $(n = 0)$ integral equations with Eqs. (5) and (6) for the flat interface $[f(\bar{r}_{\perp}') = 0]$, we notice that they are the same except for an additional superscript $^{(0)}$ at the surface variables $\bar{a}_{\perp}$ and $\bar{b}_{\perp}$. Therefore the solutions $\bar{a}_{\perp}^{(0)}$ and $\bar{b}_{\perp}^{(0)}$ for the zero-th order equations should be the same as Eqs. (5) and (6) for which the surface is considered to be flat. For the higher order equations $(n \geq 1)$, we also notice that they are in the same form as the equations for flat surface, except for the substitution of $\overline{E}_i$ by $\overline{E}_i^{(n)}$, and the additional "source" term $\overline{E}_{i2}^{(n)}$ in the lower region V_2. We call the terms $\overline{E}_i^{(n)}$ and $\overline{E}_{i2}^{(n)}$ are the equivalent sources (ES) placing on the mean surface S_o of the rough surface as illustrated in Fig. 3. By denoting the corresponding reflected field as $\overline{E}_r^{(n)}$ for the equivalent source $\overline{E}_i^{(n)}$ in the upper region V_1, and the transmitted field as $\overline{E}_{t2}^{(n)}$ for the equivalent source $\overline{E}_{i2}^{(n)}$ in the lower region, the total scattered field from the rough surface illuminated by the incident wave $\overline{E}_i$ can be expressed by

$$\overline{E}_s(\bar{r}) = \sum_{n=1}^{\infty} \left(\overline{E}_i^{(n)}(\bar{r}) + \overline{E}_r^{(n)}(\bar{r}) \right) + \sum_{n=1}^{\infty} \overline{E}_{t2}^{(n)}(\bar{r}). \tag{21}$$

C. Iterative Scheme for Total Scattered Field

Eqs. (19) and (20) provide the spatial-domain formulation of the electric field from the equivalent source in terms of the lower order surface variables. The following is the iterative procedure to calculate the scattering field from the rough surface:
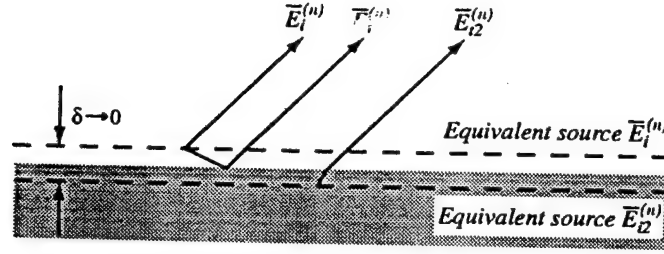
Fig. 3. Radiation, reflection and transmission of equivalent sources on the mean surface.

1. The zero-th order scattered field: Calculate the reflected $\overline{E}_r(\bar{r})$ and $\overline{H}_r(\bar{r})$ of the incident fields $\overline{E}_i(\bar{r})$ and $\overline{H}_i(\bar{r})$ from the mean surface. Thus the zero-th order scattered field is the same as the reflected field $\overline{E}_s^{(0)}(\bar{r}) = \overline{E}_r(\bar{r})$ and $\overline{H}_s^{(0)}(\bar{r}) = \overline{H}_r(\bar{r})$.

2. The first-order scattered field: Calculate the total zero-th order fields on the mean surface

$$\overline{E}^{(0)}(\bar{r}) = \overline{E}_i(\bar{r}) + \overline{E}_s^{(0)}(\bar{r}) \tag{22}$$

$$\overline{H}^{(0)}(\bar{r}) = \overline{H}_i(\bar{r}) + \overline{H}_s^{(0)}(\bar{r}). \tag{23}$$

Then calculate the surface variables of the zero-th order can be obtained by

$$\bar{a}_\perp^{(0)}(\bar{r}_\perp') = \eta_1 \hat{z} \times \overline{H}^{(0)}(\bar{r}_\perp') \tag{24}$$

$$\bar{b}_\perp^{(0)}(\bar{r}_\perp') = \hat{z} \times \overline{E}^{(0)}(\bar{r}_\perp'). \tag{25}$$

Thus the first-order scattered field can be calculated by

$$\overline{E}_s^{(1)}(\bar{r}) = \overline{E}_i^{(1)}(\bar{r}) + \overline{E}_r^{(1)}(\bar{r}) + \overline{E}_{t2}^{(1)}(\bar{r}) \tag{26}$$

$$\overline{H}_s^{(1)}(\bar{r}) = \overline{H}_i^{(1)}(\bar{r}) + \overline{H}_r^{(1)}(\bar{r}) + \overline{H}_{t2}^{(1)}(\bar{r}) \tag{27}$$

where $\overline{E}_i^{(1)}(\bar{r})$ and $\overline{H}_i^{(1)}(\bar{r})$ are the fields of the first-order equivalent source which can be calculated by using Eq. (19) for $n = 1$. $\overline{E}_r^{(1)}(\bar{r})$ and $\overline{H}_r^{(1)}(\bar{r})$ are the reflected fields of the equivalent source in the upper region V_1, and $\overline{E}_{t2}^{(1)}(\bar{r})$ and $\overline{H}_{t2}^{(1)}(\bar{r})$ are the transmitted fields from the equivalent source in the lower region V_2.

3. Calculate the n-th order scattered field: Calculate the surface variables

$$\bar{a}_\perp^{(n)}(\bar{r}_\perp') = \eta_1 \hat{z}$$
$$\times \left[\nabla_\perp' f(\bar{r}_\perp') H_z^{(n-1)}(\bar{r}_\perp') + \overline{H}^{(n)}(\bar{r}_\perp') \right] \tag{28}$$

$$\bar{b}_{\perp}^{(n)}(\bar{r}'_{\perp}) = \hat{z}$$
$$\times \left[\nabla'_{\perp} f(\bar{r}'_{\perp}) E_z^{(n-1)}(\bar{r}'_{\perp}) + \overline{E}^{(n)}(\bar{r}'_{\perp}) \right]. \qquad (29)$$

Thus the n-th order scattered field can be calculated by

$$\overline{E}_s^{(n)}(\bar{r}) = \overline{E}_i^{(n)}(\bar{r}) + \overline{E}_r^{(n)}(\bar{r}) + \overline{E}_{t2}^{(n)}(\bar{r}) \qquad (30)$$

$$\overline{H}_s^{(n)}(\bar{r}) = \overline{H}_i^{(n)}(\bar{r}) + \overline{H}_r^{(n)}(\bar{r}) + \overline{H}_{t2}^{(n)}(\bar{r}) \qquad (31)$$

where $\overline{E}_i^{(n)}(\bar{r})$ and $\overline{H}_i^{(n)}(\bar{r})$ are the fields of the n-th order equivalent source, $\overline{E}_r^{(n)}(\bar{r})$ and $\overline{H}_r^{(n)}(\bar{r})$ are the reflected fields of the equivalent source in the upper region V_1, and $\overline{E}_{t2}^{(n)}(\bar{r})$ and $\overline{H}_{t2}^{(n)}(\bar{r})$ are the transmitted fields from the equivalent source in the lower region V_2.

III. Integral Representation of Equivalent Source

The integral representation of dyadic Green's function in region V_1 and V_2 can be written as [7], respectively,

$$\overline{\overline{G}}_1(\bar{r}, \bar{r}') = -\hat{z}\hat{z}\frac{\delta(\bar{r}, \bar{r}')}{k_1^2} + \frac{i}{8\pi^2}$$
$$\cdot \begin{cases} \int d\bar{k}_{\perp} \dfrac{1}{k_{1z}} \overline{\overline{A}}_1(k_{1z}) e^{i\bar{k}_1 \cdot (\bar{r}-\bar{r}')} & z > z' \\[2mm] \int d\bar{k}_{\perp} \dfrac{1}{k_{1z}} \overline{\overline{A}}_1(-k_{1z}) e^{i\overline{K}_1 \cdot (\bar{r}-\bar{r}')} & z < z' \end{cases} \qquad (32)$$

and

$$\overline{\overline{G}}_2(\bar{r}, \bar{r}') = -\hat{z}\hat{z}\frac{\delta(\bar{r}, \bar{r}')}{k_2^2} + \frac{i}{8\pi^2}$$
$$\cdot \begin{cases} \int d\bar{k}_{\perp} \dfrac{1}{k_{2z}} \overline{\overline{A}}_2(k_{2z}) e^{i\bar{k}_2 \cdot (\bar{r}-\bar{r}')} & z > z' \\[2mm] \int d\bar{k}_{\perp} \dfrac{1}{k_{2z}} \overline{\overline{A}}_2(-k_{2z}) e^{i\overline{K}_2 \cdot (\bar{r}-\bar{r}')} & z < z' \end{cases} \qquad (33)$$

where we define

$$\overline{\overline{A}}_1(k_{1z}) = \hat{e}_1(k_{1z})\hat{e}_1(k_{1z}) + \hat{h}_1(k_{1z})\hat{h}_1(k_{1z}) \qquad (34)$$

$$\overline{\overline{A}}_2(k_{2z}) = \hat{e}_2(k_{2z})\hat{e}_2(k_{2z}) + \hat{h}_2(k_{2z})\hat{h}_2(k_{2z}) \qquad (35)$$

and $\hat{e}_{1,2}$ and $\hat{h}_{1,2}$ are unit polarization vectors defined in Appendix. The up-going wave vectors $\bar{k}_1$ and $\bar{k}_2$ are expressed as $\bar{k}_1 = \hat{x}k_x + \hat{y}k_y + \hat{z}k_{1z}$ and $\bar{k}_2 = \hat{x}k_x + \hat{y}k_y + \hat{z}k_{2z}$,

respectively, and the down-going wave vectors $\overline{K}_1$ and $\overline{K}_2$ are expressed as $\overline{K}_1 = \hat{x}k_x + \hat{y}k_y - \hat{z}k_{1z}$ and $\overline{K}_2 = \hat{x}k_x + \hat{y}k_y - \hat{z}k_{2z}$, respectively. Defining the dyads

$$
\begin{aligned}
\overline{\overline{B}}_1(k_{1z}) &= \hat{k}_1 \times \overline{\overline{A}}_1(k_{1z}) \\
&= -\hat{h}_1(k_{1z})\hat{e}_1(k_{1z}) + \hat{e}_1(k_{1z})\hat{h}_1(k_{1z}) \quad (36) \\
\overline{\overline{B}}_2(k_{2z}) &= \hat{k}_2 \times \overline{\overline{A}}_2(k_{2z}) \\
&= -\hat{h}_2(k_{2z})\hat{e}_2(k_{2z}) + \hat{e}_2(k_{2z})\hat{h}_2(k_{2z}) \quad (37)
\end{aligned}
$$

we write the expressions for $\nabla \times \overline{\overline{G}}_{1,2}(\bar{r}, \bar{r}')$ in terms of the integral of $\overline{\overline{B}}_{1,2}$. The operator $\partial^m/\partial z^m$ applying on $\overline{\overline{G}}_{1,2}(\bar{r}, \bar{r}')$ and $\nabla \times \overline{\overline{G}}_{1,2}(\bar{r}, \bar{r}')$ creates the following eigenvalues:

$$
\frac{\partial^m}{\partial z^m} = \begin{cases} (ik_{1,2z})^m & z > z' \\ (-ik_{1,2z})^m & z < z'. \end{cases} \quad (38)
$$

Therefore, the radiation field from the equivalent source on top of the mean surface can be written as follows:

For up-going wave $(z > z')$

$$
\begin{aligned}
\overline{E}_i^{(n)}(\bar{r}) = &-\frac{i}{8\pi^2}k_1 \sum_{m=1}^{n} \frac{1}{m!} \int d\bar{r}'_\perp \left[-f(\bar{r}'_\perp)\right]^m \\
&\left\{ \int d\bar{k}_\perp (ik_{1z})^{m-1} \overline{\overline{A}}_1(k_{1z}) e^{i\bar{k}_1 \cdot (\bar{r}-\bar{r}')} \cdot \bar{a}_\perp^{(n-m)}(\bar{r}'_\perp) \right. \\
&\left. + \int d\bar{k}_\perp (ik_{1z})^{m-1} \overline{\overline{B}}_1(k_{1z}) e^{i\bar{k}_1 \cdot (\bar{r}-\bar{r}')} \cdot \bar{b}_\perp^{(n-m)}(\bar{r}'_\perp) \right\} \\
&-\frac{i}{8\pi^2}k_1 \sum_{m=1}^{n} \frac{1}{(m-1)!} \int d\bar{r}'_\perp \left[-f(\bar{r}'_\perp)\right]^{m-1} \\
&\left\{ \int d\bar{k}_\perp (ik_{1z})^{m-2} \overline{\overline{A}}_1(k_{1z}) e^{i\bar{k}_1 \cdot (\bar{r}-\bar{r}')} \right. \\
&\cdot \hat{z} \left[\nabla'_\perp f(\bar{r}'_\perp) \cdot \bar{a}_\perp^{(n-m)}(\bar{r}'_\perp)\right] \\
&+ \int d\bar{k}_\perp (ik_{1z})^{m-2} \overline{\overline{B}}_1(k_{1z}) e^{i\bar{k}_1 \cdot (\bar{r}-\bar{r}')} \\
&\left. \cdot \hat{z} \left[\nabla'_\perp f(\bar{r}'_\perp) \cdot \bar{b}_\perp^{(n-m)}(\bar{r}'_\perp)\right] \right\} \quad (39)
\end{aligned}
$$

$$
\begin{aligned}
\overline{E}_{i2}^{(n)}(\bar{r}) = &-\frac{ik_2}{8\pi^2} \sum_{m=1}^{n} \frac{1}{m!} \int d\bar{r}'_\perp \left[-f(\bar{r}'_\perp)\right]^m \\
&\left\{ \frac{\eta_2}{\eta_1} \int d\bar{k}_\perp (ik_{2z})^{m-1} \overline{\overline{A}}_2(k_{2z}) e^{i\bar{k}_2 \cdot (\bar{r}-\bar{r}')} \cdot \bar{a}_\perp^{(n-m)}(\bar{r}'_\perp) \right.
\end{aligned}
$$

$$+ \int d\bar{k}_\perp (ik_{2z})^{m-1} \overline{\overline{B}}_2(k_{2z}) e^{i\bar{k}_2 \cdot (\bar{r}-\bar{r}')} \cdot \bar{b}_\perp^{(n-m)}(\bar{r}'_\perp) \Bigg\}$$

$$- \frac{ik_2}{8\pi^2} \sum_{m=1}^n \frac{1}{(m-1)!} \int d\bar{r}'_\perp [-f(\bar{r}'_\perp)]^{m-1}$$

$$\Bigg\{ \frac{\eta_2}{\eta_1} \int d\bar{k}_\perp (ik_{2z})^{m-2} \overline{\overline{A}}_2(k_{2z}) e^{i\bar{k}_2 \cdot (\bar{r}-\bar{r}')}$$

$$\cdot \hat{z} \left[\nabla'_\perp f(\bar{r}'_\perp) \cdot \bar{a}_\perp^{(n-m)}(\bar{r}'_\perp) \right]$$

$$+ \int d\bar{k}_\perp (ik_{2z})^{m-2} \overline{\overline{B}}_2(k_{2z}) e^{i\bar{k}_2 \cdot (\bar{r}-\bar{r}')}$$

$$\cdot \hat{z} \left[\nabla'_\perp f(\bar{r}'_\perp) \cdot \bar{b}_\perp^{(n-m)}(\bar{r}'_\perp) \right] \Bigg\}. \tag{40}$$

For down-going wave $(z < z')$

$$\overline{E}_i^{(n)}(\bar{r}) = \frac{ik_1}{8\pi^2} \sum_{m=1}^n \frac{1}{m!} \int d\bar{r}'_\perp [-f(\bar{r}'_\perp)]^m$$

$$\Bigg\{ \int d\bar{k}_\perp (-ik_{1z})^{m-1} e^{i\overline{K}_1 \cdot (\bar{r}-\bar{r}')}$$

$$\overline{\overline{A}}_1(-k_{1z}) \cdot \bar{a}_\perp^{(n-m)}(\bar{r}'_\perp)$$

$$+ \int d\bar{k}_\perp (-ik_{1z})^{m-1} e^{i\overline{K}_1 \cdot (\bar{r}-\bar{r}')} \Bigg\}$$

$$\overline{\overline{B}}_1(-k_{1z}) \cdot \bar{b}_\perp^{(n-m)}(\bar{r}'_\perp)$$

$$+ \frac{ik_1}{8\pi^2} \sum_{m=1}^n \frac{1}{(m-1)!} \int d\bar{r}'_\perp [-f(\bar{r}'_\perp)]^{m-1}$$

$$\Bigg\{ \int d\bar{k}_\perp (-ik_{1z})^{m-2} \overline{\overline{A}}_1(-k_{1z}) e^{i\overline{K}_1 \cdot (\bar{r}-\bar{r}')}$$

$$\cdot \hat{z} \left[\nabla'_\perp f(\bar{r}'_\perp) \cdot \bar{a}_\perp^{(n-m)}(\bar{r}'_\perp) \right]$$

$$+ \int d\bar{k}_\perp (-ik_{1z})^{m-2} \overline{\overline{B}}_1(-k_{1z}) e^{i\overline{K}_1 \cdot (\bar{r}-\bar{r}')}$$

$$\cdot \hat{z} \left[\nabla'_\perp f(\bar{r}'_\perp) \cdot \bar{b}_\perp^{(n-m)}(\bar{r}'_\perp) \right] \Bigg\} \tag{41}$$

$$\overline{E}_{i2}^{(n)}(\bar{r}) = \frac{ik_2}{8\pi^2} \sum_{m=1}^n \frac{1}{m!} \int d\bar{r}'_\perp [-f(\bar{r}'_\perp)]^m$$

$$\Bigg\{ \frac{\eta_2}{\eta_1} \int d\bar{k}_\perp (-ik_{2z})^{m-1} e^{i\overline{K}_2 \cdot (\bar{r}-\bar{r}')}$$

$$\overline{\overline{A}}_2(-k_{2z}) \cdot \bar{a}_\perp^{(n-m)}(\bar{r}'_\perp)$$

$$+ \int d\bar{k}_\perp (-ik_{2z})^{m-1} e^{i\overline{K}_2 \cdot (\bar{r}-\bar{r}')}$$

$$\overline{\overline{B}}_2(-k_{2z}) \cdot \bar{b}_\perp^{(n-m)}(\bar{r}'_\perp) \Big\}$$

$$+\frac{ik_2}{8\pi^2} \sum_{m=1}^{n} \frac{1}{(m-1)!} \int d\bar{r}'_\perp \left[-f(\bar{r}'_\perp)\right]^{m-1}$$

$$\left\{ \frac{\eta_2}{\eta_1} \int d\bar{k}_\perp (-ik_{2z})^{m-2} \overline{\overline{A}}_2(-k_{2z}) e^{i\overline{K}_2 \cdot (\bar{r}-\bar{r}')} \right.$$

$$\cdot \hat{z} \left[\nabla'_\perp f(\bar{r}'_\perp) \cdot \bar{a}_\perp^{(n-m)}(\bar{r}'_\perp) \right]$$

$$+ \int d\bar{k}_\perp (-ik_{2z})^{m-2} \overline{\overline{B}}_2(-k_{2z}) e^{i\overline{K}_2 \cdot (\bar{r}-\bar{r}')}$$

$$\left. \cdot \hat{z} \left[\nabla'_\perp f(\bar{r}'_\perp) \cdot \bar{b}_\perp^{(n-m)}(\bar{r}'_\perp) \right] \right\}. \tag{42}$$

The down-going wave $\overline{E}_i^{(n)}$ and up-going wave $\overline{E}_{i2}^{(n)}$ will be reflected by and transmitted through the mean surface, respectively.

A. Reflected Field of Equivalent Source

To calculate the reflected wave of the equivalent source, we decompose $\overline{E}_i^{(n)}$ into a sum of TE and TM waves. Recalling the definition for $\overline{\overline{A}}_1$, $\overline{\overline{B}}_1$, $\overline{\overline{A}}_2$, and $\overline{\overline{B}}_2$, we know that the product of $\hat{e}_1(-k_{1z})\hat{e}_1(-k_{1z})$ or $\hat{e}_1(-k_{1z})\hat{h}_1(-k_{1z})$ with any polarization will be a TE wave, and the product of $\hat{h}_1(-k_{1z})\hat{h}_1(-k_{1z})$ or $\hat{h}_1(-k_{1z})\hat{e}_1(-k_{1z})$ with any polarization will be a TM wave. To get the reflected wave for the down-going wave $\overline{E}_i^{(n)}$ for $z < z'$, we do the following:

1. Multiply the TE wave terms by $R^{TE}(k_{1z})$ and the TM wave terms by $R^{TM}(k_{1z})$ in the integral representation of the down-going wave $\overline{E}_i^{(n)}$,

2. Change the sign of k_{1z} for the first unit polarization vector in the tensors $\overline{\overline{A}}_1$ and $\overline{\overline{B}}_1$, and

3. Change the down-going wave vector $\overline{K}_1$ to the up-going wave vector $\bar{k}_1$ in the exponential terms.

Thus we find

$$\overline{E}_r^{(n)}(\bar{r}) = \frac{ik_1}{8\pi^2} \sum_{m=1}^{n} \frac{1}{m!} \int d\bar{r}'_\perp \left[-f(\bar{r}'_\perp)\right]^m$$

$$\left\{ \int d\bar{k}_\perp (-ik_{1z})^{m-1} \left(R^{TE}(k_{1z})\hat{e}_1(k_{1z})\hat{e}_1(-k_{1z}) \right.\right.$$

$$\left. + R^{TM}(k_{1z})\hat{h}_1(k_{1z})\hat{h}_1(-k_{1z}) \right) e^{i\bar{k}_1 \cdot (\bar{r}-\bar{r}')} \cdot \bar{a}_\perp^{(n-m)}(\bar{r}'_\perp)$$

$$+ \int d\bar{k}_\perp \, (-ik_{1z})^{m-1} \left(-R^{TM}(k_{1z})\hat{h}_1(k_{1z})\hat{e}_1(-k_{1z}) \right.$$

$$\left. +R^{TE}(k_{1z})\hat{e}_1(k_{1z})\hat{h}_1(-k_{1z}) \right) e^{i\bar{k}_1 \cdot (\bar{r}-\bar{r}')} \cdot \bar{b}_\perp^{(n-m)}(\bar{r}'_\perp) \bigg\}$$

$$+\frac{ik_1}{8\pi^2} \sum_{m=1}^{n} \frac{1}{(m-1)!} \int d\bar{r}'_\perp \, [-f(\bar{r}'_\perp)]^{m-1}$$

$$\left\{ \int d\bar{k}_\perp \, (-ik_{1z})^{m-2} \, e^{i\bar{k}_1 \cdot (\bar{r}-\bar{r}')} \right.$$

$$\left(R^{TE}(k_{1z})\hat{e}_1(k_{1z})\hat{e}_1(-k_{1z}) \right.$$

$$\left. +R^{TM}(k_{1z})\hat{h}_1(k_{1z})\hat{h}_1(-k_{1z}) \right)$$

$$\cdot\hat{z} \left[\nabla'_\perp f(\bar{r}'_\perp) \cdot \bar{a}_\perp^{(n-m)}(\bar{r}'_\perp) \right]$$

$$+ \int d\bar{k}_\perp \, (-ik_{1z})^{m-2} \, e^{i\bar{k}_1 \cdot (\bar{r}-\bar{r}')}$$

$$\left(-R^{TM}(k_{1z})\hat{h}_1(k_{1z})\hat{e}_1(-k_{1z}) \right.$$

$$\left. +R^{TE}(k_{1z})\hat{e}_1(k_{1z})\hat{h}_1(-k_{1z}) \right)$$

$$\left. \cdot\hat{z} \left[\nabla'_\perp f(\bar{r}'_\perp) \cdot \bar{b}_\perp^{(n-m)}(\bar{r}'_\perp) \right] \right\}. \tag{43}$$

In the above equation, the Fresnel reflection coefficients are defined as follows:

$$R^{TE}(k_{1z}) = \frac{k_{1z} - k_{2z}}{k_{1z} + k_{2z}} \tag{44}$$

$$R^{TM}(k_{1z}) = \frac{\epsilon_2 k_{1z} - \epsilon_1 k_{2z}}{\epsilon_2 k_{1z} + \epsilon_1 k_{2z}} \tag{45}$$

$$R^{TE}(k_{2z}) = -R^{TE}(k_{1z}) = -\frac{k_{1z} - k_{2z}}{k_{1z} + k_{2z}} \tag{46}$$

$$R^{TM}(k_{2z}) = -R^{TM}(k_{1z}) = -\frac{\epsilon_2 k_{1z} - \epsilon_1 k_{2z}}{\epsilon_2 k_{1z} + \epsilon_1 k_{2z}} \tag{47}$$

where $R^{TE}(k_{1z})$ and $R^{TM}(k_{1z})$ are the reflection coefficients for TE and TM waves incident from region V_1 to region V_2, respectively. $R^{TE}(k_{2z})$ and $R^{TM}(k_{2z})$ are the reflection coefficients for TE and TM waves incident from region V_2 to region V_1, respectively.

B. Transmitted Field of Equivalent Source

To get the transmitted wave from the equivalent source in the lower region V_2, we work on the up-going wave $\overline{E}_{i2}^{(n)}$ in Eq. (40) as following steps:

1. Multiply the terms with $\hat{e}_2$ as the first vector in the tensors with T^{TE}, and multiply the terms with $\hat{h}_2$ as the first vector in the tensors $\overline{\overline{A}}_2$ and $\overline{\overline{B}}_2$ with T^{TM} ,

2. Change the first vectors $\hat{e}_2(k_{2z})$ and $\hat{h}_2(k_{2z})$ in the polarization tensors to $\hat{e}_1(k_{1z})$ and $\hat{h}_1(k_{1z})$, and

3. Change the up-going wave vector $\overline{k}_2$ to $\overline{k}_1$ in the exponential terms.

Thus we get

$$
\begin{aligned}
\overline{E}_{t2}^{(n)}(\overline{r}) = &-\frac{ik_2}{8\pi^2} \sum_{m=1}^{n} \frac{1}{m!} \int d\overline{r}'_\perp \left[-f(\overline{r}'_\perp)\right]^m \\
&\left\{ \frac{\eta_2}{\eta_1} \int d\overline{k}_\perp (ik_{2z})^{m-1} \left(T^{TE}(k_{2z})\hat{e}_1(k_{1z})\hat{e}_2(k_{2z}) \right.\right. \\
&\left. + T^{TM}(k_{2z})\hat{h}_1(k_{1z})\hat{h}_2(k_{2z}) \right) e^{i\overline{k}_1 \cdot (\overline{r}-\overline{r}')} \cdot \overline{a}_\perp^{(n-m)}(\overline{r}'_\perp) \\
&+ \int d\overline{k}_\perp (ik_{2z})^{m-1} \left(-T^{TM}(k_{2z})\hat{h}_1(k_{1z})\hat{e}_2(k_{2z}) \right. \\
&\left.\left. + T^{TE}(k_{2z})\hat{e}_1(k_{1z})\hat{h}_2(k_{2z}) \right) e^{i\overline{k}_1 \cdot (\overline{r}-\overline{r}')} \cdot \overline{b}_\perp^{(n-m)}(\overline{r}'_\perp) \right\} \\
&- \frac{ik_2}{8\pi^2} \sum_{m=1}^{n} \frac{1}{(m-1)!} \int d\overline{r}'_\perp \left[-f(\overline{r}'_\perp)\right]^{m-1} \\
&\left\{ \frac{\eta_2}{\eta_1} \int d\overline{k}_\perp (ik_{2z})^{m-2} \left(T^{TE}(k_{2z})\hat{e}_1(k_{1z})\hat{e}_2(k_{2z}) \right.\right. \\
&\left. + T^{TM}(k_{2z})\hat{h}_1(k_{1z})\hat{h}_2(k_{2z}) \right) e^{i\overline{k}_1 \cdot (\overline{r}-\overline{r}')} \\
&\cdot \hat{z} \left[\nabla'_\perp f(\overline{r}'_\perp) \cdot \overline{a}_\perp^{(n-m)}(\overline{r}'_\perp) \right] \\
&+ \int d\overline{k}_\perp (ik_{2z})^{m-2} \left(-T^{TM}(k_{2z})\hat{h}_1(k_{1z})\hat{e}_2(k_{2z}) \right. \\
&\left. + T^{TE}(k_{2z})\hat{e}_1(k_{1z})\hat{h}_2(k_{2z}) \right) e^{i\overline{k}_1 \cdot (\overline{r}-\overline{r}')} \\
&\left.\cdot \hat{z} \left[\nabla'_\perp f(\overline{r}'_\perp) \cdot \overline{b}_\perp^{(n-m)}(\overline{r}'_\perp) \right] \right\}
\end{aligned}
\tag{48}
$$

where the transmission coefficients are defined as follows:

$$
\begin{aligned}
T^{TE}(k_{1z}) &= 1 + R^{TE}(k_{1z}) = \frac{2k_{1z}}{k_{1z} + k_{2z}} & (49) \\
T^{TM}(k_{1z}) &= \frac{\eta_2}{\eta_1} \left(1 + R^{TM}(k_{1z}) \right) \\
&= \frac{\eta_2}{\eta_1} \frac{2\epsilon_2 k_{1z}}{\epsilon_2 k_{1z} + \epsilon_1 k_{2z}} & (50) \\
T^{TE}(k_{2z}) &= 1 + R^{TE}(k_{2z}) = \frac{2k_{2z}}{k_{1z} + k_{2z}} & (51) \\
T^{TM}(k_{2z}) &= \frac{\eta_1}{\eta_2} \left(1 + R^{TM}(k_{2z}) \right)
\end{aligned}
$$

$$= \frac{\eta_1}{\eta_2} \frac{2\epsilon_1 k_{2z}}{\epsilon_2 k_{1z} + \epsilon_1 k_{2z}}. \tag{52}$$

C. The First-Order Field Scattered by PEC Rough Surface

For a perfectly conducting rough surface, the tangential electric field is zero, thus $\bar{b}_\perp^{(0)} = 0$. Therefore the first-order field of the equivalent source can be written as [from Eq. (39)]

$$
\begin{aligned}
\overline{E}_i^{(1)}(\bar{r}) = {}& \frac{ik_1}{8\pi^2} \int d\bar{r}'_\perp f(\bar{r}'_\perp) \\
& \int d\bar{k}_\perp \overline{\overline{A}}_1(k_{1z}) e^{i\bar{k}_1 \cdot (\bar{r}-\bar{r}')} \cdot \bar{a}_\perp^{(0)}(\bar{r}'_\perp) \\
& - \frac{ik_1}{8\pi^2} \int d\bar{r}'_\perp \int d\bar{k}_\perp \frac{1}{ik_{1z}} \overline{\overline{A}}_1(k_{1z}) e^{i\bar{k}_1 \cdot (\bar{r}-\bar{r}')} \cdot \hat{z} \\
& \left[\nabla'_\perp f(\bar{r}'_\perp) \cdot \bar{a}_\perp^{(0)}(\bar{r}'_\perp) \right].
\end{aligned} \tag{53}
$$

Notice that the Fresnel reflection coefficients of the TE and TM waves for perfectly conducting surface are $R^{TE}(k_{1z}) = -1$ and $R^{TM}(k_{1z}) = 1$. Therefore, from Eq. (43), the first-order ($n = 1$) reflected wave of the equivalent source from the perfectly conducting surface is

$$
\begin{aligned}
\overline{E}_r^{(1)}(\bar{r}) = {}& \frac{ik_1}{8\pi^2} \int d\bar{r}'_\perp f(\bar{r}'_\perp) \int d\bar{k}_\perp \bigg(\hat{e}_1(k_{1z})\hat{e}_1(k_{1z}) \\
& + \hat{h}_1(k_{1z})\hat{h}_1(k_{1z}) \bigg) e^{i\bar{k}_1 \cdot (\bar{r}-\bar{r}')} \cdot \bar{a}_\perp^{(0)}(\bar{r}'_\perp) \\
& - \frac{ik_1}{8\pi^2} \int d\bar{r}'_\perp \int d\bar{k}_\perp \frac{1}{ik_{1z}} \bigg(\hat{e}_1(k_{1z})\hat{e}_1(k_{1z}) \\
& + \hat{h}_1(k_{1z})\hat{h}_1(k_{1z}) \bigg) e^{i\bar{k}_1 \cdot (\bar{r}-\bar{r}')} \\
& \cdot \hat{z} \left[\nabla'_\perp f(\bar{r}'_\perp) \cdot \bar{a}_\perp^{(0)}(\bar{r}'_\perp) \right] \\
= {}& \frac{ik_1}{8\pi^2} \int d\bar{r}'_\perp f(\bar{r}'_\perp) \int d\bar{k}_\perp \overline{\overline{A}}_1(k_{1z}) e^{i\bar{k}_1 \cdot (\bar{r}-\bar{r}')} \cdot \bar{a}_\perp^{(0)}(\bar{r}'_\perp) \\
& - \frac{ik_1}{8\pi^2} \int d\bar{r}'_\perp \int d\bar{k}_\perp \frac{1}{ik_{1z}} \overline{\overline{A}}_1(k_{1z}) e^{i\bar{k}_1 \cdot (\bar{r}-\bar{r}')} \cdot \hat{z} \\
& \left[\nabla'_\perp f(\bar{r}'_\perp) \cdot \bar{a}_\perp^{(0)}(\bar{r}'_\perp) \right].
\end{aligned} \tag{54}
$$

Notice that the first-order reflected wave from the mean surface of the perfectly conducting rough surface [Eq. (54)] is the same as the first-order radiated field of the equivalent source [Eq. (53)]. The transmitted field $\overline{E}_{t2}^{(1)}$ is zero, thus the total scattered field is

$$\overline{E}_s^{(1)}(\bar{r}) = \overline{E}_i^{(1)}(\bar{r}) + \overline{E}_{1r}^{(1)}(\bar{r}) = 2\overline{E}_i^{(1)}(\bar{r})$$

$$\begin{aligned}
= \ & -2ik_1 \int d\bar{r}'_\perp f(\bar{r}'_\perp) \frac{\partial}{\partial z} \left\{ \overline{\overline{G}}_1(\bar{r}, \bar{r}'_\perp) \cdot \bar{a}^{(0)}_\perp(\bar{r}'_\perp) \right\} \\
& + 2ik_1 \int d\bar{r}'_\perp \overline{\overline{G}}_1(\bar{r}, \bar{r}'_\perp) \\
& \cdot \hat{z} \left[\nabla'_\perp f(\bar{r}'_\perp) \cdot \bar{a}^{(0)}_\perp(\bar{r}'_\perp) \right].
\end{aligned} \tag{55}$$

IV. Comparison with Conventional SPM Result

Consider a plane wave $\overline{E}_i(\bar{r}) = \overline{E}_i^{(0)}(\bar{r}) = \hat{e}_i E_o e^{i\bar{k}_i \cdot \bar{r}}$ incident upon a perfectly conducting rough surface. The SPM solution of the zero-th order surface variable $\bar{a}^{(0)}_\perp$ is [7]

$$\bar{a}^{(0)}_\perp(\bar{r}'_\perp) = \tilde{a}^{(0)}_\perp(\bar{k}_{i\perp}) e^{i\bar{k}_{i\perp} \cdot \bar{r}'_\perp} \tag{56}$$

where

$$\tilde{a}^{(0)}_\perp(\bar{k}_{i\perp}) = \hat{q}_i a^{(0)}_q(\bar{k}_{i\perp}) + \hat{p}_i a^{(0)}_p(\bar{k}_{i\perp}) \tag{57}$$

$$\begin{aligned}
a^{(0)}_q(\bar{k}_{i\perp}) &= 2 \left[\hat{e}_i \cdot \hat{e}(-k_{iz}) \right] E_o \frac{k_{iz}}{k_1} \\
a^{(0)}_p(\bar{k}_{i\perp}) &= 2 \left[\hat{e}_i \cdot \hat{h}(-k_{iz}) \right] E_o
\end{aligned} \tag{58}$$

and the basis vectors are defined as follows:

$$\begin{aligned}
\hat{q}_i &= \frac{1}{k_{i\rho}} (\hat{x} k_{iy} - \hat{y} k_{ix}) \\
\hat{p}_i &= \hat{z}_i \times \hat{q}_i = \frac{1}{k_{i\rho}} (\hat{x} k_{ix} + \hat{y} k_{iy}) \\
\hat{z}_i &= \hat{z}.
\end{aligned} \tag{59}$$

Defining the Fourier transform pair

$$F(\bar{k}_\perp) = \frac{1}{(2\pi)^2} \int d\bar{r}'_\perp e^{-i\bar{k}_\perp \cdot \bar{r}'_\perp} f(\bar{r}'_\perp) \tag{60}$$

$$f(\bar{r}'_\perp) = \int d\bar{k}'_\perp e^{i\bar{k}'_\perp \cdot \bar{r}'_\perp} F(\bar{k}'_\perp) \tag{61}$$

and the delta function

$$\delta(\bar{k}_\perp) = \frac{1}{(2\pi)^2} \int d\bar{r}'_\perp e^{-i\bar{k}_\perp \cdot \bar{r}'_\perp} \tag{62}$$

we can write the following relations as:

$$\frac{\partial f(\bar{r}'_\perp)}{\partial x'} = i \int d\bar{k}'_\perp e^{i\bar{k}'_\perp \cdot \bar{r}'_\perp} k'_x F(\bar{k}'_\perp) \tag{63}$$

$$\frac{\partial f(\bar{r}'_\perp)}{\partial y'} = i \int d\bar{k}'_\perp e^{i\bar{k}'_\perp \cdot \bar{r}'_\perp} k'_y F(\bar{k}'_\perp) \tag{64}$$

$$\nabla'_\perp f(\bar{r}'_\perp) = i \int d\bar{k}'_\perp e^{i\bar{k}'_\perp \cdot \bar{r}'_\perp} \left(k'_x \hat{x} + k'_y \hat{y} \right) F(\bar{k}'_\perp). \tag{65}$$

By making use of the vector products

$$(\hat{x}k_x + \hat{y}k_y) \cdot \hat{q}_i = \frac{k_x k_{iy} - k_y k_{ix}}{k_{i\rho}}$$

$$(\hat{x}k_x + \hat{y}k_y) \cdot \hat{p}_i = \frac{k_x k_{ix} + k_y k_{iy}}{k_{i\rho}}$$

$$(\hat{x}k_{ix} + \hat{y}k_{iy}) \cdot \hat{q}_i = 0$$

$$(\hat{x}k_{ix} + \hat{y}k_{iy}) \cdot \hat{p}_i = k_{i\rho}$$

$$\hat{e}_1(k_{1z}) \cdot \hat{q}_i = \frac{k_{iy}k_y + k_{ix}k_x}{k_\rho k_{i\rho}}$$

$$\hat{e}_1(k_{1z}) \cdot \hat{p}_i = \frac{k_{ix}k_y - k_{iy}k_x}{k_\rho k_{i\rho}}$$

and integrating the transverse wavenumber, the first-order scattered field in Eq. (55) rewritten as

$$\overline{E}_s^{(1)}(\bar{r}) = E_o \int d\bar{k}_\perp e^{i\bar{k}_1 \cdot \bar{r}} iF(\bar{k}_\perp - \bar{k}_{i\perp})\hat{e}_1(k_{1z})$$

$$\left(2k_1 \frac{k_{iy}k_y + k_{ix}k_x}{k_\rho k_{i\rho}} \frac{k_{iz}}{k_1}\right)[\hat{e}_i \cdot \hat{e}(-k_{iz})]$$

$$+E_o \int d\bar{k}_\perp e^{i\bar{k}_1 \cdot \bar{r}} iF(\bar{k}_\perp - \bar{k}_{i\perp})\hat{e}_1(k_{1z})$$

$$\left(2k_1 \frac{k_{ix}k_y - k_{iy}k_x}{k_\rho k_{i\rho}}\right)\left[\hat{e}_i \cdot \hat{h}(-k_{iz})\right]$$

$$+E_o \int d\bar{k}_\perp e^{i\bar{k}_1 \cdot \bar{r}} iF(\bar{k}_\perp - \bar{k}_{i\perp})\hat{h}_1(k_{1z})$$

$$\left(-2\frac{k_1 k_{iz}}{k_{1z}k_\rho} \frac{k_x k_{iy} - k_y k_{ix}}{k_{i\rho}}\right)[\hat{e}_i \cdot \hat{e}(-k_{iz})]$$

$$+E_o \int d\bar{k}_\perp e^{i\bar{k}_1 \cdot \bar{r}} iF(\bar{k}_\perp - \bar{k}_{i\perp})\hat{h}_1(k_{1z})$$

$$\left(-2\frac{k_1^2}{k_{1z}k_\rho} \frac{k_x k_{ix} + k_y k_{iy}}{k_{i\rho}} + 2\frac{k_\rho k_{i\rho}}{k_{1z}}\right)$$

$$\left[\hat{e}_i \cdot \hat{h}(-k_{iz})\right]. \tag{66}$$

By rewriting the scattered electric field in a matrix form

$$\overline{E}^{(1)}(\bar{r}) = \begin{bmatrix} E_e^{(1)}(\bar{r}) \\ E_h^{(1)}(\bar{r}) \end{bmatrix}$$

$$= \int d\bar{k}_\perp e^{i\bar{k}_1 \cdot \bar{r}} iF(\bar{k}_\perp - \bar{k}_{i\perp})$$

$$\begin{bmatrix} f_{ee} & f_{eh} \\ f_{he} & f_{hh} \end{bmatrix} \begin{bmatrix} \hat{e}_i \cdot \hat{e}(-k_{iz})E_o \\ \hat{e}_i \cdot \hat{h}(-k_{iz})E_o \end{bmatrix} \tag{67}$$

the scattering matrix is then obtained as

$$
\begin{bmatrix} f_{ee} & f_{eh} \\ f_{he} & f_{hh} \end{bmatrix} =
$$
$$
\begin{bmatrix} 2k_1 \frac{k_{iy}k_y + k_{ix}k_x}{k_\rho k_{i\rho}} \frac{k_{iz}}{k_1} & 2k_1 \frac{k_{ix}k_y - k_{iy}k_x}{k_\rho k_{i\rho}} \\ -\frac{2k_1 k_{iz}}{k_{1z}k_\rho} \frac{k_z k_{iy} - k_y k_{iz}}{k_{i\rho}} & -\frac{2k_1^2}{k_{1z}k_\rho} \frac{k_z k_{ix} + k_y k_{iy}}{k_{i\rho}} + \frac{2k_\rho k_{i\rho}}{k_{1z}} \end{bmatrix} .
$$

(68)

Expressing the wavenumber components by using angles θ, ϕ, θ_i, and ϕ_i, we find the scattering matrix to be

$$
\begin{bmatrix} f_{ee} & f_{eh} \\ f_{he} & f_{hh} \end{bmatrix} =
$$
$$
\begin{bmatrix} 2k_{iz}\cos(\phi - \phi_i) & 2k_1 \sin(\phi - \phi_i) \\ \frac{2k_1 k_{iz}}{k_{1z}} \sin(\phi - \phi_i) & \frac{2k_1^2}{k_{1z}} [\sin\theta \sin\theta_i - \cos(\phi - \phi_i)] \end{bmatrix} .
$$

(69)

Notice that the components of the scattering matrix [Eq. (68)] derived above using the equivalent source formulation for a plane incident wave are the same as the ones using conventional SPM as given in [8] for the limiting case of $k_2 \to \infty$.

V. NUMERICAL RESULT

In this section, the backscattering coefficients will be calculated by using the first-order equivalent source formulation for a Gaussian-tapered incident wave and compared with the standard method of moments. The backscattering coefficient is defined as

$$
\sigma_{ab} = \lim_{r \to \infty} 4\pi r^2 \frac{\left\langle |E_a^s - \langle E_a^s \rangle|^2 \right\rangle}{P_i}
$$

(70)

where $P_i = \int |E_b^i|^2 \, dA$ is the power of the incident wave on the illuminated area with the integral over the mean surface. On the mean surface, the electric field of a Gaussian-tapered wave can be written as $E_b^i = E_o e^{-r^2/g^2}$, where g is a factor specifying the beam width. Therefore we get, for the Gaussian-tapered incident wave,

$$
P_i = \int_0^\infty r\,dr \int_0^{2\pi} d\phi \, |E_o|^2 \, e^{-2r^2/g^2} = |E_o|^2 \frac{\pi g^2}{2} .
$$

(71)

In the numerical calculation, the expected backscattering coefficient are calculated by averaging the samples of the scattered field, thus

$$\sigma_{ab} = \lim_{r \to \infty} 4\pi r^2 \frac{\left\langle |E_a^s - \langle E_a^s \rangle|^2 \right\rangle}{P_i}$$

$$\sim \lim_{r \to \infty} \frac{4\pi r^2}{P_i} \frac{1}{N-1} \left[\sum_{n=1}^N |E_a^s|^2 - \frac{1}{N} \left| \sum_{n=1}^N E_a^s \right|^2 \right]$$

$$= \lim_{r \to \infty} \frac{4\pi r^2}{P_i} \frac{N}{N-1} \left[\frac{1}{N} \sum_{n=1}^N |E_a^s|^2 - \left| \frac{1}{N} \sum_{n=1}^N E_a^s \right|^2 \right]$$

$$(72)$$

where N is the number of realizations in the Monte Carlo simulation and "$\sim$" means statistically estimated. It is convenient if we use the standard deviation to normalize the calculated profile $f(x, y)$. The standard deviation σ can be obtained as

$$\sigma^2 = \int_0^\infty k \, dk \int_0^{2\pi} d\alpha W(k, \alpha). \tag{73}$$
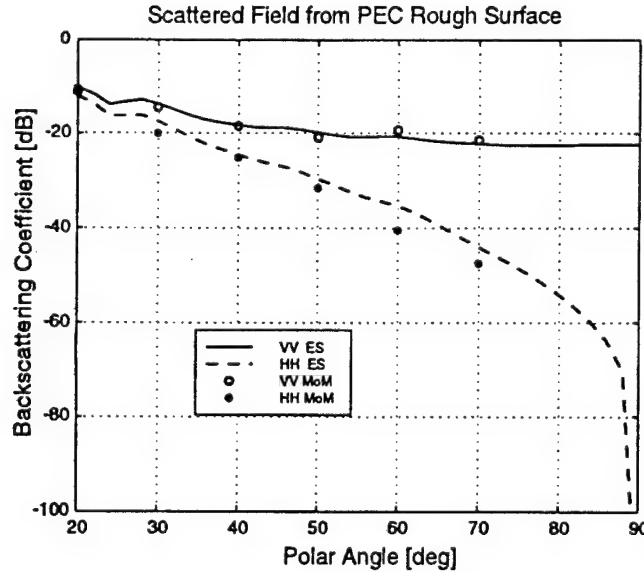

Fig. 4. Comparison of the scattered field calculated by using the spatial-domain formulation with the result by the method of moments (MoM).

In the numerical simulation, we use the power law spectrum to generate random rough

surfaces. The power law spectrum function for rough surfaces is defined as

$$W(k, \alpha) = \frac{\sigma^2 k_c^2 k_{max}^2}{\pi \left(k_{max}^2 - k_c^2 \right) k^4} \tag{74}$$

where σ is the rms height, and k_c and k_{max} are the low and high cutoff wavenumber of the rough surface, respectively.

Fig. 4 is the numerical result for the backscattering coefficients of the co-polarized waves σ_{hh} and σ_{vv} by using the spatial-domain formulation in comparison with the standard MoM. The rms height of the rough surface is $\sigma = 0.01\lambda$ and the number of realizations is $N = 30$. The incident wave is tapered with the factor $g = 3.0\lambda$. The central plane wave of the tapered incident wave varies its polar angle from 20° in order to avoid the strong specular reflection of the incident beam close to the normal incident angle. The comparison of the results demonstrates good agreement between the two different methods. At low grazing angles, the MoM code does not provide correct results due to the difficulty to increase the size of rough surface at these angles [9]. The spatial-domain formulation gives reasonable results at low grazing angles where σ_{hh} drops to zero and σ_{vv} tends to a constant when the grazing angle approaches zero.

VI. DISCUSSIONS

In this paper, we have derived the spatial-domain formulation of the equivalent sources for any orders and the simple spatial-domain formulation of the first-order field scattered by a PEC rough surface. Up to the first order, we have proved that the total field of the equivalent source on a PEC rough surface is the field scattered by the rough surface. The advantage of using the spatial-domain formulation instead of frequency domain as in the conventional SPM formulation is that there is no need of integration over the spatial frequency and the non-averaged complex scattered field is well-defined. However the derivation for the total scattered field of higher order ($n \geq 2$) or the field scattered from a dielectric rough surface requires much more effort since the Sommerfeld integrals are involved. By considering a plane incident wave, we have found that the total field of the equivalent source is the same as the field scattered by a rough surface obtained by using the conventional small perturbation method (SPM). Particularly for the PEC rough surface, the equivalent source formulation in Eq. (55) is more suited than the conventional

SPM in the calculation of the scattered field, since

1. The incident wave $\overline{E}_i$ is not restricted to be a plane wave as in SPM, therefore it works well at low-grazing angles.

2. The spatial-domain formulation can be used to calculate the near field.

3. The non-averaged complex scattered field in spatial-domain formulation does not use the Fourier integral over the rough surface, therefore it is well-defined.

4. The spatial-domain formulation is computationally efficient, since there is no integration over the spatial frequency as in the convention SPM.

ACKNOWLEDGMENTS

APPENDIX

The integral representation of the dyadic Green's function in unbounded space is given by [7]

$$
\overline{\overline{G}}_1(\bar{r}, \bar{r}') = -\hat{z}\hat{z}\frac{\delta(\bar{r}, \bar{r}')}{k_1^2} + \frac{i}{8\pi^2} \iint dk_x dk_y \frac{1}{k_{1z}}
$$
$$
\cdot \begin{cases} \left[\hat{e}(k_{1z})\hat{e}(k_{1z}) + \hat{h}(k_{1z})\hat{h}(k_{1z})\right] e^{i\bar{k}_1 \cdot (\bar{r}-\bar{r}')} \\ \qquad\qquad\qquad\qquad\qquad\qquad\qquad z > z' \\ \left[\hat{e}(-k_{1z})\hat{e}(-k_{1z}) + \hat{h}(-k_{1z})\hat{h}(-k_{1z})\right] e^{i\overline{K}_1 \cdot (\bar{r}-\bar{r}')} \\ \qquad\qquad\qquad\qquad\qquad\qquad\qquad z < z' \end{cases}
\tag{75}
$$

where

$$
\hat{e}(\pm k_{1z}) = \frac{\hat{x}k_y - \hat{y}k_x}{\sqrt{k_x^2 + k_y^2}}
\tag{76}
$$

$$
\hat{h}(\pm k_{1z}) = \mp\frac{k_{1z}}{k_1\sqrt{k_x^2 + k_y^2}}(\hat{x}k_x + \hat{y}k_y)
$$
$$
+\hat{z}\frac{\sqrt{k_x^2 + k_y^2}}{k_1}
\tag{77}
$$

$$
\bar{k}_1 = k_x\hat{x} + k_y\hat{y} + k_{1z}\hat{z}
\tag{78}
$$

$$\overline{K}_1 = k_x\hat{x} + k_y\hat{y} - k_{1z}\hat{z} \tag{79}$$

$$k_{1z} = \sqrt{k_1^2 - k_x^2 - k_y^2}. \tag{80}$$

REFERENCES

[1] S. O. Rice, "Reflection of electromagnetic waves from slightly rough surface," *Commun. Pure Appl. Math.*, vol. 4, pp. 351–378, 1951.

[2] A. A. Maradudin, "Iterative solutions for electromagnetic scattering by gratings," *J. Opt. Soc. Am.*, vol. 73, no. 6, pp. 759–764, June 1983.

[3] G. S. Agarwal, "Interaction of electromagnetic waves at rough dielectric surface," *Phys. Rev. B*, vol. 15, no. 4, pp. 2371–2383, Feb. 1977.

[4] M. Nieto-Vesperinas, "Depolarization of electromagnetic waves scattered from slightly rough random surfaces: a study by means of the extinctin theorem," *J. Opt. Soc. Am.*, vol. 72, no. 5, pp. 539–547, May 1982.

[5] Y. Zhang, Y. E. Yang, H. Braunisch, and J. A. Kong, "Electromagnetic wave interaction of conducting object with rough surface by hybrid SPM/MoM technique — summary," *J. Electro. Waves Appl.*, vol. 13, pp. 983–984, 1999.

[6] Y. Zhang, Y. E. Yang, H. Braunisch, and J. A. Kong, "Electromagnetic wave interaction of conducting object with rough surface by hybrid SPM/MoM technique," in *Progress in Electromagnetics Research (PIER 22)*, J. A. Kong, Ed., pp. 315–335. EMW Publishing, Cambridge, 1999.

[7] J. A. Kong, *Electromagnetic Wave Theory*, Wiley, New York, second edition, 1990.

[8] S. H. Yueh, R. Kwok, F. K. Li, S. V. Nghiem, and W. J. Wilson, "Polarimetric passive remote sensing of ocean wind vectors," *Radio Sci.*, vol. 29, no. 4, pp. 799–814, July–Aug. 1994.

[9] L. Tsang, C. H. Chan, K. Pak, and H. Sangani, "Monte-Carlo simulation of large-scale problems of random rough surface scattering and applications to grazing incidence with the BMIA/canonical grid method," *IEEE Trans. Antennas Propagat.*, vol. AP-43, no. 2, pp. 851–859, Aug. 1995.

Appendix B

Electromagnetic Wave Interaction of Conducting Object with Rough Surface by
Hybrid SPM/MoM Technique

I   INTRODUCTION

Recently, there has been a great interest of studying the electromagnetic wave scattering from object situated above rough surface [1, 2, 3, 4, 5, 6, 7]. Previously, electromagnetic wave scattering by arbitrarily shaped objects in free space has been well developed using wire [8, 9, 10] and surface-patch model [11, 12, 13, 14, 15, 16, 17, 18]. The theory and numerical approaches associated with object near flat interface of layered medium have also be studied extensively by many researchers [26, 27, 19, 20, 21, 22, 7, 31, 32, 25]. However, the consideration of the interface to be rough surface is a new challenge, and little work has been reported. In theory, the standard MoM can be used to solved unknowns both on object and rough surface [4, 28, 29]. However, the discretization of the rough surface can significantly increase the computational resource compared to calculating the scattering from object alone, therefore little literature has been reported on the study of scattering for full scale gemetry.

In this paper, we present a hybrid SPM/MoM technique to calculate the EM scattering from 3-D conducting object above rough surface. Under the hybrid technique, the Green's function and surface variables are expanded in terms of the surface height function on the mean surface, and the electric integral equations based on the extinction theorem and the surface boundary conditions are decomposed into different orders. Each order of equations represents a scattering problem with the same geometry and different equivalent incident wave, so that it can be solved efficiently by using the dyadic Green's function in layered medium. The separation of solution into different orders also helps us identify and characterize the individual interaction terms between the object and the rough surface.

II   CONFIGURATION AND FORMULATION

Consider an electromagnetic wave $\overline{E}_i(\overline{r})$ incident upon a perfectly conducting object with arbitrary shape S_1 above a rough surface S_r as shown in Fig. 1. The upper space V_1 is air which is specified by ϵ_1 and μ_1, the lower space V_2 is a homogeneous medium and characterized by ϵ_2 and μ_2. The rough surface profile is defined by the surface height function $z = f(\overline{r}'_\perp)$ with mean surface S_o on the x-y plane.
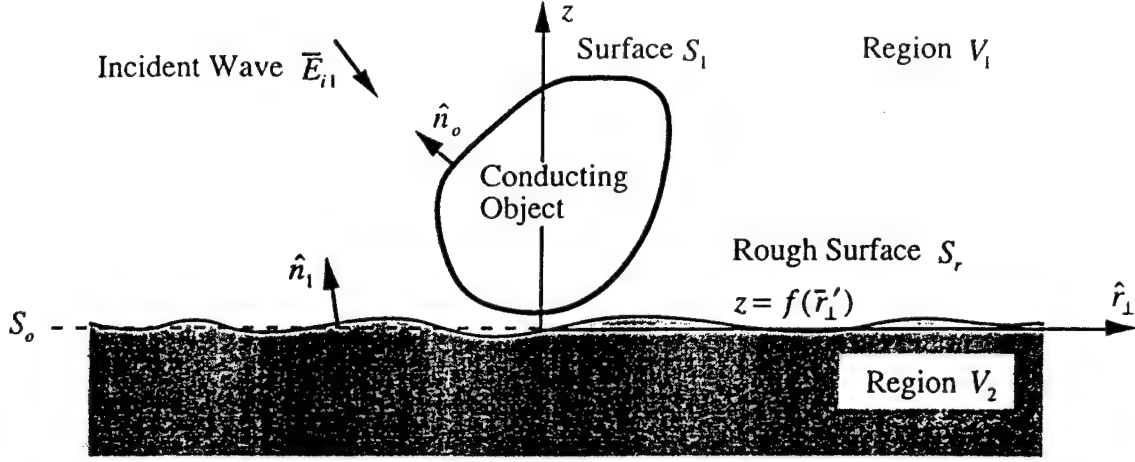
2

Figure 1: Configuration of the problem.

A Electric Field Integral Equations

On the conducting surface, the tangential electric field is zero, thus we can write the integral equation for electric field as following,

for $\bar{r} \in S_1$,

$$\left(\overline{E}_i(\bar{r}) + \iint_{S_o} dS' \left\{ i\omega\mu_1 \overline{\overline{G}}_1(\bar{r}, \bar{r}') \cdot \left[\hat{n}_1(\bar{r}') \times \overline{H}_1(\bar{r}')\right] + \nabla \times \overline{\overline{G}}_1(\bar{r}, \bar{r}') \cdot \left[\hat{n}_1(\bar{r}') \times \overline{E}_1(\bar{r}')\right]\right\}\right.$$
$$\left. + i\omega\mu_1 \iint_{S_1} dS' \overline{\overline{G}}_1(\bar{r}, \bar{r}') \cdot \overline{J}_1(\bar{r}')\right) \times \hat{n}_o(\bar{r}) = 0. \tag{1}$$

By Extinction Theorem, we get,

for $\bar{r} \in V_2$,

$$\overline{E}_i(\bar{r}) \quad + \quad \iint_{S_o} dS' \left\{ i\omega\mu_1 \overline{\overline{G}}_1(\bar{r}, \bar{r}') \cdot \left[\hat{n}_1(\bar{r}') \times \overline{H}_1(\bar{r}')\right] + \nabla \times \overline{\overline{G}}_1(\bar{r}, \bar{r}') \cdot \left[\hat{n}_1(\bar{r}') \times \overline{E}_1(\bar{r}')\right]\right\}$$
$$+ i\omega\mu_1 \iint_{S_1} dS' \overline{\overline{G}}_1(\bar{r}, \bar{r}') \cdot \overline{J}_1(\bar{r}') = 0, \tag{2}$$

and for $\bar{r} \in V_1$,

$$\iint_{S_o} dS' \left\{ i\omega\mu_2 \overline{\overline{G}}_2(\bar{r}, \bar{r}') \cdot \left[\hat{n}_2(\bar{r}') \times \overline{H}_2(\bar{r}')\right] + \nabla \times \overline{\overline{G}}_2(\bar{r}, \bar{r}') \cdot \left[\hat{n}_2(\bar{r}') \times \overline{E}_2(\bar{r}')\right]\right\} = 0, \tag{3}$$

where $\overline{\overline{G}}_1$ and $\overline{\overline{G}}_2$ are dyadic Green's functions in unbounded regions with (ϵ_1, μ_1) and (ϵ_2, μ_2) respectively. The vector $\hat{n}_1(\bar{r}')$ denotes a local normal pointing from rough surface

3

S_r to upper region V_1. The vector $\hat{n}_2(\bar{r}')$ is opposite to $\hat{n}_1(\bar{r}')$, thus $\hat{n}_2(\bar{r}') = -\hat{n}_1(\bar{r}')$. $\overline{E}_1(\bar{r}')$ and $\overline{H}_1(\bar{r}')$ are electric and magnetic fields on the rough surface in region V_1, while $\overline{E}_2(\bar{r}')$ and $\overline{H}_2(\bar{r}')$ are surface fields on rough surface in region V_2. $\overline{J}_1(\bar{r}')$ is the induced surface current on the object. If region V_2 is dielectric, the tangential fields are continuous, thus

$$\hat{n}_1(\bar{r}') \times \overline{H}_1(\bar{r}') = \hat{n}_1(\bar{r}') \times \overline{H}_2(\bar{r}') \equiv \frac{d\bar{r}'_\perp}{dS'\eta_1} \bar{a}(\bar{r}'_\perp), \tag{4}$$

$$\hat{n}_1(\bar{r}') \times \overline{E}_1(\bar{r}') = \hat{n}_1(\bar{r}') \times \overline{E}_2(\bar{r}') \equiv \frac{d\bar{r}'_\perp}{dS'} \bar{b}(\bar{r}'_\perp), \tag{5}$$

where $\bar{a}(\bar{r}'_\perp)$ and $\bar{b}(\bar{r}'_\perp)$ are new surface variables defined on the mean surface S_o, η_1 is the characteristic impedance of upper region and can be written as $\eta_1 = (\mu_1/\epsilon_1)^{1/2}$, and

$$\frac{d\bar{r}'_\perp}{dS'} = \frac{1}{\sqrt{1 + (\partial f(x', y')/\partial x')^2 + (\partial f(x', y')/\partial y')^2}}. \tag{6}$$

With the new surface variables, we can rewrite the integral equations as

$$\left(\overline{E}_i(\bar{r}) + \iint_{S_o} d\bar{r}'_\perp \left\{ ik_1 \overline{\overline{G}}_1(\bar{r}, \bar{r}') \cdot \bar{a}(\bar{r}'_\perp) + \nabla \times \overline{\overline{G}}_1(\bar{r}, \bar{r}') \cdot \bar{b}(\bar{r}'_\perp) \right\} \right.$$
$$\left. + i\omega\mu_1 \iint_{S_1} dS' \overline{\overline{G}}_1(\bar{r}, \bar{r}') \cdot \overline{J}_1(\bar{r}') \right) \times \hat{n}_o(\bar{r}) = 0 \qquad \text{for } \bar{r} \in S_1 \tag{7}$$

,

$$\overline{E}_i(\bar{r}) + \iint_{S_o} d\bar{r}'_\perp \left\{ ik_1 \overline{\overline{G}}_1(\bar{r}, \bar{r}') \cdot \bar{a}(\bar{r}'_\perp) + \nabla \times \overline{\overline{G}}_1(\bar{r}, \bar{r}') \cdot \bar{b}(\bar{r}'_\perp) \right\}$$
$$+ i\omega\mu_1 \iint_{S_1} dS' \overline{\overline{G}}_1(\bar{r}, \bar{r}') \cdot \overline{J}_1(\bar{r}') = 0 \qquad \text{for } \bar{r} \in V_{2,} \tag{8}$$

$$\iint_{S_o} d\bar{r}'_\perp \left\{ ik_2 \frac{\eta_2}{\eta_1} \overline{\overline{G}}_2(\bar{r}, \bar{r}') \cdot \bar{a}(\bar{r}'_\perp) + \nabla \times \overline{\overline{G}}_2(\bar{r}, \bar{r}') \cdot \bar{b}(\bar{r}'_\perp) \right\} = 0 \qquad \text{for } \bar{r} \in V_1. \tag{9}$$

Theoretical, given the rough surface S_r and the perfectly conducting object surface profiles S_1, the unknown surface variables $\bar{a}(\bar{r}'_\perp)$, $\bar{b}(\bar{r}'_\perp)$ and the induced current $\bar{J}_1(\bar{r}')$ can be solved from Eqs. (7–9). For the special case in which the interface is flat, the surface variables $\bar{a}(\bar{r}'_\perp)$ and $\bar{b}(\bar{r}'_\perp)$ are in the horizontal plane and the local coordinate $\bar{r}'$ can be replaced by $\bar{r}'_\perp$ in the dyadic Green's functions $\overline{\overline{G}}_1(\bar{r}, \bar{r}')$ and $\overline{\overline{G}}_2(\bar{r}, \bar{r}')$.

B *Expansion of Green's Function and Surface Variables*

We assume that the rough surface height is small. Therefore the scalar Green's function in region α (where $\alpha = 1, 2$) can be expanded in terms of surface height function $f(\bar{r}'_\perp)$ on the mean surface S_o,

$$
\begin{aligned}
g_\alpha(\bar{r}, \bar{r}') &= g_\alpha\left(\bar{r}, \bar{r}'_\perp + \hat{z} f(\bar{r}'_\perp)\right) \\
&= \sum_{m=0}^{\infty} \frac{1}{m!} \frac{\partial^m}{\partial z'^m} g_\alpha\left(\bar{r}, \bar{r}'_\perp\right) f^m(\bar{r}'_\perp) = \sum_{m=0}^{\infty} \frac{1}{m!} \frac{\partial^m}{\partial z^m} g_\alpha\left(\bar{r}, \bar{r}'_\perp\right) \left(-f(\bar{r}'_\perp)\right)^m, \quad (10)
\end{aligned}
$$

in which the following property of the Green's function has been used

$$
\frac{\partial}{\partial z'} g_\alpha\left(\bar{r}, \bar{r}'\right) = -\frac{\partial}{\partial z} g_\alpha\left(\bar{r}, \bar{r}'\right). \tag{11}
$$

Thus the dyadic Green's function can be written as

$$
\overline{\overline{G}}_\alpha(\bar{r}, \bar{r}') = \left(\overline{\overline{I}} + \frac{1}{k^2} \nabla\nabla\right) g_\alpha(\bar{r}, \bar{r}') = \sum_{m=0}^{\infty} \frac{1}{m!} \left(-f(\bar{r}'_\perp)\right)^m \frac{\partial^m}{\partial z^m} \overline{\overline{G}}_\alpha\left(\bar{r}, \bar{r}'_\perp\right). \tag{12}
$$

Consequently, the surface variables and induced current can be written as the series expansions as following

$$
\overline{J}_1(\bar{r}') = \sum_{m=0}^{\infty} \overline{J}_1^{(m)}(\bar{r}'), \tag{13}
$$

$$
\bar{a}(\bar{r}'_\perp) = \sum_{m=0}^{\infty} \left[\bar{a}_\perp^{(m)}(\bar{r}'_\perp) + \hat{z} a_z^{(m)}(\bar{r}'_\perp)\right], \tag{14}
$$

$$
\bar{b}(\bar{r}'_\perp) = \sum_{m=0}^{\infty} \left[\bar{b}_\perp^{(m)}(\bar{r}'_\perp) + \hat{z} b_z^{(m)}(\bar{r}'_\perp)\right]. \tag{15}
$$

In Eqs. (14) and (15), the separation of the z-components for the surface variables $\bar{a}$ and $\bar{b}$ allows the unknown surface variables become only the tangential components since the z-components of the m-th order can be expressed in terms of the tangential components of lower order $(m-1)$ as we will see below. By the definition of $\bar{a}$ and $\bar{b}$ as in Eqs. (4) and (5), we get the following identities,

$$
\hat{n}_1(\bar{r}'_\perp) \cdot \bar{a}(\bar{r}'_\perp) = 0, \tag{16}
$$

$$
\hat{n}_1(\bar{r}'_\perp) \cdot \bar{b}(\bar{r}'_\perp) = 0, \tag{17}
$$

where

$$
\hat{n}_1(\bar{r}'_\perp) = \frac{\nabla'_\perp f(\bar{r}'_\perp) + \hat{z}}{|\nabla'_\perp f(\bar{r}'_\perp) + \hat{z}|} \tag{18}
$$

5

Substituting the series expressions of $\bar{a}$ and $\bar{b}$ as in Eqs. (14) and (15) into Eqs. (16) and (17) respectively, and considering that $\partial f(\bar{r}'_\perp)/\partial x'$ and $\partial f(\bar{r}'_\perp)/\partial y'$ are in the same order as $f(\bar{r}'_\perp)$, we then get the m-th order z-components of surface variables $\bar{a}$ and $\bar{b}$ in terms of the $(m-1)$-th order tangential components,

$$
\begin{cases}
a_z^{(m)}(\bar{r}'_\perp) = \nabla'_\perp f(\bar{r}'_\perp) \cdot \bar{a}_\perp^{(m-1)}(\bar{r}'_\perp), \\
b_z^{(m)}(\bar{r}'_\perp) = \nabla'_\perp f(\bar{r}'_\perp) \cdot \bar{b}_\perp^{(m-1)}(\bar{r}'_\perp).
\end{cases}
\tag{19}
$$

Substituting the series expression of dyadic Green's functions as in Eq. (12) and the surface variables $\bar{a}$ and $\bar{b}$ as in Eqs. (14) and (15) into the integral equations (7-9), we get the n-th order equations in terms of the surface height function $f(\bar{r}'_\perp)$ as following.

C   The n-th Order Equations

$$
\left(\overline{E}_i^{(n)}(\bar{r}) + \iint_{S_o} d\bar{r}'_\perp \left\{ ik_1 \overline{\overline{G}}_1(\bar{r}, \bar{r}'_\perp) \cdot \bar{a}_\perp^{(n)}(\bar{r}'_\perp) + \nabla \times \overline{\overline{G}}_1(\bar{r}, \bar{r}'_\perp) \cdot \bar{b}_\perp^{(n)}(\bar{r}'_\perp) \right\} \right.
$$
$$
\left. + i\omega\mu_1 \iint_{S_1} dS' \overline{\overline{G}}_1(\bar{r}, \bar{r}') \cdot \overline{J}_1^{(1)}(\bar{r}') \right) \times \hat{n}_o(\bar{r}) = 0 \qquad \text{for } \bar{r} \in S_1, \tag{20}
$$

$$
\overline{E}_i^{(n)}(\bar{r}) \; + \; \iint_{S_o} d\bar{r}'_\perp \left\{ ik_1 \overline{\overline{G}}_1(\bar{r}, \bar{r}'_\perp) \cdot \bar{a}_\perp^{(n)}(\bar{r}'_\perp) + \nabla \times \overline{\overline{G}}_1(\bar{r}, \bar{r}'_\perp) \cdot \bar{b}_\perp^{(n)}(\bar{r}'_\perp) \right\}
$$
$$
+ i\omega\mu_1 \iint_{S_1} dS' \overline{\overline{G}}_1(\bar{r}, \bar{r}') \cdot \overline{J}_1^{(1)}(\bar{r}') = 0 \qquad \text{for } \bar{r} \in V_2, \tag{21}
$$

$$
\overline{E}_{i2}^{(n)}(\bar{r}) + \iint_{S_o} d\bar{r}'_\perp \left\{ ik_2 \frac{\eta_2}{\eta_1} \overline{\overline{G}}_2(\bar{r}, \bar{r}'_\perp) \cdot \bar{a}_\perp^{(n)}(\bar{r}'_\perp) + \nabla \times \overline{\overline{G}}_2(\bar{r}, \bar{r}'_\perp) \cdot \bar{b}_\perp^{(n)}(\bar{r}'_\perp) \right\} = 0 \qquad \text{for } \bar{r} \in V_1, \tag{22}
$$

where for $n = 0$,

$$
\overline{E}_i^{(0)}(\bar{r}) = \overline{E}_i(\bar{r}), \tag{23}
$$
$$
\overline{E}_{i2}^{(0)}(\bar{r}) = 0, \tag{24}
$$

for $n \geq 1$,

$$
\overline{E}_i^{(n)}(\bar{r}) = \sum_{m=1}^{n} \frac{1}{m!} \iint d\bar{r}'_\perp \, [-f(\bar{r}'_\perp)]^m \frac{\partial^m}{\partial z^m}
$$
$$
\left\{ ik_1 \overline{\overline{G}}_1(\bar{r}, \bar{r}'_\perp) \cdot \bar{a}_\perp^{(n-m)}(\bar{r}'_\perp) + \nabla \times \overline{\overline{G}}_1(\bar{r}, \bar{r}'_\perp) \cdot \bar{b}_\perp^{(n-m)}(\bar{r}'_\perp) \right\}
$$

6

$$+ \sum_{m=1}^{n} \frac{1}{(m-1)!} \iint d\bar{r}'_\perp \left[-f(\bar{r}'_\perp)\right]^{m-1} \frac{\partial^{m-1}}{\partial z^{m-1}}$$

$$\left\{ i k_1 \overline{\overline{G}}_1 \left(\bar{r}, \bar{r}'_\perp\right) \cdot \hat{z} \left[\nabla'_\perp f(\bar{r}'_\perp) \cdot \bar{a}_\perp^{(n-m)}(\bar{r}'_\perp)\right] \right.$$

$$\left. + \nabla \times \overline{\overline{G}}_1 \left(\bar{r}, \bar{r}'_\perp\right) \cdot \hat{z} \left[\nabla'_\perp f(\bar{r}'_\perp) \cdot \bar{b}_\perp^{(n-m)}(\bar{r}'_\perp)\right] \right\}, \tag{25}$$

$$\overline{E}_{i2}^{(n)}(\bar{r}) = \sum_{m=1}^{n} \frac{1}{m!} \iint d\bar{r}'_\perp \left[-f(\bar{r}'_\perp)\right]^{m} \frac{\partial^{m}}{\partial z^{m}}$$

$$\left\{ i k_2 \frac{\eta_2}{\eta_1} \overline{\overline{G}}_2 \left(\bar{r}, \bar{r}'_\perp\right) \cdot \bar{a}_\perp^{(n-m)}(\bar{r}'_\perp) + \nabla \times \overline{\overline{G}}_2(\bar{r}, \bar{r}'_\perp) \cdot \bar{b}_\perp^{(n-m)}(\bar{r}'_\perp) \right\}$$

$$+ \sum_{m=1}^{n} \frac{1}{(m-1)!} \iint d\bar{r}'_\perp \left[-f(\bar{r}'_\perp)\right]^{m-1} \frac{\partial^{m-1}}{\partial z^{m-1}}$$

$$\left\{ i k_2 \frac{\eta_2}{\eta_1} \overline{\overline{G}}_2 \left(\bar{r}, \bar{r}'_\perp\right) \cdot \hat{z} \left[\nabla'_\perp f(\bar{r}'_\perp) \cdot \bar{a}_\perp^{(n-m)}(\bar{r}'_\perp)\right] \right.$$

$$\left. + \nabla \times \overline{\overline{G}}_2(\bar{r}, \bar{r}'_\perp) \cdot \hat{z} \left[\nabla'_\perp f(\bar{r}'_\perp) \cdot \bar{b}_\perp^{(n-m)}(\bar{r}'_\perp)\right] \right\}. \tag{26}$$

Comparing the zeroth order ($n = 0$) integral equations with Eqs. (7-9) for flat interface ($f(\bar{r}'_\perp) = 0$), we found that they are the same except adding a superscript (0) to the surface variables $\bar{a}_\perp$ and $\bar{b}_\perp$ and the induced current $\overline{J}_1$. Therefore, the solutions $\bar{a}_\perp^{(0)}$, $\bar{b}_\perp^{(0)}$ and $\overline{J}_1^{(0)}$ for the zeroth order equations should be the same as the ones for Eqs. (7-9) in which the rough surface is considered to be flat. For the higher order equations ($n \geq 1$), we found that they are also in the same form as the zeroth order equations, except for the substitution of $\overline{E}_i$ by $\overline{E}_i^{(n)}$, and the additional "source" term $\overline{E}_{i2}^{(n)}$ in the lower region. Therefore we only need to know how to solve the zeroth order equations, i.e. the equations for object on a flat interface.

Since the equations of any order are equivalent the ones for flat interface, they can be rewritten by introducing the dyadic Green's function for layered media. The advantage for this approach is avoiding solving surface unknowns $\bar{a}_\perp^{(n)}$ and $\bar{b}_\perp^{(n)}$ on interface, but only need to solved the induced current $\overline{J}_1^{(n)}$ on the conducting body. Therefore both the computational time and memory can be dramatically saved.

D *Application to Non-penetrable Rough Surface*

Without losing the generality, we consider the rough surface to be non-penetrable. In this case the zeroth order electric field integral equation (EFIE) can be written as

$$\hat{n}_o(\bar{r}) \times \left(\overline{E}_i^{(0)}(\bar{r}) + \overline{E}_r^{(0)}(\bar{r}) + i\omega\mu_1 \int_{S_1} dS' \overline{\overline{G}}_L(\bar{r}, \bar{r}') \cdot \overline{J}_1^{(0)}(\bar{r}') \right) = 0 \qquad \text{for } \bar{r} \in S_1, \qquad (27)$$

and the n-th order ($n \geq 1$) EFIE can be written as

$$\hat{n}_o(\bar{r}) \times \left(\overline{E}_i^{(n)}(\bar{r}) + \overline{E}_r^{(n)}(\bar{r}) + i\omega\mu_1 \int_{S_1} dS' \overline{\overline{G}}_L(\bar{r}, \bar{r}') \cdot \overline{J}_1^{(n)}(\bar{r}') \right) = 0 \qquad \text{for } \bar{r} \in S_1, \qquad (28)$$

where

$$
\begin{aligned}
\overline{E}_i^{(n)}(\bar{r}) &= \sum_{m=1}^{n} \frac{1}{m!} \iint d\bar{r}'_\perp \, [-f(\bar{r}'_\perp)]^m \frac{\partial^m}{\partial z^m} \left\{ ik_1 \overline{\overline{G}}_1 (\bar{r}, \bar{r}'_\perp) \cdot \bar{a}_\perp^{(n-m)}(\bar{r}'_\perp) \right\} \\
&\quad + \sum_{m=1}^{n} \frac{1}{(m-1)!} \iint d\bar{r}'_\perp \, [-f(\bar{r}'_\perp)]^{m-1} \frac{\partial^{m-1}}{\partial z^{m-1}} \\
&\qquad \left\{ ik_1 \overline{\overline{G}}_1 (\bar{r}, \bar{r}'_\perp) \cdot \hat{z} \left[\nabla'_\perp f(\bar{r}'_\perp) \cdot \bar{a}_\perp^{(n-m)}(\bar{r}'_\perp) \right] \right\},
\end{aligned}
\qquad (29)
$$

and the dyadic Green's function for conducting interface is

$$\overline{\overline{G}}_L(\bar{r}, \bar{r}') = \overline{\overline{G}}_1(\bar{r}, \bar{r}') - \overline{\overline{G}}_1(\bar{r}, (\overline{\overline{I}} - 2\hat{z}\hat{z}) \cdot \bar{r}') \cdot (\overline{\overline{I}} - 2\hat{z}\hat{z}), \qquad (30)$$

where $\overline{\overline{G}}_1$ is the dyadic Green's function in unbounded medium of region V_1.

The surface field $\bar{a}_\perp$ of lower order can be obtained from the lower order scattered field from object and equivalent source. For example, the first order surface variable $\bar{a}_\perp^{(1)}$ can be calculated by using the solution of the zeroth order induced current $\overline{J}_1^{(0)}$ and the incident and reflected magnetic fields in absence of the object,

$$\bar{a}_\perp^{(0)}(\bar{r}'_\perp) = \eta_1 \hat{z} \times \left(\overline{H}_{i1}(\bar{r}'_\perp) + \overline{H}_{r1}(\bar{r}'_\perp) + \int_{S_1} dS'' \nabla' \times \overline{\overline{G}}_L(\bar{r}'_\perp, \bar{r}'') \cdot \overline{J}_1^{(0)}(\bar{r}'') \right). \qquad (31)$$

The higher order ($n \geq 2$) surface variable $\bar{a}_\perp^{(n)}$ can be obtained similarly but involving much more manipulation.

Up to the first order, the total returned field can be written as

$$\overline{E}_s(\bar{r}) = \overline{E}_r(\bar{r}) + \overline{E}_b(\bar{r}) + \overline{E}_c(\bar{r}) + \overline{E}_d(\bar{r}), \qquad (32)$$

where

$$\overline{E}_b(\bar{r}) = i\omega\mu_1 \int_{S_1} dS' \overline{\overline{G}}_L(\bar{r}, \bar{r}') \cdot \overline{J}_1^{(0)}(\bar{r}'), \qquad (33)$$

$$\overline{E}_c(\bar{r}) = \overline{E}_i^{(1)}(\bar{r}) + \overline{E}_r^{(1)}(\bar{r}), \qquad (34)$$

$$\overline{E}_d(\bar{r}) = i\omega\mu_1 \int_{S_1} dS' \overline{\overline{G}}_L(\bar{r}, \bar{r}') \cdot \overline{J}_1^{(1)}(\bar{r}'). \qquad (35)$$
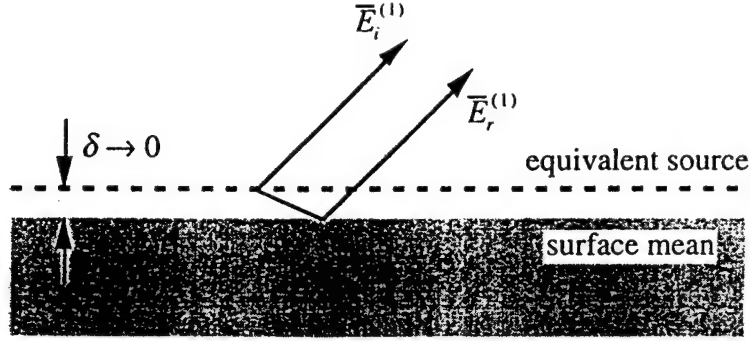
8

Figure 2: Radiation and reflection of the equivalent source.

and

$$\begin{aligned}
\overline{E}_i^{(1)}(\bar{r}) &= -ik_1 \iint d\bar{r}'_\perp f(\bar{r}'_\perp) \frac{\partial}{\partial z} \overline{\overline{G}}_1(\bar{r}, \bar{r}'_\perp) \cdot \bar{a}_\perp^{(0)}(\bar{r}'_\perp) \\
&\quad + ik_1 \iint d\bar{r}'_\perp \overline{\overline{G}}_1(\bar{r}, \bar{r}'_\perp) \cdot \hat{z} \left[\nabla'_\perp f(\bar{r}'_\perp) \cdot \bar{a}_\perp^{(0)}(\bar{r}'_\perp) \right].
\end{aligned} \tag{36}$$

In Eq. (32), the $\overline{E}_r(\bar{r})$ is simply the reflected field from the flat interface in absence of conducting object. In the expression of $\overline{E}_b(\bar{r})$ as in Eq. (33), the induced current $\overline{J}_1^{(0)}$ is obtained by solving the integral equation (27) with layered Green's function, therefore the returned field $\overline{E}_b(\bar{r})$ includes all interactions between object and flat interface. The $\overline{E}_c(\bar{r})$ as in Eq. (34) is the sum of radiation field from the "equaivalent source" and its reflection are illustrated in Fig. 2. The reflected field of the equivalent source can be obtained by writing unbounded dyadic Green's function in the integral form as in Appendix A, thus the radiation field of the equivalent source $\overline{E}_i^{(1)}$ is repressed as the sum of plane waves. By knowing the Fresnel reflection coefficient of each plane wave component, it is easy to write the reflected field $\overline{E}_r^{(1)}$ by multiplying R^{TE} and R^{TM} to the reflected TE and TM waves respectively. For non-penetrable surface $R^{TE} = -1$ and $R^{TM} = 1$, thus we find

$$\overline{E}_r^{(1)}(\bar{r}) = \overline{E}_i^{(1)}(\bar{r}). \tag{37}$$

Therefore the return field due to the equivalent source is simply

$$\overline{E}_c(\bar{r}) = 2\overline{E}_i^{(1)}(\bar{r}). \tag{38}$$

It can also be shown that the returned field $\overline{E}_c(\bar{r})$ as in Eq. (38) is the same as the first order SPM solution for conducting rough surface if we let the induced current $\overline{J}_1^{(0)} = 0$ when evaluating the surface field $\bar{a}_\perp^{(0)}(\bar{r}'_\perp)$ in Eq. (31). Therefore, we call the return field $\overline{E}_c(\bar{r})$ to be the "incoherent" returned field from rough surface under the influence of the object. The returned

9

field $\overline{E}_d(\bar{r})$ is the radiation field of the first order induced current $\overline{J}_1^{(1)}$ excited by the "incoherent" field $\overline{E}_c(\bar{r})$. Since the layered Green's function are used to calculate the induced current $\overline{J}_1^{(1)}$ and its radiation field, therefore the returned field $\overline{E}_d(\bar{r})$ includes all multiple interactions between object and conducting interface.

III *Numerical Results*

In the numerical simulation, a horizontal conducting cylinder along x-axis with 2.0λ in length and 1.0λ in diameter is considered. The distance between the bottom of the cylinder and the mean height of conducting rough surface is 0.1λ so that large interaction between object and rough surface can be involved. A rough surface with well-known Gaussian power spectrum is used for the validation with the standard method of moment (MoM). The size of the rough surface is 15.0λ by 15.0λ. The deviation and correlation length of the rough surface are $\sigma = 0.03\lambda$ and $l = 1.0\lambda$ respectively. The incident wave $\overline{E}_i$ is tapered and formed as the summation of plane waves with Gaussian-shaped footprint on the mean surface. The tapered incident wave satisfies Maxwell's equations and minimizes the edge effect in numerical calculations. The factor g, which is used to control the beam width of the tapered wave is $g = 3.0\lambda$, so that the incident electric field density on the rough surface drops $1/e$ at $|\bar{r}'_\perp| = 3.0\lambda$.

In the numerical calculation, the radar cross section (RCS) is defined as

$$RCS = \lim_{r \to \infty} 4\pi r^2 \frac{|E_s(\theta, \phi)|^2}{|E_o(\theta_i, \phi_i)|^2}, \tag{39}$$

where E_o is the maximum magnitude of tapered incident electric field on the mean surface S_o. For monostatic (backscattering) RCS, the scattering angles $\theta = \theta_i$ and $\phi = \phi_i$. In the numerical simulation for bistatic RCS, we let the scattering θ angle be $40°$ and vary the azimuthal angle ϕ from $0°$ to $360°$, hence $\phi = 0°$ is the backscattering direction. For monostatic RCS simulation, the incident $\bar{k}_i$ vector remains in the $x - z$ plane and the incident angle θ_i varies from $0°$ to $90°$.

The plots shown in Fig. 3 and Fig. 4 are bistatic RCSs for individual terms of Eq. (32) for TE and TM incident waves respectively. The plot labeled as E_r is the reflected field of the incident tapered wave from flat interface in absence of object. A peak of co-pol component of E_r appears in the specular direction $\phi = 180°$ as expected. The plot labeled as E_b is the returned field as in Eq. (33). The E_c plot is evaluated by using Eq. (34), and the E_d plot is calculated from Eq. (35). It can be found that most of the energy of the "incoherent" field E_c concentrates in the forward scattering direction. The fields shown in the E_b plot are the scattering from object excited by fields E_i and E_r, while the secondary scattering field in the E_d plot is the returned field from the

10

object excited by the "incoherent" field E_c from the rough surface. We note that the cross-pol returned fields VH and HV in the backscattering direction are zero in the E_b plot. This is due to the symmetrical property of the geometry and the incident wave. The secondary returned fields of cross-pol VH and HV in the plot E_d are no longer zero in the backscattering direction due to the asymmetry of the "incoherent" field E_c. The "incoherent" field E_c as well as the secondary returned field E_d from the object are both proportional to the surface height function $f(\bar{r}'_\perp)$ of the rough surface. It can be easily checked that both E_c and E_d become zero when the surface height function is zero.

The sum of the four terms $E_r + E_b + E_c + E_d$ as in Eq. (32) is the total returned field up to the first order as shown in Fig. 5 and Fig. 6 for TE and TM incident wave respectively. The bistatic RCS for the total returned field with TE incident wave are compared with standard MoM results. In the MoM simulation, both the rough surface and the conducting object are discretized and the surface unknowns are solved together by using the conjugate gradient algorithm. The plots in the top columns in Fig. 5 and Fig. 6 show the bistatic RCS of the zeroth order solution using the hybrid technique and the standard MoM solution. Good agreement is found in the comparison of the results. The co-pol VV of the zeroth order solution matches better than the co-pol HH, since the TE incident wave may induce unnegligible currents on the front and back edges of the rough surface, which may add more returns for the MoM result. This edge effect can be minimized if the TM wave is used as incident as we can see in Fig.6. In the simulations as shown in Fig. 5 and 6, a single rough surface with Gaussian power spectrum is used. The deviation of the surface height is $\sigma = 0.03\lambda$ and the correlation length is $l = 1.0\lambda$. The results also show good agreement in comparison of the results obtained by hybrid technique with the standard MoM. It is noted that the curves are no long symmetrical with respect to the incident plane when the surface is rough.

The Monte Carlo simulation results with 100 realizations are shown in Fig. 7 and Fig. 8 for TE and TM incident waves respectively. The rough surfaces with power law spectrum are generated and they are independent to each other. The power law spectrum function is $W(k) = a_o/k^4$ which more closely represents ocean state, where k is the spatial wavenumber of the rough surface and $a_o = 0.008/2\pi$ which corresponds to the amplitude used for Durden-Vesecky spectrum [35]. The higher cut-off spatial wavenumber k_h is chosen to be $k_h = 2.5k_1$ which corresponds the band width for $1/5\lambda_1$ spatial resolution of sampling on the rough surface, where k_1 and λ_1 are electromagnetic wavenumber and wavelength of incident wave respectively. The lower cut-off spatial wavenumber

11

	MoM	Hybrid
Number of unknowns	17,252	972
CPU time		
single bistatic	1 hr 14 min	5 min
100 realizations	5 days (estimated)	40 min
single monostatic	23 hr	3 hrs 15 min
100 monostatic	3 months (estimated)	17 hrs

Table 1: Comparison of computational effort for standard MoM and hybrid codes, respectively.

k_l is chosen according to the deviation of rough surface height using the following relation

$$\sigma^2 = \int W(k)d^2k = \pi a_o \left(\frac{1}{k_l^2} - \frac{1}{k_h^2} \right). \tag{40}$$

In Fig. 7 and Fig. 8, the deviations of rough surface $k_1\sigma = 0.1$, 0.2, 0.4 correspond to the lower cut-off spatial wavenumbers $k_l = 0.6131$, 0.3137, $0.1578k_1$ respectively. It is shown that the Monte Carlo simulation converges with respect to the number of realizations, and the averaged cross-pol RCSs increase with the deviation of rough surface at a wide range of scattering angles.

Fig. 9 and 10 show the Monte Carlo simulation of monostatic (backscattering) RCS for TE and TM incident waves respectively. Here 100 rough surfaces with power law spectrum and $k_1\sigma = 0.4$ are used. The backscattering direction varies from $\theta = 0°$ to $\theta = 90°$ with 45 steps in between. The azimuthal angle ϕ remains 0 degree. We note that the cross-pol VH and HV are significant in the presence of rough surface. Analytically the cross-pols should be zero for the geometry we are considering when the surface is flat. We note that the non-zero cross-pols for flat surface shown in the solid lines are produced numerically. The changes of co-pol monostatic RCS due to the rough surface can be found at some scattering angles. At small grazing angle, the rough surface effect on co-pol backscattering RCS is not significant.

The computational performance of the hybrid technique and the standard MoM are listed in Table 1 for the testing cases discussed above, in which the Alpha 21164 machine with 2MB L2 Cache, 500 MHz clock rate and 1GB RAM are used for the simulation. The CPU time for monostatic simulations are based on 45 incident angles.

12

IV CONCLUSION

This paper presents a hybrid technique of SPM and MoM for EM scattering from object above rough surface. With the expansion of the Green's function and surface variables in terms of the surface height function on the mean surface, the electric field integral equations are decomposed into different orders. The equations of each order represent the EM scattering problem with the same object above the mean surface (flat) and different incident field from equivalent source which can be evaluated by using lower order solutions. The equivalence of the flat surface problem allows us to use the dyadic Green's function for layered media, so that we do not need to solve for tangential fields on the rough surface, leaving only unknowns on the conducting object. Comparison with standard MoM, this hybrid technique demonstrates a dramatic increase in computational efficiency without losing the accuracy. The separation of return field into the sum of individual interaction terms allows us to identify the coherent and incoherent returned field, therefore the rough surface affect can be quantitatively characterized.

ACKNOWLEDGMENT

APPENDIX A

The integral representation of dyadic Green's function in unbounded space is

$$\overline{\overline{G}}_1(\bar{r}, \bar{r}') = -\hat{z}\hat{z}\frac{\delta(\bar{r}, \bar{r}')}{k_1^2}$$

$$+ \begin{cases} \frac{i}{8\pi^2} \iint dk_x dk_y \frac{1}{k_{1z}} \left[\hat{e}(k_{1z})\hat{e}(k_{1z}) + \hat{h}(k_{1z})\hat{h}(k_{1z}) \right] e^{i\bar{k}_1 \cdot (\bar{r} - \bar{r}')} & z > z', \\ \frac{i}{8\pi^2} \iint dk_x dk_y \frac{1}{k_{1z}} \left[\hat{e}(-k_{1z})\hat{e}(-k_{1z}) + \hat{h}(-k_{1z})\hat{h}(-k_{1z}) \right] e^{i\overline{K}_1 \cdot (\bar{r} - \bar{r}')} & z < z', \end{cases} \quad (41)$$

where

$$\hat{e}(\pm k_{1z}) = \frac{\hat{x}k_y - \hat{y}k_x}{\sqrt{k_x^2 + k_y^2}}, \tag{42}$$

$$\hat{h}(\pm k_{1z}) = \mp \frac{k_{1z}}{k_1\sqrt{k_x^2 + k_y^2}}(\hat{x}k_x + \hat{y}k_y) + \hat{z}\frac{\sqrt{k_x^2 + k_y^2}}{k_1}, \tag{43}$$

$$\bar{k}_1 = k_x\hat{x} + k_y\hat{y} + k_{1z}\hat{z} \tag{44}$$

13

$$\overline{K}_1 = k_x\hat{x} + k_y\hat{y} - k_{1z}\hat{z} \tag{45}$$

$$k_{1z} = \sqrt{k_1^2 - k_x^2 - k_y^2} \tag{46}$$

References

[1] T. Dogaru, L. Carlin, B. L. Merchant, and C. F. Lee, "Electromagnetic scattering and detection of mines near a rough air-ground interface," *Proc. SPIE - Int. Soc. Opt. Eng. (USA)*, vol. 3079, p. 704-15, April 1997.

[2] Jin-Seob Kang and Weng Cho Chew, "Time-domain distorted Born iterative method for imaging buried dielectric cylinder in underground lossy media," *IEEE Antennas and Propagation Society International Symposium. 1996·Digest*, p. 3 vol. viii+2252, p. 2156-9 vol. 3, 1996.

[3] D.J. Daniels, "Surface-penetrating radar," *Electronics & Communication Engineering Journal*, vol. 8, no. 4, p. 165-82, Aug. 1996.

[4] K. O'Neill, R. F. Lussky, Jr., and K. D. Paulsen, "Scattering from a metallic object embedded near the randomly rough surface of a lossy dielectric," *IEEE Transactions on Geoscience and Remote Sensing*, vol. 34, no. 2, p. 367-6, March 1996.

[5] A. Helaly, A. Sebak, and L. Shafai, "Scattering by a buried conducting object of general shape at low frequencies," *IEE Proceedings H (Microwaves, Antennas and Propagation)*, vol. 138, no. 3, p. 213-18, June 1991.

[6] K. Tajima and S.-I. Iiguchi, "Analysis of electromagnetic wave scattered from cylinders buried in the ground," *Electronics and Communications in Japan*, Part 1, (Communications), vol. 70, no. 5, p. 86-94, May 1987.

[7] P. G. Cottis and J. D. Kanellopoulos, "Scattering from a conducting cylinder above a lossy medium," *International Journal of Electronics*, vol. 65, no. 5, p. 1031-8, Nov. 1988.

[8] J. H. Richmond, "A wire-grid model for scattering by conducting bodies," *IEEE Trans. Antennas Propagat.*, vol. AP-14, No. 6, p. 782-6, Nov. 1966.

[9] E. K. Miller and F. J. Deadrick, "Some computational aspects of thin-wire modeling," in *Numerical and Asymptotic Techniques in Electromagnetics*, R. Mittra, Ed. ch. 4, Springer-Verlag, New York, 1975.

[10] K. S. H. Lee, L. Marin, and J. P. Castillo, "Limitations of wire-grid modeling of a closed surface," IEEE trans. Electromagn. Compat., vol. EMC-18, no. 3, p. 123-29, Aug. 1976.

[11] D. L. Knepp and J. Goldhirsh, "Numerical analysis of electromagnetic radiation properties of smooth conducting bodies of arbitrary shape," *IEEE Trans. Antennas Propagat.*, vol. AP-20, no. 3, p. 383-8, May 1972.

[12] N. C. Albertsen, J. E. Hansen, and N. E. Jensen, "Computation of radiation from wire antennas on conducting bodies," *IEEE Trans. Antennas Propagat.*, vol. AP-22, no. 2, p. 200-6, Mar. 1974.

[13] N. N. Wang, J. H. Richmond, and M. C. Gilreath, "Simusoidal reaction formulation for radiation and scattering from conducting surfaces," *IEEE Trans. Antennas Propagat.*, vol. AP-23, no. 3, p. 376-82, May 1975.

[14] E. H. Newman and D. M. Pozar, "Electromagnetic modeling of composite wire and surface geometries," *IEEE Trans. Antennas Propagat.*, vol. AP-26, no. 6, p. 784-9, Nov. 1978.

[15] A. Sankar and T. C. Tong, "Current computation on complex structures by finite element method," *Electron. Lett.*, vol. 11, no. 20, p. 481-2, Oct. 1975.

[16] J. J. H. Wang, "Numerical analysis of three-dimensional arbitrarily-shaped conducting scatterers by trilateral surface cell modelling," *Radio Sci.*, vol. 13, no. 6, p. 947-52, Nov.-Dec. 1978.

[17] J. Singh and A. T. Adams, "A non rectangular patch model for scattering from surfaces," *IEEE Trans. Antennas Propagat.*, vol. AP-27, no. 4, p. 531-5, July 1979.

[18] S. M. Rao, D. R. Wilton, and A. W. Glisson, "Elecctromagnetic scattering by surfaces of arbitrary shape," *IEEE Trans. Antennas Propagat.*, vol. AP-30, no. 3, p. 409-18, May 1982.

[19] C. M. Butler, "Current induced on a conducting strip which resides on the planar interface between two semi-infinite half-spaces," *IEEE Transactions on Antennas and Propagation*, vol. AP-32, no. 3, p. 226-31, March 1984.

[20] C. M. Butler, X. B. Xu, and A. W. Glisson, "Current induced on a conducting cylinder located near the planar interface between two semi-infinite half-spaces," *IEEE Transactions on Antennas and Propagation*, vol. AP-33, no. 6, p. 616-24, June 1985.

[21] X. B. Xu and C. M. Butler, "Current induced by TE excitation on a conducting cylinder located near the planar interface between two semi-infinite half-spaces," *IEEE Transactions on Antennas and Propagation*, vol. AP-34, no. 7, p. 880-90, July 1986.

[22] X. B. Xu and C. M. Butler, "Scattering of TM excitation by coupled and partially buried cylinders at the interface between two media," *IEEE Transactions on Antennas and Propagation*, vol. AP-35, no. 5, p. 529-38, May 1987.

[23] K.A. Michalski and D. Zheng, "Electromagnetic scattering and radiation by surfaces of arbitrary shape in layered media. I. Theory," *IEEE Transactions on Antennas and Propagation*, vol. 38, no. 3, p. 335-44, March 1990.

[24] K.A. Michalski and D. Zheng, "Electromagnetic scattering and radiation by surfaces of arbitrary shape in layered media. II. Implementation and results for contiguous half-spaces," *IEEE Transactions on Antennas and Propagation*, vol. 38, no. 3, p. 345-52, March 1990.

[25] S. F. Mahmoud, S. M. Ali, and J. R. Wait, "Electromagnetic scattering from a buried cylindrical inhomogeneity inside a lossy Earth," *Radio Science*, vol. 16, no. 6, p. 1285-98, Nov.-Dec. 1981.

[26] A. Q. Howard, "The electromagnetic fields of a subterranean cylindrical inhomogeneity excited by a line source," *Geophysics*, vol. 37, no. 6, p. 975-84, Dec. 1972.

[27] J. R. Parry and S. H. Ward "Electromagnetic scattering from cylinders of arbitrary cross-section in a conductive half-space," *Geophysics*, vol. 36, no. 1, p. 67-100, Feb. 1971.

[28] Leung Tsang, Guifu Zhang, and Kyung Pak, "Detection of a buried object under a single random rough surface with angular correlation function in EM wave scattering," *Microwave and Optical Technology Letters*, vol. 11, no. 6, p. 300-4, 20 April 1996.

[29] J. Ripoll, A. Madrazo, and M. Nieto-Vesperinas, "Scattering of electromagnetic waves from a body over a random rough surface," *Optics Communications*, vol. 142, no. 4-6, p. 173-8, 15 Oct. 1997.

[30] J. A. Kong, "*Electromagnetic Wave Theory*,", 2nd ed., John Wiley & Sons, New York, 1990.

[31] K.A. Michalski and D. Zheng, "Electromagnetic scattering and radiation by surfaces of arbitrary shape in layered media. I. Theory," *IEEE Transactions on Antennas and Propagation*, vol.38, no.3, p. 335-44, March 1990.

[32] K.A. Michalski and D. Zheng, "Electromagnetic scattering and radiation by surfaces of arbitrary shape in layered media. II. Implementation and results for contiguous half-spaces," *IEEE Transactions on Antennas and Propagation*, vol.38, no.3, p. 345-52, March 1990.

[33] Tie Jun Cui, W. Wiesbeck, and A. Herschlein, "Electromagnetic scattering by multiple three-dimensional scatterers buried under multilayered media. I. Theory," *IEEE Transactions on Geoscience and Remote Sensing*, vol. 36, no. 2, p. 526-34, March 1998.

[34] Tie Jun Cui, W. Wiesbeck, and A. Herschlein, "Electromagnetic scattering by multiple three-dimensional scatterers buried under multilayered media. II. Numerical," *IEEE Transactions on Geoscience and Remote Sensing*, vol. 36, no. 2, p. 535-46, March 1998.

[35] S. P. Durden and J. F. Vesecky, "A physical radar cross-section model for a wind-driven sea with swell," *IEEE J. Oceanic Eng.*, vol. 10, p. 445-51, 1985.
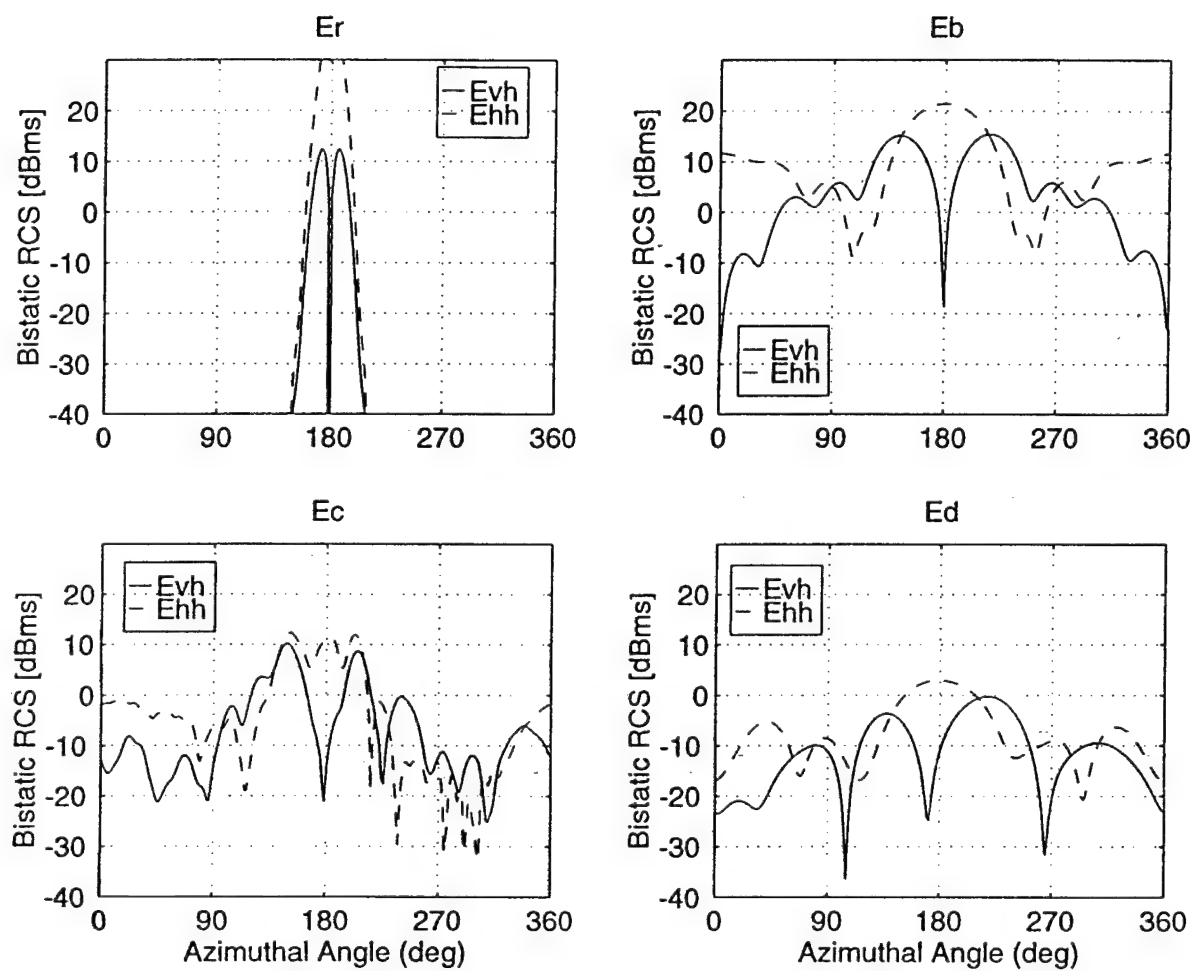
Figure 3: Bistatic RCS of individual terms for TE incident wave.
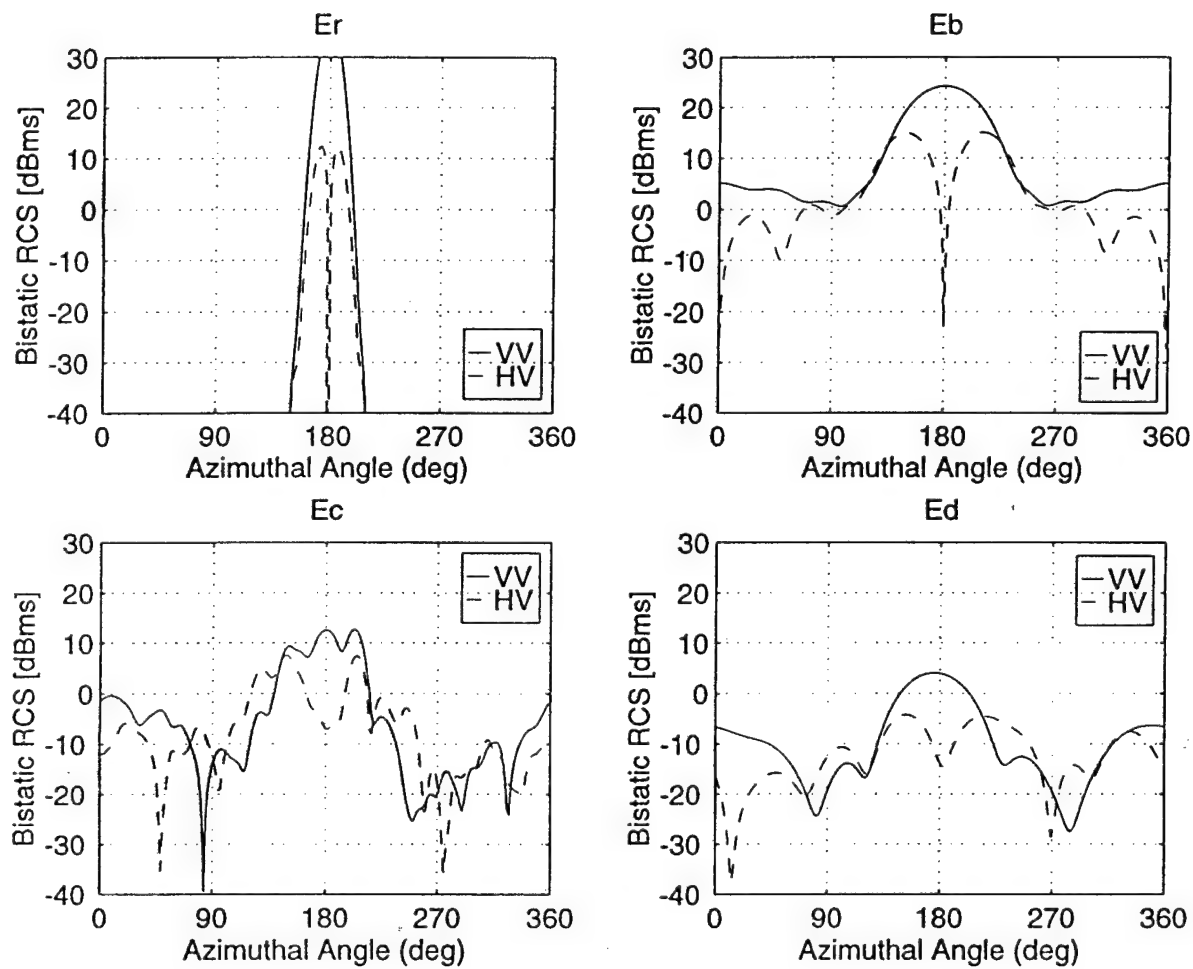
Figure 4: Bistatic RCS of individual terms for TM incident wave.
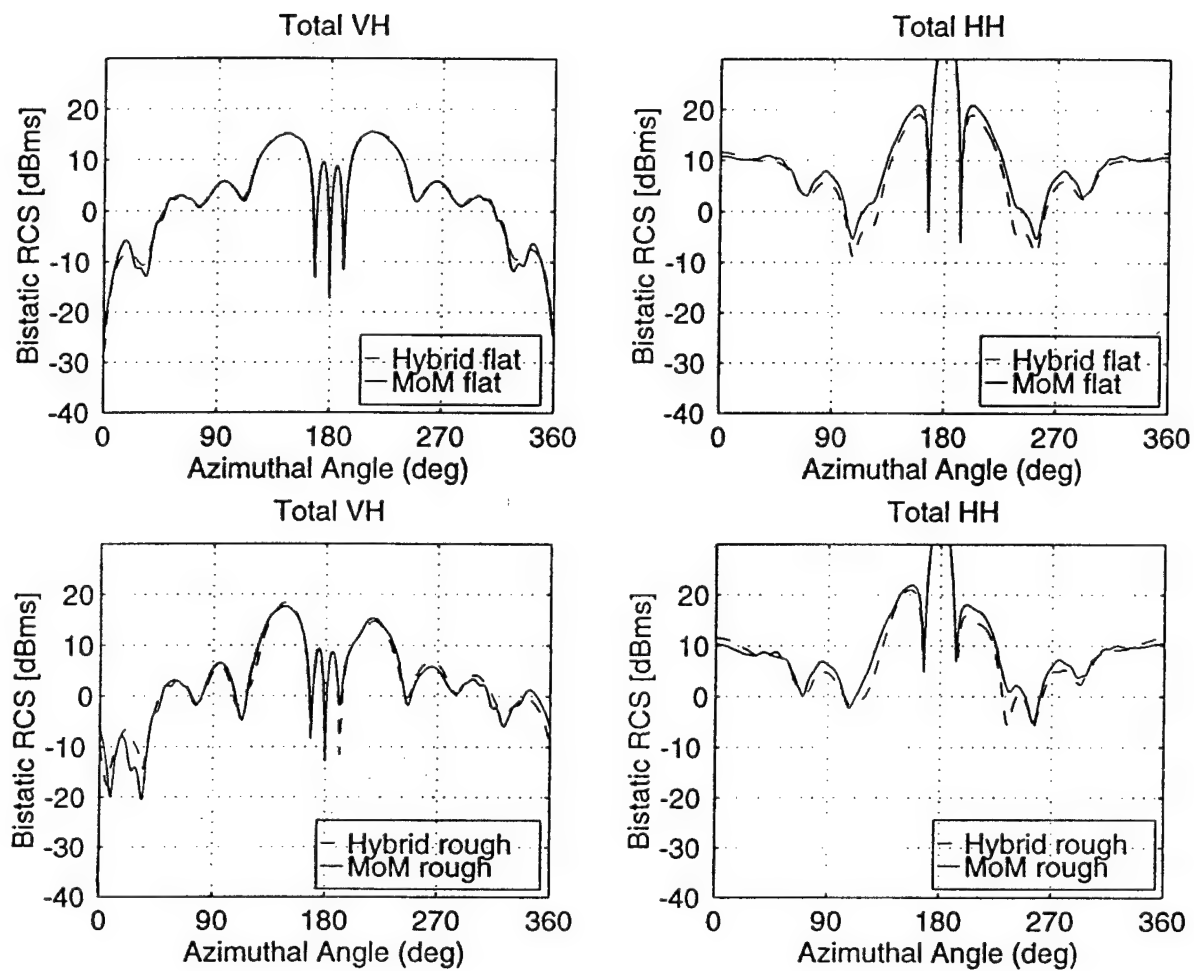
Figure 5: Bistatic RCS of the total returned field $E_r + E_b + E_c + E_d$ for TE incident wave.
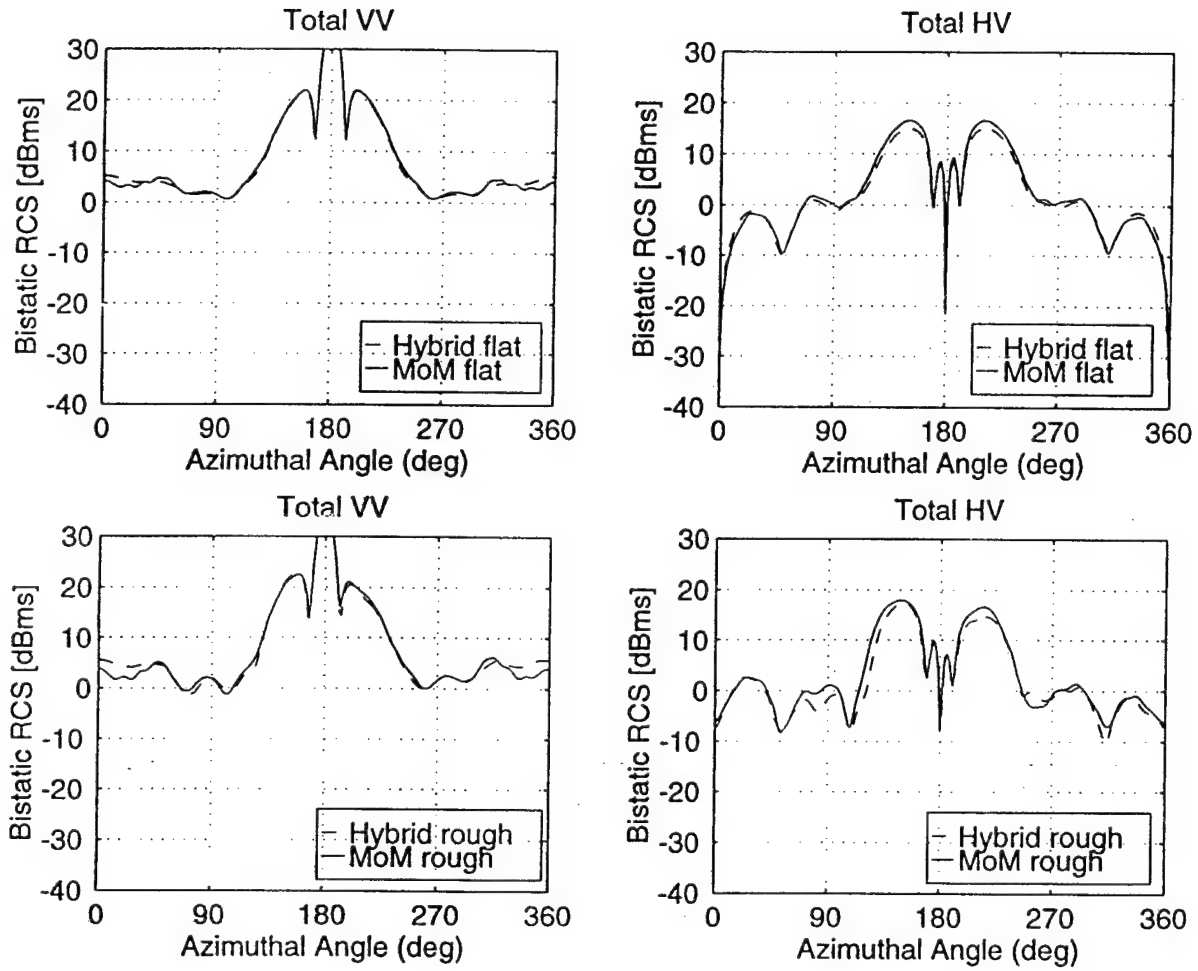
Figure 6: Bistatic RCS of the total returned field $E_r + E_b + E_c + E_d$ for TM incident wave.
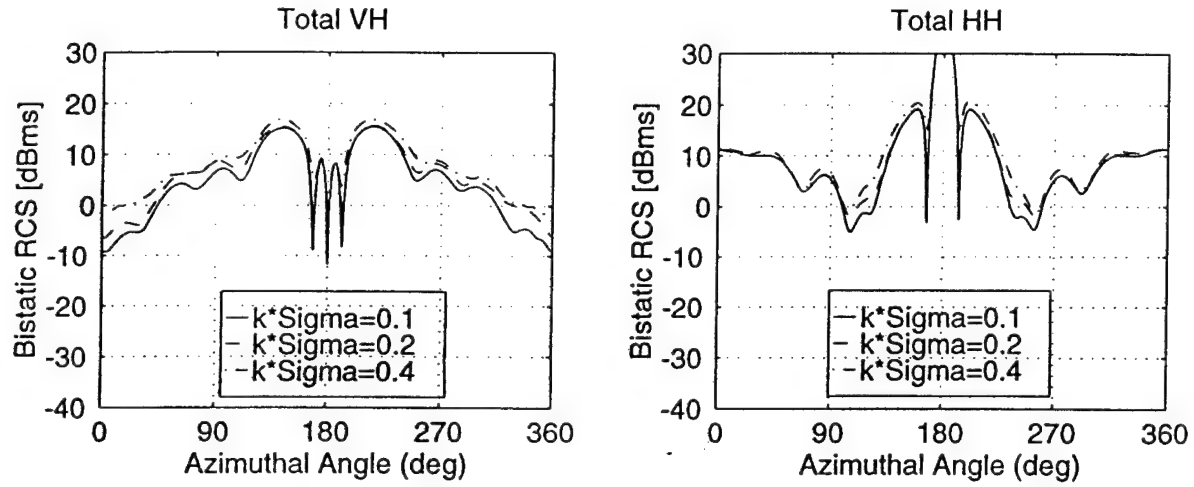
Figure 7: Monte Carlo simulation of bistatic RCS of the total returned field $E_r + E_b + E_c + E_d$ for TE incident wave.
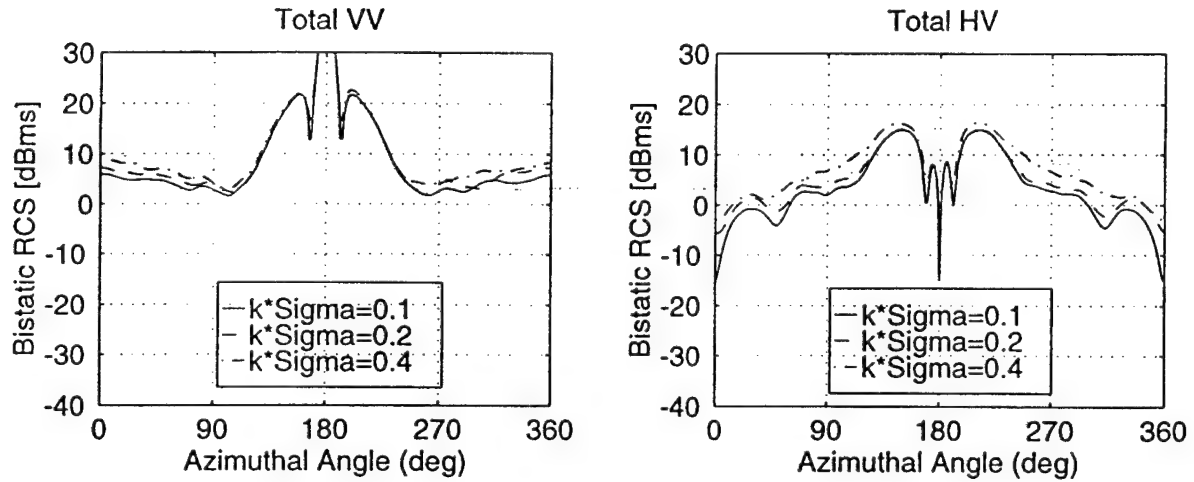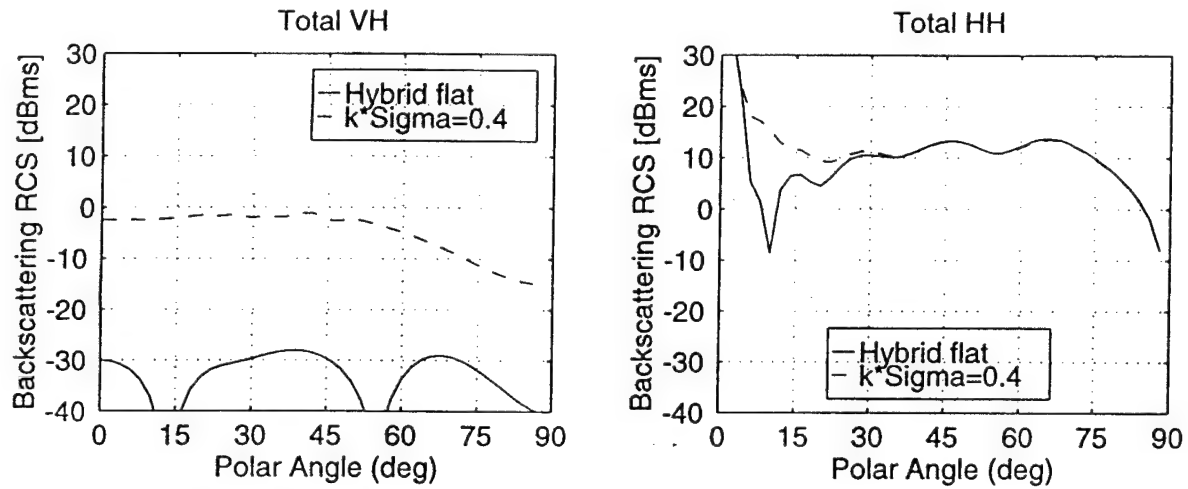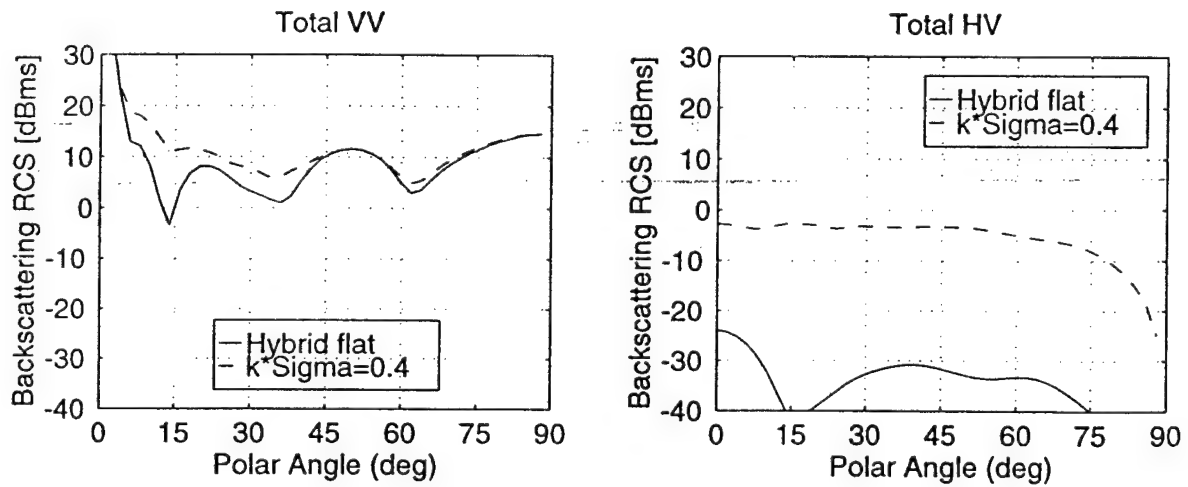

Figure 8: Monte Carlo simulation of bistatic RCS of the total returned field $E_r + E_b + E_c + E_d$ for TM incident wave.

Figure 9: Monte Carlo simulation of monostatic RCS of the total returned field $E_r + E_b + E_c + E_d$ for TE incident wave.

Figure 10: Monte Carlo simulation of monostatic RCS of the total returned field $E_r + E_b + E_c + E_d$ for TM incident wave.

Appendix C

Tapered Wave with Dominant Polarization State for All Angles of Incidence

Abstract

Typical applications of the method of moments (MoM) to rough surface 3-D electromagnetic scattering require a truncation of the surface considered and call for a tapered incident wave. It is shown how such wave can be constructed as a superposition of plane waves, avoiding problems near both normal and grazing incidence and providing clean footprints and clear polarization at all angles of incidence. The proposed special choice of polarization vectors removes an irregularity at the origin of the wavenumber space and leads to a least squared error property of the wave. Issues in the application to 3-D scattering from an object over a rough surface are discussed. Approximate 3-D scalar and vector tapered waves which can be evaluated without resorting to any numerical integrations are derived and important limitations to the accuracy and applicability of these approximations are pointed out.

Keywords

I. INTRODUCTION

Recent years have seen major advances in the development of fast MoM solvers for 3-D scattering of electromagnetic vector waves from rough surfaces [1], [2], [3], [4], [5], [6], [7], [8]. Efforts are now also being directed towards inclusion of objects situated in the neighborhood of the rough surface [9], [10], [11], [12]. Since the problem of scattering from an object next to a rough surface is computationally complex, 2-D investigations are also of importance [13], [14], [15], [16], [17], [18], [19], [20]. The 3-D case with or without objects is aimed at by the present paper.

The methods employed usually require a truncation of the rough surface because of limited computing resources which leads to erroneous results due to artificial edge diffraction when ideal plane waves are used to excite the system. The tapered wave concept is based on providing an illumination for the numerical simulation that resembles the plane wave case to be modeled closely at the center of the scattering scenario (including a particular arbitrary polarization) while its intensity becomes negligibly small upon approaching the artificially introduced edges of the rough surface. Thus unwanted edge effects due to the primary incident wave are avoided and the proper normalization of computed scattering coefficients allows a meaningful comparison with the ideal plane wave case; near-field quantities such as current distributions induced near the center of the tapered wave are also expected to be similar.

Furthermore, the tapered wave should be constructed in such a way that it satisfies the Maxwell equations without any approximation. This helps to increase the confidence in the results obtained from the in general rather complex MoM simulation codes. It should also be possible to substitute it for a plane wave of arbitrary polar and azimuthal angles of incidence without loss of polarization and degradation of tapering.

The above requirements led us to revise and modify the tapered wave found in the open literature which is based on a superposition of plane waves.

II. Superposition of Plane Waves

Consider a homogeneous, isotropic medium with real wavenumber k and wave impedance η. Then the following superposition of a 2-D spectrum of plane waves is an exact solution to the Maxwell equations and represents a wave incident upon the x-y plane from $z > 0$:

$$\overline{E}_i(\overline{r}) = \int\limits_{-\infty}^{\infty} d\overline{k}_\rho \, e^{i(\overline{k}_\rho \cdot \overline{\rho} - k_z z)} \, \psi(\overline{k}_\rho) \, \overline{e}(\overline{k}_\rho) \tag{1}$$

$$\overline{H}_i(\overline{r}) = \int\limits_{-\infty}^{\infty} d\overline{k}_\rho \, e^{i(\overline{k}_\rho \cdot \overline{\rho} - k_z z)} \, \frac{\psi(\overline{k}_\rho)}{\eta} \, \overline{h}(\overline{k}_\rho) \tag{2}$$

where

$$\overline{r} = \overline{\rho} + \hat{z} \, z \tag{3}$$

$$\overline{k}_\rho = \hat{x} \, k_x + \hat{y} \, k_y \tag{4}$$

and

$$k_z = k_z(k_\rho) = \begin{cases} \sqrt{k^2 - k_\rho^2} & 0 \le k_\rho \le k \\ -i\sqrt{k_\rho^2 - k^2} & k_\rho > k \end{cases} \tag{5}$$

The spectrum ψ carries the information on the shape of the footprint (defined as the distribution of the magnitude in the x-y plane) of the incident field and also on the direction of incidence. It is assumed to be centered about

$$\overline{k}_{i\rho} = \hat{x} \, k_{ix} + \hat{y} \, k_{iy} \tag{6}$$

$$= k \, \sin\theta_i \, (\hat{x} \, \cos\phi_i + \hat{y} \, \sin\phi_i) \tag{7}$$

where θ_i and ϕ_i are the polar and azimuthal angles of incidence of the central plane wave and—*pars pro toto*—of the tapered wave. In an application the central plane wave would

coincide with the plane wave which was replaced by the tapered wave in the numerical simulation. Details about the functional dependence of ψ are given in Section III.

The polarization vectors $\overline{e}$ and $\overline{h}$ are of the general form

$$\overline{e}(\overline{k}_\rho) = e_h(\overline{k}_\rho)\,\hat{h}(\overline{k}_\rho) + e_v(\overline{k}_\rho)\,\hat{v}(\overline{k}_\rho) \tag{8}$$

and

$$\overline{h}(\overline{k}_\rho) = e_v(\overline{k}_\rho)\,\hat{h}(\overline{k}_\rho) - e_h(\overline{k}_\rho)\,\hat{v}(\overline{k}_\rho) \tag{9}$$

The notations

$$\hat{h}(\overline{k}_\rho) = \begin{cases} \hat{x}\,\sin\phi_i - \hat{y}\,\cos\phi_i & k_\rho = 0 \\ \frac{1}{k_\rho}\left(\hat{x}\,k_y - \hat{y}\,k_x\right) & k_\rho > 0 \end{cases} \tag{10}$$

and

$$\hat{v}(\overline{k}_\rho) = \begin{cases} \hat{x}\,\cos\phi_i + \hat{y}\,\sin\phi_i & k_\rho = 0 \\ \frac{k_z}{k\,k_\rho}\left(\hat{x}\,k_x + \hat{y}\,k_y\right) + \hat{z}\,\frac{k_\rho}{k} & k_\rho > 0 \end{cases} \tag{11}$$

are found in similar form in [21], [22]. The chosen definitions for $k_\rho = 0$ take care of the special case of a normally incident pure plane wave. $k_\rho > k$ corresponds to evanescent waves (Section III) and the horizontal part of $\hat{v}(\overline{k}_\rho)$ is imaginary in this case. It is important to note the discontinuity of $\hat{h}$ and $\hat{v}$ at $\overline{k}_\rho = 0$; both *unit* vectors change sign when crossing the origin along a straight line in the $\overline{k}_\rho$ plane.

The general superposition integrals (1), (2) were stated similarly in [23], [7]; however, only normal incidence is considered in what follows there. If e_h and e_v in (8), (9) are set to constants then (1), (2) specializes to the tapered wave used in [1], [2], [4], [9], [8], with a particular spectrum ψ briefly discussed in Section III. Problems with this tapered wave encountered near the grazing incidence (for discussion and references see Section III) and near the normal incidence (Section IV) motivated our formulation of a different kind of tapered wave, especially with respect to the polarization vectors.

III. Amplitude Spectrum

If the polarization vector $\overline{e}$ on the right-hand side of (1) is replaced by a scalar constant then the resulting integral

$$\mathcal{E}_i(\overline{r}) = e_i \int\limits_{-\infty}^{\infty} d\overline{k}_\rho\, e^{i(\overline{k}_\rho \cdot \overline{\rho} - k_z z)}\, \psi(\overline{k}_\rho) \tag{12}$$

is the plane-wave representation of a scalar wave satisfying the scalar Helmholtz equation and ψ can be identified with the well-known angular spectrum in scalar diffraction theory [24], [25]. Thus by obtaining ψ via 2-D Fourier transformation and making sure that $\overline{e}$ and $\overline{h}$ vary only moderately over the spatial frequency range where ψ is not negligible, arbitrary footprints of the vector tapered wave can be approximated. [The mentioned requirement leads to a problem with the tapering in [1], [2], [4], [9], [8] near normal incidence (Section IV).] The information on the direction of incidence of the tapered wave is included by shifting ψ in the k_x-k_y plane to be centered about $\overline{k}_{i\rho}$. The prescribed footprint itself is fixed with respect to angle of incidence.

A Gaussian-shaped footprint (Fig. 1) whose amplitude at $\rho = g$ is down to $1/e$ times the level at the center is implemented by choosing

$$\psi(\overline{k}_\rho) = \frac{g^2}{4\pi}\, e^{-\frac{g^2}{4}\left|\overline{k}_\rho - \overline{k}_{i\rho}\right|^2} \tag{13}$$

A pure plane wave is described by $\psi(\overline{k}_\rho) = \delta(\overline{k}_\rho - \overline{k}_{i\rho})$, or $g \to \infty$ in (13). It should be pointed out that—as is well known from signal theory—among all footprints of given finite energy and width, the Gaussian leads to the smallest bandwidth (for the appropriate definition of space and frequency domain widths) which is desirable for synthesis.

Spectral components with $k_\rho > k$ are the amplitudes of plane waves that travel along the x-y plane and are evanescent for $z > 0$. Their inclusion makes it possible to synthesize a given footprint near or at grazing incidence.

The spectrum in [1], [2], [4], [9], [8] is given as a 2-D Fourier integral that needs to be evaluated numerically. It cannot be used near grazing incidence where the field distribution in the x-y plane becomes highly oscillatory. Its continued use is rooted in its close relation to a scalar tapered wave employed previously [26], [27]. The latter wave, on the other hand, goes back to a popular incident field introduced by E. I. Thorsos [28] who—for the 2-D case—derived it as an approximation to a summation of plane waves, accurate for sufficiently *small* angles of incidence θ_i (also employed in [29], [30], [15], [31], [32], [33].) The limitations of the 2-D scalar Thorsos wave at low grazing angles were analyzed and discussed in [34], [35]. The bound in the resolvability criterion discussed by Ngo and Rino [36] also becomes significant at low grazing angles. The recommendation for the 3-D vector case is to start over and simply use the spectrum given by (13) which has the additional

benefit of being given in closed form. Taking advantage of the functional dependence of the Gaussian spectrum, an option in the 2-D case is to use path deformation techniques to speed up the evaluation of the exact expression for the incident field [37]. In the 3-D case we can at least band-limit the integration to a disk about $\overline{k}_\rho = \overline{k}_{i\rho}$ within which the spectrum exhibits a significant magnitude (disk radius a few multiples of $2/g$). This leads to an approximation of the original incident field which satisfies Maxwell's equations exactly. The derivation of approximate non-Maxwellian 3-D tapered waves which can be evaluated without integration is discussed in Section VI.

IV. POLARIZATION

In order to construct a wave that is both reliably tapered and clearly polarized, for all angles of incidence, we suggest choosing the polarization of the individual plane wave components as follows:

$$e_h(\overline{k}_\rho) = \overline{e}_i \cdot \hat{h}(\overline{k}_\rho) \tag{14}$$

$$e_v(\overline{k}_\rho) = \overline{e}_i \cdot \hat{v}(\overline{k}_\rho) \tag{15}$$

with the polarization vector of the central plane wave

$$\overline{e}_i = \overline{e}(\overline{k}_{i\rho}) = E_h \, \hat{h}(\overline{k}_{i\rho}) + E_v \, \hat{v}(\overline{k}_{i\rho}) \tag{16}$$

Hence, in dyadic notation

$$\overline{e}(\overline{k}_\rho) = \overline{e}_i \cdot \left[\hat{h}(\overline{k}_\rho) \, \hat{h}(\overline{k}_\rho) + \hat{v}(\overline{k}_\rho) \, \hat{v}(\overline{k}_\rho) \right] \tag{17}$$

and

$$\overline{h}(\overline{k}_\rho) = \overline{e}_i \cdot \left[\hat{v}(\overline{k}_\rho) \, \hat{h}(\overline{k}_\rho) - \hat{h}(\overline{k}_\rho) \, \hat{v}(\overline{k}_\rho) \right] \tag{18}$$

The dominant polarization state of the tapered wave is then determined by the choice of E_h and E_v in (16) which describe the (in general elliptical) polarization of the central plane wave.

Note that with this choice the integrands of (1), (2) are continuous at $\overline{k}_\rho = 0$ [as follows from Section VI, we have in fact analyticity throughout the k_x-k_y plane excluding the circle $|\overline{k}_\rho| = k$ provided an analytic spectrum such as (13) is used; at $|\overline{k}_\rho| = k$ the integrands are still continuous] as opposed to the tapered wave in [1], [2], [4], [9], [8]. The latter wave

is characterized by the choice $e_h(\overline{k}_\rho) = E_h$ and $e_v(\overline{k}_\rho) = E_v$, leading to rapidly varying polarization vectors $\overline{e}$ and $\overline{h}$ near $\overline{k}_\rho = 0$. For the near normal incidence case this will violate the basic assumption of the footprint design technique described in Section III. When examined numerically it is found that the approximation of a prescribed, e.g., Gaussian, footprint is poor; the result for normal incidence shows the largest intensity along a ring in the x-y plane rather than at the center (Fig. 2). This effect is also evident from the following consideration: For a spectrum that satisfies $\psi(\overline{k}_\rho) = \psi(-\overline{k}_\rho)$ it can be shown that, for $E_v = 0$, we have $\overline{E}_i(\overline{\rho}, z) = -\overline{E}_i(-\overline{\rho}, z)$ with the consequence $\overline{E}_i(\overline{\rho} = 0, z) = 0$ for all z [Fig. 2(a)]. Similarly, for $E_h = 0$ it is found that $\hat{z} \times \overline{E}_i(\overline{\rho}, z) = -\hat{z} \times \overline{E}_i(-\overline{\rho}, z)$ and $\hat{z} \times \overline{E}_i(\overline{\rho} = 0, z) = 0$ [Fig. 2(b)]. Other problems are leakage of the intensity to larger radii than expected (Fig. 2) and the non-existence of a clear polarization of the wave. By using (17), (18) these problems are removed (Fig. 3). [The 101×101 tapered wave field values for the results in Fig. 2, 3, 6, and 7 were calculated using a summation of 128×128 plane waves with a 2-D DFT sampling of the $\overline{k}_\rho$ space. The spectrum after [1], [2], [4], [9], [8] was calculated using a 2-D FFT algorithm. The horizontal periodicity of the fields in the space domain was in all cases $30\,\lambda$, i.e., twice the surface length shown in the figures, in order to avoid aliasing (Section V).]

The tapered wave with polarization vectors (17), (18) is optimal in a least squared error sense. Consider a vector field

$$\overline{\mathcal{E}}_i(\overline{r}) = \overline{e}_i \int\limits_{-\infty}^{\infty} d\overline{k}_\rho \, e^{i(\overline{k}_\rho \cdot \overline{\rho} - k_z z)} \, \psi(\overline{k}_\rho) \tag{19}$$

obtained by multiplying a scalar tapered wave with the constant polarization vector $\overline{e}_i$ as in (16). This field combines the desirable properties of well defined polarization and controllable tapering. (Note that $|\overline{\mathcal{E}}_i(\overline{\rho}, z = 0)|/|\overline{e}_i|$ corresponds to the prescribed footprint as discussed in Section III and illustrated in Fig. 1.) However, the field defined by (19) is not a valid electric field because in general $\nabla \cdot \overline{\mathcal{E}}_i \neq 0$. We can therefore ask for a permissible wave of form (1) with the same spectrum ψ that approximates $\overline{\mathcal{E}}_i$ as close as possible. Defining

$$S(z) = \int\limits_{-\infty}^{\infty} d\overline{\rho} \, \left| \overline{E}_i(\overline{\rho}, z) - \overline{\mathcal{E}}_i(\overline{\rho}, z) \right|^2 \tag{20}$$

we find from Parseval's theorem for 2-D Fourier transforms

$$S(z) = 4\pi^2 \int\limits_{-\infty}^{\infty} d\overline{k}_\rho \left| e^{-ik_z z} \psi(\overline{k}_\rho) \right|^2 \left| \overline{e}(\overline{k}_\rho) - \overline{e}_i \right|^2 \tag{21}$$

To minimize S for all z note that

$$\left| \overline{e}(\overline{k}_\rho) - \overline{e}_i \right|^2 = \left| \overline{e}(\overline{k}_\rho) - \overline{e}_i \cdot \left[\hat{h}(\overline{k}_\rho)\,\hat{h}(\overline{k}_\rho) + \hat{v}(\overline{k}_\rho)\,\hat{v}(\overline{k}_\rho) \right] \right|^2 + \left| \overline{e}_i \cdot \hat{k}(\overline{k}_\rho) \right|^2 \tag{22}$$

where

$$\hat{k}(\overline{k}_\rho) = \hat{v}(\overline{k}_\rho) \times \hat{h}(\overline{k}_\rho) = \frac{1}{k} \left(\hat{x}\,k_x + \hat{y}\,k_y - \hat{z}\,k_z \right) \tag{23}$$

Hence, (17) yields the optimal $\overline{E}_i$ and the minimum S_m is given by

$$S_m(z) = 4\pi^2 \int\limits_{-\infty}^{\infty} d\overline{k}_\rho \left| e^{-ik_z z} \psi(\overline{k}_\rho) \right|^2 \left| \overline{e}_i \cdot \hat{k}(\overline{k}_\rho) \right|^2 \tag{24}$$

It is emphasized that we refer to $S(z)$ and $S_m(z)$ as "errors" only in the familiar mathematical sense. The purpose of comparing with the non-Maxwellian field $\overline{\mathcal{E}}_i(\overline{r})$ is to uniquely identify a functional dependence of $\overline{e}(\overline{k}_\rho)$ which can be expected to guarantee tapering and a dominant polarization state of the total field (both as prescribed). In other words, $\overline{\mathcal{E}}_i(\overline{r})$ which is ideal with respect to tapering and polarization is projected into the space of waves constructed as 2-D superpositions of plane waves, lending its desirable properties to an exact solution of Maxwell's equations.

To illustrate the approximation behavior numerically we computed the relative root mean squared (RMS) error

$$\sqrt{ S(0) \left/ \int\limits_{-\infty}^{\infty} d\overline{\rho} \left| \overline{\mathcal{E}}_i(\overline{\rho}, 0) \right|^2 \right. } = \frac{\sqrt{2\,S(0)/\pi}}{g\,|\overline{e}_i|} \tag{25}$$

where $\overline{\mathcal{E}}_i$ is formed using the spectrum (13), for varying tapering parameter g and incidence angle θ_i (in Fig. 4 and 5 contour levels decrease monotonically for fixed θ_i and increasing g and are separated by 2 dB steps.) The results in Fig. 4 for the tapered wave in [1], [2], [4], [9], [8] exhibit the previously mentioned problems near normal and grazing incidence. It is noted that for intermediate angles θ_i and larger g the error can be smaller than 1% (-20 dB) and that the approximation behavior for horizontally polarized [Fig. 4(a)] and vertically polarized [Fig. 4(b)] plane wave components is similar. For the tapered

wave composed according to (17) and (13) and for horizontal polarization [Fig. 5(a)] the error is small everywhere and practically independent of θ_i. For vertical polarization [Fig. 5(b)] the error grows larger towards grazing but does not exceed moderate levels. The fact that approximating a vertically polarized plane wave near grazing incidence is harder can be understood intuitively by noting that the energy flow of the tapered wave has to "bend down" in order to form the exponentially space-limited footprint, a requirement in contradiction with maintaining a vertical polarization state. However, Fig. 5(b) shows that the optimal approximation finds a reasonable compromise. [For the results shown in Fig. 4 and 5 the RMS error was evaluated using a Gauss-Legendre quadrature over a surface of size $7\,g \times 7\,g$, choosing in both dimensions 5 times the number of sampling points obtained when rounding $7\,g/\lambda$ to the nearest integer. 128×128 plane waves were summed to space domain fields with horizontal periodicity of $7\,g$. The tapering parameter g was changed in steps of $\lambda/2$ and the angle of incidence θ_i in steps of 5°.]

Another important property of the wave based on (17) is found from (18) by noting that

$$\overline{e}_i \cdot \overline{h}(\overline{k}_\rho) = \overline{h}(\overline{k}_\rho) \cdot \overline{e}_i = \overline{e}_i \cdot \left[\hat{v}(\overline{k}_\rho)\,\hat{h}(\overline{k}_\rho) - \hat{h}(\overline{k}_\rho)\,\hat{v}(\overline{k}_\rho) \right] \cdot \overline{e}_i = 0 \qquad (26)$$

and thus, according to (2), $\overline{e}_i \cdot \overline{H}_i(\overline{r}) = 0$. The total magnetic field of the tapered wave is everywhere perpendicular to the electric field of the central plane wave.

It is remarked that this is reminiscent of the tapered wave (given for the case of normal incidence only) in [23], designed to have no y component of the magnetic field. Setting $\overline{e}_i = -\hat{y}$ in (17), (18) or, more conveniently, in (34), (37) of Section VI and comparing to (7), (8) in [23] it is found that the waves are different. In particular, the polarization vectors in [23] are unbounded as $|\overline{k}_\rho| \to k$ while being analytic throughout the k_x-k_y plane excluding the circle $|\overline{k}_\rho| = k$.

The tapered wave given previously by Tran and Maradudin [38] and for the case of vertical polarization employed in [3], [5], [6]—when generalized to arbitrary azimuthal angle of incidence and cast into our formalism—turns out to be somewhat related. Their magnetic polarization vector for horizontal polarization is collinear to (18) when $E_v = 0$. However, it is normalized to unit length and the magnetic polarization vector for vertical polarization is then obtained by taking the vector product with $\hat{k}(\overline{k}_\rho)$. It is seen that this

construction will not lead to an optimal approximation of (19) and thus to a different wave.

Finally, we point out that our tapered wave has been derived by optimizing the electric field with respect to an ideal field $\overline{\mathcal{E}}_i$. The magnetic field of the tapered wave then followed from the familiar relation between the electric and magnetic field of a plane wave (Faraday's law). It is clear that in a similar manner we could derive a dual tapered wave which is obtained by choosing the magnetic polarization vectors $\overline{h}$ with respect to a non-Maxwellian field $\overline{\mathcal{H}}_i$ and applying Ampere's law to find the electric field.

V. ISSUES IN THE APPLICATION TO 3-D SCATTERING

The tapered wave introduced in this paper can be used for the simulation of scattering from randomly rough surfaces with a planar mean surface. In a more complex scenario, objects are embedded in a layered background with rough interfaces. If the objects are at least partially situated in the half space where the sources of the incident wave reside it is important also to pay attention to the distribution of the tapered wave for $z > 0$.

Fig. 6 and 7 illustrate the cases of oblique and grazing incidence, respectively. Fig. 6(a) shows how the tapered wave forms a slightly converging beam, approximating the prescribed footprint at $z = 0$ [Fig. 6(b)]. The non-zero intensity in the top-right corner of Fig. 6(a) is due to the periodic nature of the discretized versions of (1), (2) with respect to $\overline{p}$. This aliasing effect, which in the present case would have no effect on the illumination of objects situated relatively close to the surface at $z = 0$, can be reduced—as usual—by sampling finer with respect to $\overline{k}_\rho$. For footprints where $\psi(\overline{k}_\rho)$ is not given in closed form as in (13) but is computed by 2-D FFT this is achieved by applying zero padding before carrying out the transformation. The remarkable fact about Fig. 7 is that the inclusion and correct treatment of evanescent waves enables synthesis of the prescribed footprint even for $\theta_i = 90°$ [Fig. 7(b)]. Aliasing for $z > 0$ in this case is more severe [Fig. 7(a)].

In typical applications of the tapered wave concept, electromagnetic wave scattering from a conducting object over a conducting rough surface is simulated and Glisson's overlapping triangular flat vector basis functions [39], [40], [41] for the electric surface current on both object and rough surface are used in discretizing the electric field integral equation, applying a Galerkin-type method of moments. We compared the results of such a

scattering code with those obtained by the hybrid method described in [10], [11], [12]. The major advantage of this hybrid method is that the decomposition into flat surface problems with impressed equivalent sources that are determined by lower order solutions allows introduction of the tensor Green function for layered media. This removes the need to solve for the surface currents on the rough surface and to truncate its physical dimensions. In the comparison, the same rough surface profile, the same patch model for the object, and the same tapered incident wave were used for solving the problem with the two independent codes; reasonable agreement was obtained. Discrepancies, however, occurred for near-grazing angles $\theta_i = 80 \ldots 90°$ where the pure MoM results suffer from edge effects due to the truncation of the rough surface. While the incident wave can be tapered to fall off exponentially towards the edges the scattered fields from the object decay only as $1/r$, giving rise to problems at very large polar angles where the object acts as a reflector that directs energy towards the edges. This indicates the increased difficulty of the low grazing angle rough surface scattering problem when an object is present. In the hybrid method, the correct behavior of the monostatic HH return at $\theta_i = 90°$ where in the flat surface case the boundary condition on the perfectly conducting surface forces a zero is guaranteed. It should be remarked that, although the utilization of the tapered wave concept for the method in [10], [11], [12], which when implemented up to and including the first order yields accurate results for slightly rough surfaces, is not imperative, it is still useful there because only finite rough surface profiles can be processed.

VI. Approximate 3-D Tapered Waves

A clear advantage of the original 2-D scalar Thorsos wave and a major reason for its popularity is the avoidance of numerical integrations in the evaluation of the incident field. The price paid is the non-Maxwellian nature of the approximation which, as reported in [34], can lead to anomalies in the computed results of simulations that require evaluation of the incident field not only on the rough surface as, e.g., in object-surface interaction problems. Also the breakdown of the approximation near grazing incidence causes serious problems in some applications. Keeping these limitations in mind and analogous to the derivation of the Thorsos wave, in the 3-D case with the spectrum (13) we can argue, in a spirit similar to Laplace's method for the asymptotic expansion of integrals [42], [43], that

for large g the main contribution to the superposition of plane waves comes from around $\overline{k}_\rho = \overline{k}_{i\rho}$. Using the truncated bivariate Taylor expansion in k_x, k_y

$$
\begin{aligned}
\sqrt{k^2 - \left|\overline{k}_{i\rho} + \overline{k}_\rho\right|^2} &\approx k_{iz} - \frac{k_{ix}}{k_{iz}} k_x - \frac{k_{iy}}{k_{iz}} k_y \\
&- \frac{k_{ix} k_{iy}}{k_{iz}^3} k_x k_y - \frac{k^2 - k_{iy}^2}{2 k_{iz}^3} k_x^2 - \frac{k^2 - k_{ix}^2}{2 k_{iz}^3} k_y^2
\end{aligned}
\tag{27}
$$

where $k_{iz} = k \cos\theta_i$, we can obtain from (12) by carrying out the integrations and symmetrizing the result with respect to x and y (without any further approximations)

$$
\mathcal{E}_i(\overline{r}) \approx e_i\, e^{i\overline{k}_i \cdot \overline{r}}\, \frac{1}{u(z)}\, \exp\left[-\frac{s(\overline{r})}{g^2\, u^2(z)}\right]
\tag{28}
$$

where $\overline{k}_i = \overline{k}_{i\rho} - \hat{z}\, k_{iz}$ and

$$
\begin{aligned}
s(\overline{r}) &= \left(1 - \frac{2i}{g^2} \frac{k^2 - k_{ix}^2}{k_{iz}^3} z\right)\left(x + \frac{k_{ix}}{k_{iz}} z\right)^2 \\
&+ \left(1 - \frac{2i}{g^2} \frac{k^2 - k_{iy}^2}{k_{iz}^3} z\right)\left(y + \frac{k_{iy}}{k_{iz}} z\right)^2 \\
&+ \frac{4i}{g^2} \frac{k_{ix} k_{iy}}{k_{iz}^3} z\left(x + \frac{k_{ix}}{k_{iz}} z\right)\left(y + \frac{k_{iy}}{k_{iz}} z\right)
\end{aligned}
\tag{29}
$$

and

$$
u(z) = \sqrt{\left(1 - \frac{2i}{g^2} \frac{k^2}{k_{iz}^3} z\right)\left(1 - \frac{2i}{g^2} \frac{1}{k_{iz}} z\right)}
\tag{30}
$$

In deriving (27)–(30), the dispersion relation $k_{iz}^2 = k^2 - k_{ix}^2 - k_{iy}^2$ has been used. As expected, (28) coincides with (12) exactly when $z = 0$. As $g \to \infty$ the plane wave case is recovered. It is remarked that (28) is not a direct generalization of the Thorsos wave to 3-D because of the different formulation of the superposition integral used as starting point. However, using the following argument we arrive at a condition for the validity of (28) that is similar to the one given in the 2-D case [36], [34], [35], in particular the dependence on $(\frac{\pi}{2} - \theta_i)^2$ near grazing carries over to 3-D: The radius of convergence of the full Taylor series (27) is limited to $k - k_{i\rho}$ because of the branch point of the square root function. Thus

$$
kg\,(1 - \sin\theta_i) \gg 1
\tag{31}
$$

is required for (28) to be an accurate representation of (12). In addition, the error of the truncated series (27) is multiplied by z with the consequence that the largest $|z|$ considered should be small relative to g, i.e., $g \gg |z|_{\max}$.

Approximations for the 3-D vector wave case are derived in a similar fashion by additionally expanding the polarization vectors. Substituting

$$\hat{h}(\overline{k}_\rho)\,\hat{h}(\overline{k}_\rho) \;=\; \frac{1}{k_\rho^2}\left[\hat{x}\,\hat{x}\,k_y^2 - (\hat{x}\,\hat{y} + \hat{y}\,\hat{x})\,k_x\,k_y + \hat{y}\,\hat{y}\,k_x^2\right] \tag{32}$$

$$\hat{v}(\overline{k}_\rho)\,\hat{v}(\overline{k}_\rho) \;=\; \frac{k_z^2}{k^2\,k_\rho^2}\left[\hat{x}\,\hat{x}\,k_x^2 + (\hat{x}\,\hat{y} + \hat{y}\,\hat{x})\,k_x\,k_y + \hat{y}\,\hat{y}\,k_y^2\right]$$
$$+ \frac{k_z}{k^2}\left[(\hat{x}\,\hat{z} + \hat{z}\,\hat{x})\,k_x + (\hat{y}\,\hat{z} + \hat{z}\,\hat{y})\,k_y\right] + \hat{z}\,\hat{z}\,\frac{k_\rho^2}{k^2} \tag{33}$$

into (17), we find

$$\overline{e}(\overline{k}_\rho) \;=\; \frac{\overline{e}_i}{k^2}\cdot\left[\hat{x}\,\hat{x}\,(k^2 - k_x^2) + \hat{y}\,\hat{y}\,(k^2 - k_y^2) + \hat{z}\,\hat{z}\,k_\rho^2\right.$$
$$\left. - (\hat{x}\,\hat{y} + \hat{y}\,\hat{x})\,k_x\,k_y + (\hat{x}\,\hat{z} \dotplus \hat{z}\,\hat{x})\,k_x\,k_z + (\hat{y}\,\hat{z} + \hat{z}\,\hat{y})\,k_y\,k_z\right] \tag{34}$$

Equation (34) also follows from $\hat{h}\,\hat{h} + \hat{v}\,\hat{v} = \overline{\overline{I}} - \hat{k}\,\hat{k}$ with $\overline{\overline{I}}$ the identity tensor and $\hat{k}$ as in (23). Similarly, with the dyads

$$\hat{v}(\overline{k}_\rho)\,\hat{h}(\overline{k}_\rho) \;=\; \frac{k_z}{k\,k_\rho^2}\left[(\hat{x}\,\hat{x} - \hat{y}\,\hat{y})\,k_x\,k_y - \hat{x}\,\hat{y}\,k_x^2 + \hat{y}\,\hat{x}\,k_y^2\right]$$
$$+ \frac{1}{k}\left(\hat{z}\,\hat{x}\,k_y - \hat{z}\,\hat{y}\,k_x\right) \tag{35}$$

$$\hat{h}(\overline{k}_\rho)\,\hat{v}(\overline{k}_\rho) \;=\; \frac{k_z}{k\,k_\rho^2}\left[(\hat{x}\,\hat{x} - \hat{y}\,\hat{y})\,k_x\,k_y + \hat{x}\,\hat{y}\,k_y^2 - \hat{y}\,\hat{x}\,k_x^2\right]$$
$$+ \frac{1}{k}\left(\hat{x}\,\hat{z}\,k_y - \hat{y}\,\hat{z}\,k_x\right) \tag{36}$$

we obtain from (18)

$$\overline{h}(\overline{k}_\rho) \;=\; -\frac{\overline{e}_i}{k}\cdot\left[(\hat{x}\,\hat{y} - \hat{y}\,\hat{x})\,k_z + (\hat{x}\,\hat{z} - \hat{z}\,\hat{x})\,k_y - (\hat{y}\,\hat{z} - \hat{z}\,\hat{y})\,k_x\right] \tag{37}$$

It is observed from (34), (37) that the tensors in (17), (18) are symmetric and anti-symmetric, respectively. More importantly here, it is evident from (34), (37) that both $\overline{e}(\overline{k}_\rho)$ and $\overline{h}(\overline{k}_\rho)$, viewed as functions of the two real variables k_x and k_y, are analytic throughout the k_x-k_y plane excluding the 1-D set of points forming the circle $|\overline{k}_\rho| = k$. (It is emphasized that the region of analyticity includes $\overline{k}_\rho = 0$, c.f., Section IV.) Thus, the Taylor series

$$\overline{e}(\overline{k}_{i\rho} + \overline{k}_\rho) = \sum_{m,n=0}^{\infty} \overline{a}_{mn}\,k_x^m\,k_y^n \tag{38}$$

where

$$\overline{a}_{mn} = \frac{1}{m!\,n!}\left[\frac{\partial^{m+n}}{\partial k_x^m\,\partial k_y^n}\,\overline{e}(\overline{k}_\rho)\right]_{\overline{k}_\rho=\overline{k}_{i\rho}} \tag{39}$$

converges in the disk $|\overline{k}_\rho| < k - k_{i\rho}$, and similar expressions hold for $\overline{h}(\overline{k}_\rho)$. Applying the approximation (27) to (1) with the spectrum (13), inserting (38), and using twice the Fourier integral identity (c. f., 3.958.2 in [44])

$$\int\limits_{-\infty}^{\infty} dx\,x^n e^{iqx-ax^2} = \sqrt{\frac{\pi}{a}}\,i^{-n}\,\frac{d^n}{dq^n}\,e^{-\frac{q^2}{4a}}$$

$$= \sqrt{\frac{\pi}{a}}\,n!\left(\frac{i}{2a}\right)^n e^{-\frac{q^2}{4a}} \sum_{m=0}^{[n/2]} \frac{(-a)^m}{(n-2m)!\,m!}\,q^{n-2m} \tag{40}$$

where $[n/2]$ is the integral part of $n/2$, leads, again without further approximation, to an expression of the form

$$\overline{E}_i(\overline{r}) \approx e^{i\overline{k}_i\cdot\overline{r}}\,\frac{1}{u(z)}\,\exp\left[-\frac{s(\overline{r})}{g^2\,u^2(z)}\right] \sum_{m,n=0}^{\infty} \overline{a}_{mn}\,p_{mn}(\overline{r}) \tag{41}$$

where $s(\overline{r})$ and $u(z)$ are as in (29), (30), the $\overline{a}_{mn}$ are obtained from (34), and $p_{mn}(\overline{r})$ is polynomial in x, y, z up to z-dependent correction factors that, similar to (30), are unity for $z = 0$ or $g \to \infty$. It is noted that, different from the scalar case discussed above, (41) for $z = 0$ is only an approximation of the superposition of plane waves that we started out with because of the finite radius of convergence of (38) and the fact that the spectrum (13) is not band-limited. The conditions on g for (41) to be a reasonable approximation are as stated above for the scalar case. We have $\overline{a}_{00} = \overline{e}_i$ and $p_{00} = 1$. Thus the lowest-order electric field approximation following from (41) is the same as what is obtained by approximating k_z in (19) with the help of (27) or multiplying (28) by $\overline{e}_i/e_i$. The p_{mn} of higher order vanish as $g \to \infty$. The algebraic details for the p_{mn} of any order (integrating over k_y first) are as follows:

$$\begin{aligned}
p_{mn}(\overline{r}) = {} & n!\left[\frac{2i}{g^2\,u_1^2(z)}\right]^n \sum_{k=0}^{[n/2]} \frac{[-g^2\,u_1^2(z)]^k}{4^k\,k!} \\
& \times \sum_{j=0}^{n-2k} \frac{(m+j)!}{j!\,(n-2k-j)!}\left(y+\frac{k_{iy}}{k_{iz}}z\right)^{n-2k-j}\left(\frac{k_{ix}\,k_{iy}}{k_{iz}^3}z\right)^j\left[\frac{2i}{g^2\,u_2^2(z)}\right]^{m+j} \\
& \times \sum_{\ell=0}^{\left[\frac{m+j}{2}\right]} \frac{[-g^2\,u_2^2(z)]^\ell}{4^\ell\,(m+j-2\ell)!\,\ell!}\left[x+\frac{k_{ix}}{k_{iz}}z+w(y,z)\right]^{m+j-2\ell}
\end{aligned} \tag{42}$$

where

$$u_1^2(z) = 1 - \frac{2i}{g^2} \frac{k^2 - k_{ix}^2}{k_{iz}^3} z \tag{43}$$

$$u_2^2(z) = \frac{u^2(z)}{u_1^2(z)} \tag{44}$$

$$w(y,z) = \frac{2i}{g^2\, u_1^2(z)} \frac{k_{ix}k_{iy}}{k_{iz}^3} z \left(y + \frac{k_{iy}}{k_{iz}} z\right) \tag{45}$$

When choosing the number of terms to be included in (41) one should be aware of the limited radius of convergence of (38) and the underlying approximation (27) which, however, has no effect for $z = 0$. The $\overline{a}_{mn}$ with $m + n < 3$ are given by

$$\overline{a}_{00} = \overline{e}_i \tag{46}$$

$$\overline{a}_{10} = \frac{\overline{e}_i}{k^2\, k_{iz}} \cdot \Big[-2\,(\hat{x}\,\hat{x} - \hat{z}\,\hat{z})\, k_{ix}\, k_{iz} - (\hat{x}\,\hat{y} + \hat{y}\,\hat{x})\, k_{iy}\, k_{iz}$$
$$+ (\hat{x}\,\hat{z} + \hat{z}\,\hat{x})\, (k_{iz}^2 - k_{ix}^2) - (\hat{y}\,\hat{z} + \hat{z}\,\hat{y})\, k_{ix}\, k_{iy} \Big] \tag{47}$$

$$\overline{a}_{01} = \frac{\overline{e}_i}{k^2\, k_{iz}} \cdot \Big[-2\,(\hat{y}\,\hat{y} - \hat{z}\,\hat{z})\, k_{iy}\, k_{iz} - (\hat{x}\,\hat{y} + \hat{y}\,\hat{x})\, k_{ix}\, k_{iz}$$
$$- (\hat{x}\,\hat{z} + \hat{z}\,\hat{x})\, k_{ix}\, k_{iy} + (\hat{y}\,\hat{z} + \hat{z}\,\hat{y})\, (k_{iz}^2 - k_{iy}^2) \Big] \tag{48}$$

$$\overline{a}_{11} = \frac{\overline{e}_i}{k^2\, k_{iz}^3} \cdot \Big[-(\hat{x}\,\hat{y} + \hat{y}\,\hat{x})\, k_{iz}^3 - (\hat{x}\,\hat{z} + \hat{z}\,\hat{x})\, k_{iy}\, (k_{ix}^2 + k_{iz}^2)$$
$$- (\hat{y}\,\hat{z} + \hat{z}\,\hat{y})\, k_{ix}\, (k_{iy}^2 + k_{iz}^2) \Big] \tag{49}$$

$$\overline{a}_{20} = \frac{\overline{e}_i}{2\, k^2\, k_{iz}^3} \cdot \Big[-2\,(\hat{x}\,\hat{x} - \hat{z}\,\hat{z})\, k_{iz}^3 - (\hat{x}\,\hat{z} + \hat{z}\,\hat{x})\, k_{ix}\, (k_{ix}^2 + 3\, k_{iz}^2)$$
$$- (\hat{y}\,\hat{z} + \hat{z}\,\hat{y})\, k_{iy}\, (k^2 - k_{iy}^2) \Big] \tag{50}$$

$$\overline{a}_{02} = \frac{\overline{e}_i}{2\, k^2\, k_{iz}^3} \cdot \Big[-2\,(\hat{y}\,\hat{y} - \hat{z}\,\hat{z})\, k_{iz}^3 - (\hat{x}\,\hat{z} + \hat{z}\,\hat{x})\, k_{ix}\, (k^2 - k_{ix}^2)$$
$$- (\hat{y}\,\hat{z} + \hat{z}\,\hat{y})\, k_{iy}\, (k_{iy}^2 + 3\, k_{iz}^2) \Big] \tag{51}$$

Following a similar procedure, approximations for the magnetic field and the dual tapered wave (Section IV) can be derived.

VII. CONCLUSION

We considered the problem of constructing a 3-D tapered wave as a superposition of plane waves, taking into account both propagating and evanescent waves. The use of the simple Gaussian plane wave spectrum was recommended in order to avoid problems near

the grazing incidence. The introduced special choice for the polarization vectors removed the problems of losing a dominant polarization state and degradation of tapering near the normal incidence. Mathematically speaking, the proposed polarization vectors are analytic at the origin of the 2-D wavenumber space. Moreover, the choice of polarization vectors was shown to lead to an exact solution of the Maxwell equations which is an optimal approximation of an ideal but non-Maxwellian tapered field that is constructed by multiplying a scalar tapered wave with a constant polarization vector. The result is a reliably tapered wave with a dominant polarization state that can be used uniformly for all angles of incidence. We discussed the application of the proposed tapered wave in simulating 3-D electromagnetic scattering from a conducting object over a conducting rough surface. Newly encountered problems near the grazing incidence were attributed to secondary edge effects which are unrelated to the tapered incident wave but indicate the difficulty of the low grazing angle rough surface scattering problem when objects are present. It was pointed out that methods which avoid such edge effects could also benefit from the utilization of the tapered wave. In some situations it might be desirable to have an approximate 3-D tapered wave at one's disposal which does not require a 2-D numerical integration (summation of plane waves), trading accuracy in satisfying Maxwell's equations for computational speed. We presented the derivation of approximations for both the 3-D scalar and vector case. The expansion of the polarization vectors is based on their analyticity. The local character of the technique employed forces the breakdown of the approximations at grazing incidence.

REFERENCES

[1] K. Pak, L. Tsang, C. H. Chan, and J. Johnson, "Backscattering enhancement of electromagnetic waves from two-dimensional perfectly conducting random rough surfaces based on Monte Carlo simulations," *J. Opt. Soc. Am. A*, vol. 12, pp. 2491–2499, Nov. 1995.

[2] J. T. Johnson, L. Tsang, R. T. Shin, K. Pak, C. H. Chan, A. Ishimaru, and Y. Kuga, "Backscattering enhancement of electromagnetic waves from two-dimensional perfectly conducting random rough surfaces: A comparison of Monte Carlo simulations with experimental data," *IEEE Trans. Antennas Propagat.*, vol. 44, pp. 748–756, May 1996.

[3] R. L. Wagner, J. Song, and W. C. Chew, "Monte Carlo simulation of electromagnetic scattering from two-dimensional random rough surfaces," *IEEE Trans. Antennas Propagat.*, vol. 45, pp. 235–245, Feb. 1997.

[4] K. Pak, L. Tsang, and J. Johnson, "Numerical simulations and backscattering enhancement of electromagnetic waves from two-dimensional dielectric random rough surfaces with the sparse-matrix canonical grid method," *J. Opt. Soc. Am. A*, vol. 14, pp. 1515–1529, July 1997.

[5] V. Jandhyala, E. Michielssen, B. Shanker, and W. C. Chew, "A combined steepest descent-fast multipole algorithm for the fast analysis of three-dimensional scattering by rough surfaces," *IEEE Trans. Geosci. Remote Sensing*, vol. 36, pp. 738–748, May 1998.

[6] V. Jandhyala, B. Shanker, E. Michielssen, and W. C. Chew, "Fast algorithm for the analysis of scattering by dielectric rough surfaces," *J. Opt. Soc. Am. A*, vol. 15, pp. 1877–1885, July 1998.

[7] J. T. Johnson, R. T. Shin, J. A. Kong, L. Tsang, and K. Pak, "A numerical study of ocean polarimetric thermal emission," *IEEE Trans. Geosci. Remote Sensing*, vol. 37, pp. 8–20, Jan. 1999.

[8] Q. Li, L. Tsang, K. S. Pak, and C. H. Chan, "Bistatic scattering and emissivities of random rough dielectric lossy surfaces with the physics-based two-grid method in conjunction with the sparse-matrix canonical grid method," *IEEE Trans. Antennas Propagat.*, vol. 48, pp. 1–11, Jan. 2000.

[9] G. Zhang and L. Tsang, "Angular correlation function and scattering coefficient of electromagnetic waves scattered by a buried object under a two-dimensional rough surface," *J. Opt. Soc. Am. A*, vol. 15, pp. 2995–3001, Dec. 1998.

[10] Y. Zhang, *Forward and Inverse Problems in Microwave Remote Sensing of Objects in a Complex Medium*, Ph.D. thesis, Massachusetts Institute of Technology, 1999.

[11] Y. Zhang, Y. E. Yang, H. Braunisch, and J. A. Kong, "Electromagnetic wave interaction of conducting object with rough surface by hybrid SPM/MoM technique," *J. Electromagnetic Waves and Applications*, vol. 13, pp. 983–984, 1999.

[12] Y. Zhang, Y. E. Yang, H. Braunisch, and J. A. Kong, "Electromagnetic wave interaction of conducting object with rough surface by hybrid SPM/MoM technique," in *Progress in Electromagnetics Research (PIER 22)*, J. A. Kong, Ed., pp. 315–335. EMW Publishing, Cambridge, 1999.

[13] K. O'Neill, R. Lussky, Jr., and K. D. Paulsen, "Scattering from a metallic object embedded near the randomly rough surface of a lossy dielectric," *IEEE Trans. Geosci. Remote Sensing*, vol. 34, pp. 367–376, Mar. 1996.

[14] G. Zhang, L. Tsang, and Y. Kuga, "Studies of the angular correlation function of scattering by random rough surfaces with and without a buried object," *IEEE Trans. Geosci. Remote Sensing*, vol. 35, pp. 444–453, Mar. 1997.

[15] G. Zhang and L. Tsang, "Angular correlation function of wave scattering by a random rough surface and discrete scatterers and its application in the detection of a buried object," *Waves Random Media*, vol. 7, pp. 467–479, July 1997.

[16] A. Madrazo and M. Nieto-Vesperinas, "Scattering of light and other electromagnetic waves from a body buried beneath a highly rough random surface," *J. Opt. Soc. Am. A*, vol. 14, pp. 1859–1866, Aug. 1997.

[17] J. Ripoll, A. Madrazo, and M. Nieto-Vesperinas, "Scattering of electromagnetic waves from a body over a random rough surface," *Opt. Commun.*, vol. 142, pp. 173–178, Oct. 1997.

[18] A. Madrazo, J. R. Arias-González, and M. Nieto-Vesperinas, "Polarization effects in scattering of electromagnetic waves by an object beneath a random rough surface," *Opt. Commun.*, vol. 162, pp. 91–98, Apr. 1999.

[19] M. Rodríguez Pino, L. Landesa, J. L. Rodríguez, F. Obelleiro, and R. J. Burkholder, "The generalized forward-backward method for analyzing the scattering from targets on ocean-like rough surfaces," *IEEE Trans. Antennas Propagat.*, vol. 47, pp. 961–969, June 1999.

[20] J. R. Arias-González, M. Nieto-Vesperinas, and A. Madrazo, "Morphology-dependent resonances in the scattering of electromagnetic waves from an object buried beneath a plane or a random rough surface," *J. Opt. Soc. Am. A*, vol. 16, pp. 2928–2934, Dec. 1999.

[21] L. Tsang, J. A. Kong, and R. T. Shin, *Theory of Microwave Remote Sensing*, Wiley, New York, 1985.

[22] J. A. Kong, *Electromagnetic Wave Theory*, Wiley, New York, 2nd edition, 1990.

[23] J. T. Johnson, "Surface currents induced on a dielectric half-space by a Gaussian beam: An extended validation for point matching method of moment codes," *Radio Sci.*, vol. 32, pp. 923–934, May–June 1997.

[24] J. A. Ratcliffe, "Some aspects of diffraction theory and their application to the ionosphere," *Rep. Prog. Phys.*, vol. 19, pp. 188–267, 1956.

[25] J. W. Goodman, *Introduction to Fourier Optics*, McGraw-Hill, New York, 1968.

[26] L. Tsang, C. H. Chan, and K. Pak, "Monte Carlo simulation of a two-dimensional random rough surface using the sparse-matrix flat-surface iterative approach," *Electron. Lett.*, vol. 29, pp. 1153–1154, June 1993.

[27] L. Tsang, C. H. Chan, and K. Pak, "Backscattering enhancement of a two-dimensional random rough surface (three-dimensional scattering) based on Monte Carlo simulations," *J. Opt. Soc. Am. A*, vol. 11, pp. 711–715, Feb. 1994.

[28] E. I. Thorsos, "The validity of the Kirchhoff approximation for rough surface scattering using a Gaussian roughness spectrum," *J. Acoust. Soc. Am.*, vol. 83, pp. 78–92, Jan. 1988.

[29] E. I. Thorsos and D. R. Jackson, "Studies of scattering theory using numerical methods," *Waves Random Media*, vol. 1, pp. S165–S190, July 1991.

[30] L. Tsang, C. H. Chan, K. Pak, and H. Sangani, "Monte-Carlo simulations of large-scale problems of random rough surface scattering and applications to grazing incidence with the BMIA/canonical grid method," *IEEE Trans. Antennas Propagat.*, vol. 43, pp. 851–859, Aug. 1995.

[31] D. J. Donohue, H.-C. Ku, and D. R. Thompson, "Application of iterative moment-method solutions to ocean surface radar scattering," *IEEE Trans. Antennas Propagat.*, vol. 46, pp. 121–132, Jan. 1998.

[32] J. T. Johnson, "A numerical study of low-grazing-angle backscatter from ocean-like impedance surfaces with the canonical grid method," *IEEE Trans. Antennas Propagat.*, vol. 46, pp. 114–120, Jan. 1998.

[33] J. V. Toporkov, R. T. Marchand, and G. S. Brown, "On the discretization of the integral equation describing scattering by rough conducting surfaces," *IEEE Trans. Antennas Propagat.*, vol. 46, pp. 150–161, Jan. 1998.

[34] J. V. Toporkov, R. S. Awadallah, and G. S. Brown, "Issues related to the use of a Gaussian-like incident field for low-grazing-angle scattering," *J. Opt. Soc. Am. A*, vol. 16, pp. 176–187, Jan. 1999.

[35] R. T. Marchand and G. S. Brown, "On the use of finite surfaces in the numerical prediction of rough surface scattering," *IEEE Trans. Antennas Propagat.*, vol. 47, pp. 600–604, Apr. 1999.

[36] H. D. Ngo and C. L. Rino, "Application of beam simulation to scattering at low grazing angles: 1. Methodology and validation," *Radio Sci.*, vol. 29, pp. 1365–1379, Nov.–Dec. 1994.

[37] C. H. Chan, L. Tsang, and Q. Li, "Monte Carlo simulations of large-scale one-dimensional random rough-surface scattering at near-grazing incidence: penetrable case," *IEEE Trans. Antennas Propagat.*, vol. 46, pp. 142–149, Jan. 1998.

[38] P. Tran and A. A. Maradudin, "The scattering of electromagnetic waves from a randomly rough 2D metallic surface," *Opt. Commun.*, vol. 110, pp. 269–273, Aug. 1994.

[39] A. W. Glisson, *On the Development of Numerical Techniques for Treating Arbitrarily-Shaped Surfaces*, Ph.D. thesis, University of Mississippi, 1978.

[40] S. M. Rao, *Electromagnetic Scattering and Radiation of Arbitrarily-Shaped Surfaces by Triangular Patch Modeling*, Ph.D. thesis, University of Mississippi, 1980.

[41] S. M. Rao, D. R. Wilton, and A. W. Glisson, "Electromagnetic scattering by surfaces of arbitrary shape," *IEEE Trans. Antennas Propagat.*, vol. AP-30, pp. 409–418, May 1982.

[42] N. Bleistein and R. A. Handelsman, *Asymptotic Expansions of Integrals*, Holt, Rinehart and Winston, New York, 1975.

[43] C. M. Bender and S. A. Orszag, *Advanced Mathematical Methods for Scientists and Engineers*, McGraw-Hill, New York, 1978.

[44] I. S. Gradshteyn, I. M. Ryzhik, and A. Jeffrey (Ed.), *Table of Integrals, Series, and Products*, Academic Press, Boston, 5th edition, 1994.
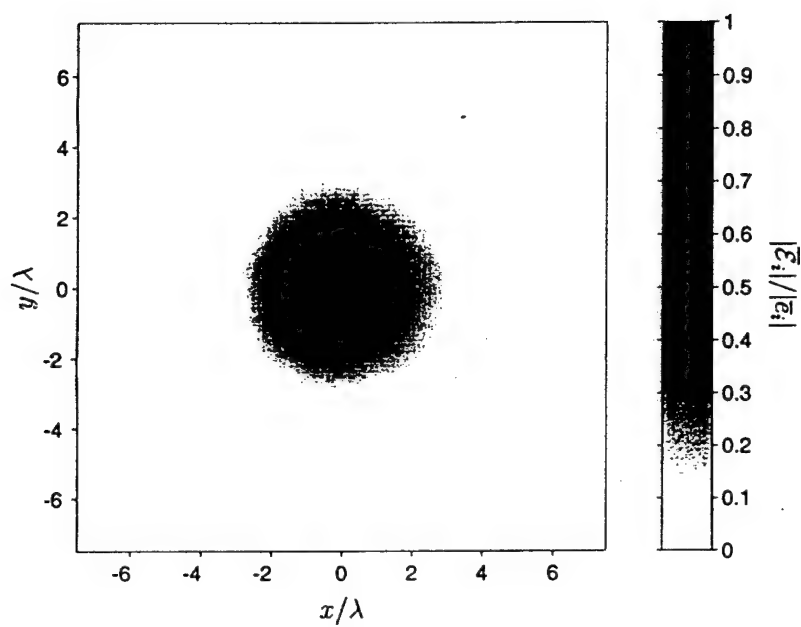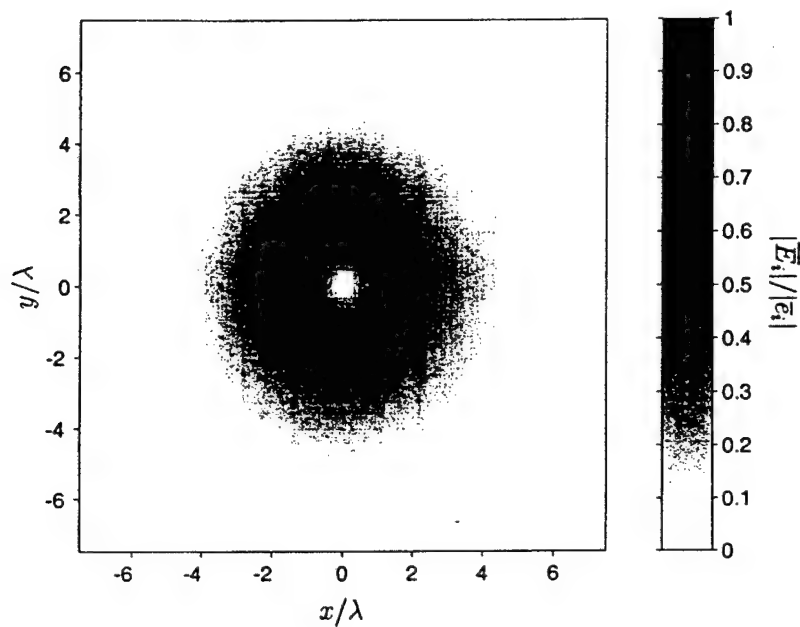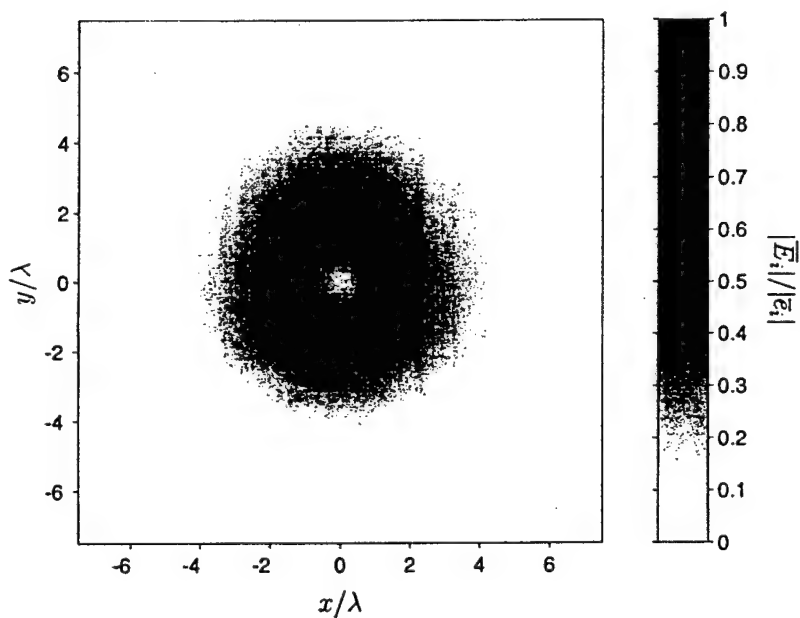
LIST OF FIGURES

Fig. 1. Example of a prescribed Gaussian-shaped footprint to be approximated by the vector tapered wave ($g = 2\,\lambda$).
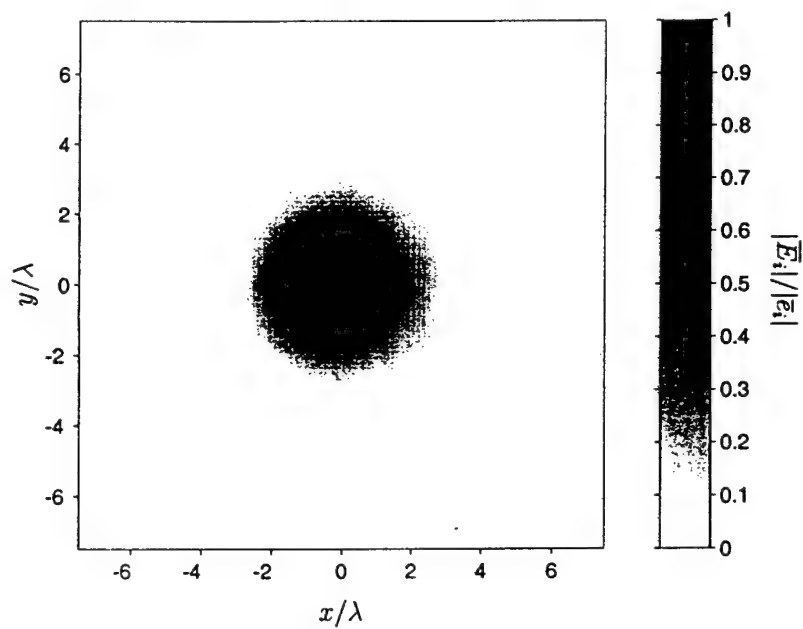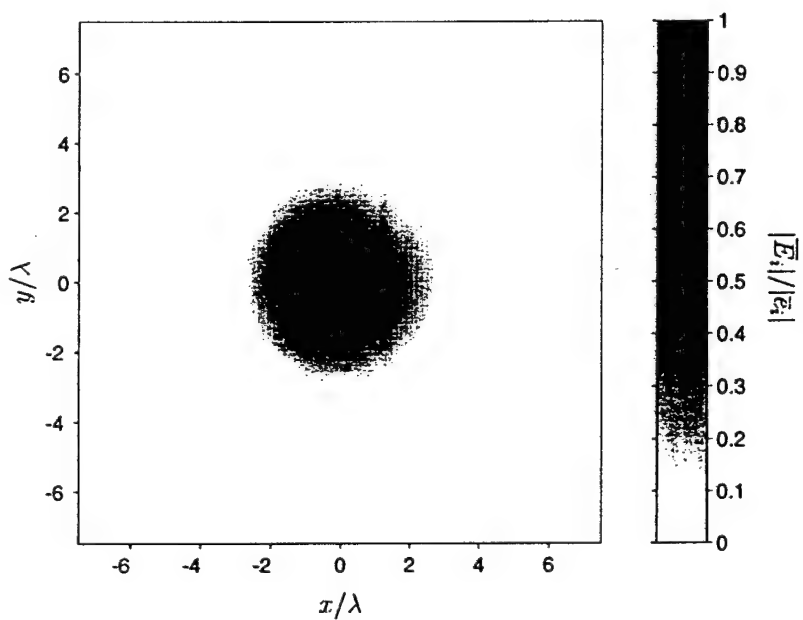
(a) Horizontally polarized plane wave components.

(b) Vertically polarized plane wave components.

Fig. 2. Resulting footprints at normal incidence for the tapered wave after [1], [2], [4], [9], [8]. The approximation of the prescribed footprint (Fig. 1) is not satisfactory.

(a) Horizontal polarization.

(b) Vertical polarization.

Fig. 3. Resulting footprints at normal incidence for the tapered wave introduced in the present paper and approximating the prescribed footprint of Fig. 1.

(a) Horizontally polarized components.

(b) Vertically polarized components.
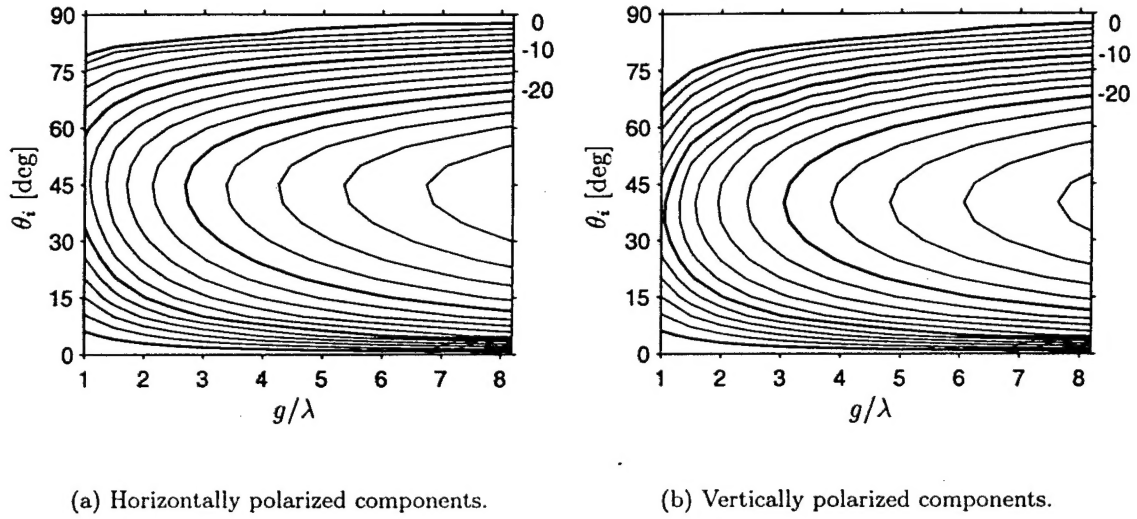
Fig. 4. Relative RMS error [dB] at $z = 0$ for the tapered wave after [1], [2], [4], [9], [8] as compared to a non-Maxwellian field with prescribed tapering and polarization.
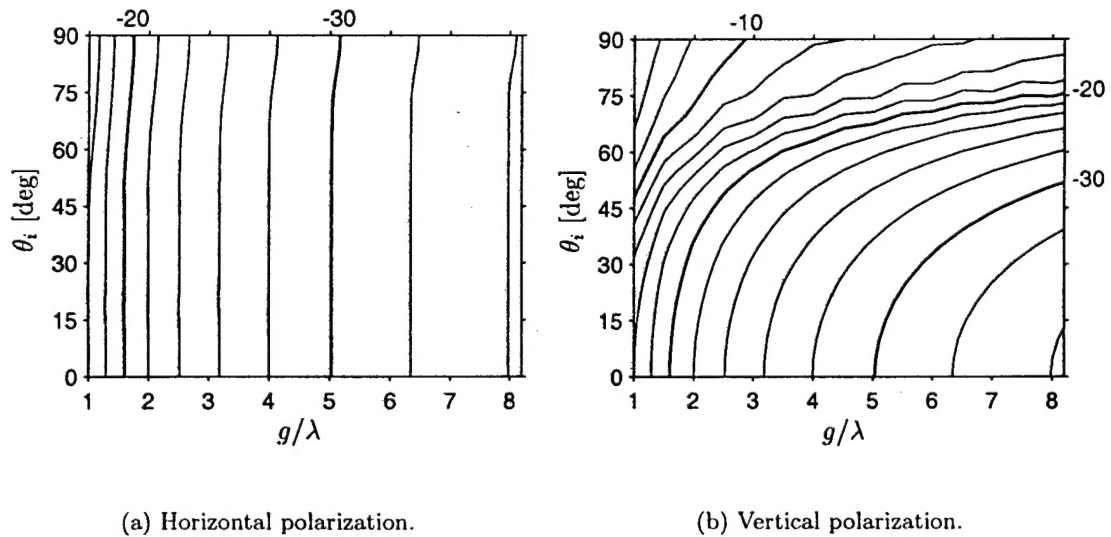

(a) Horizontal polarization.
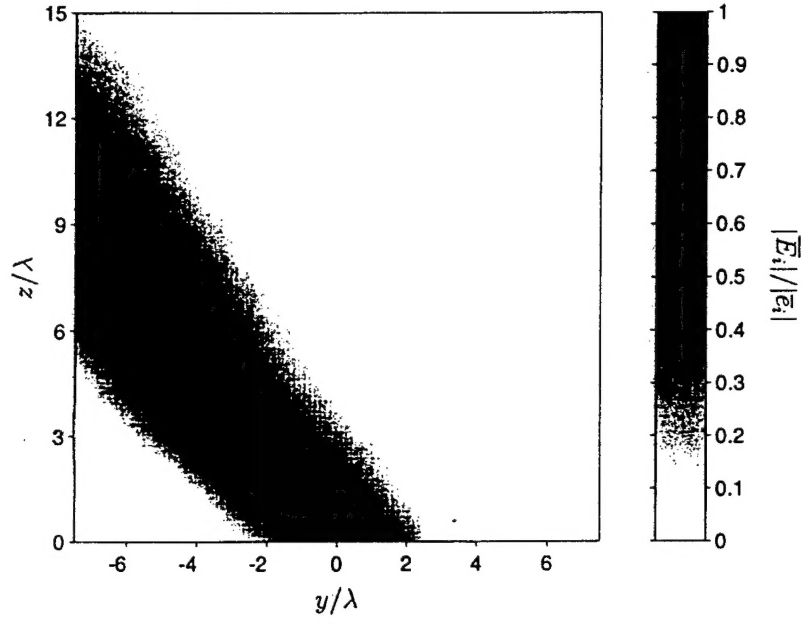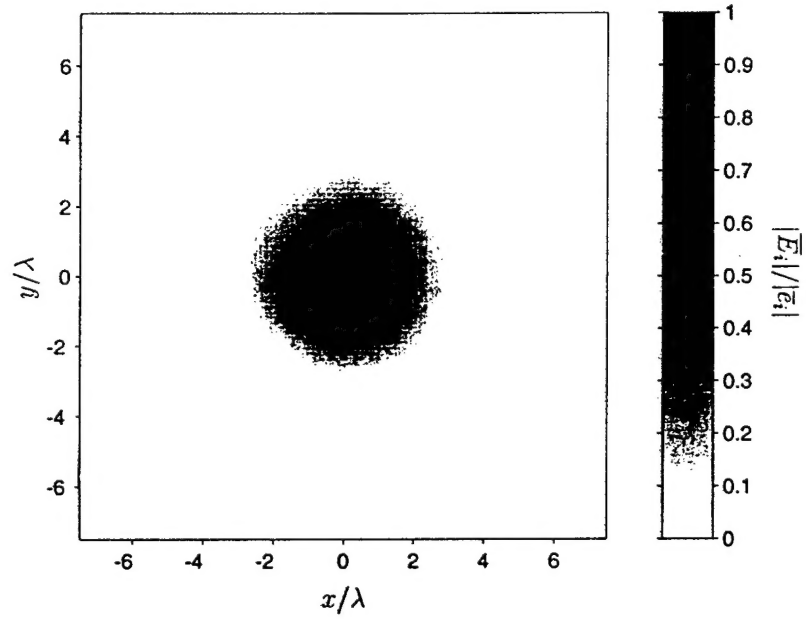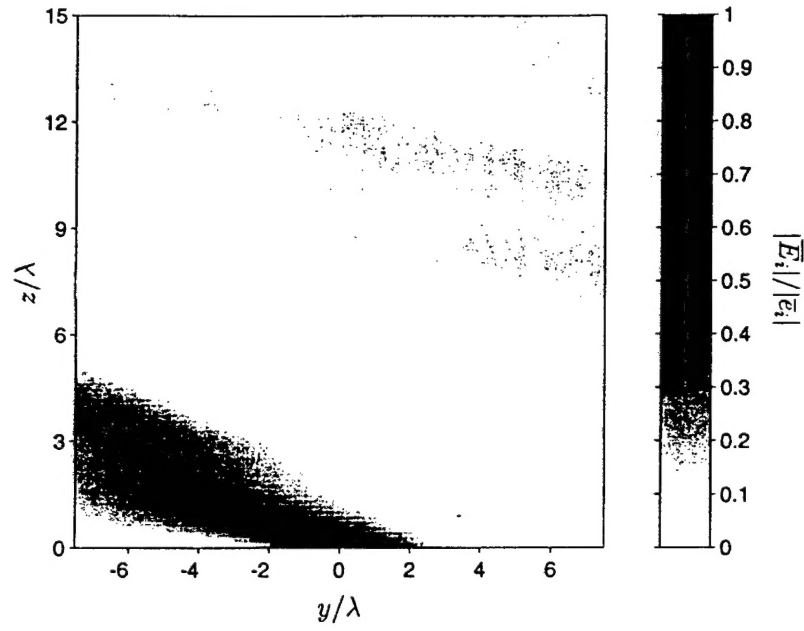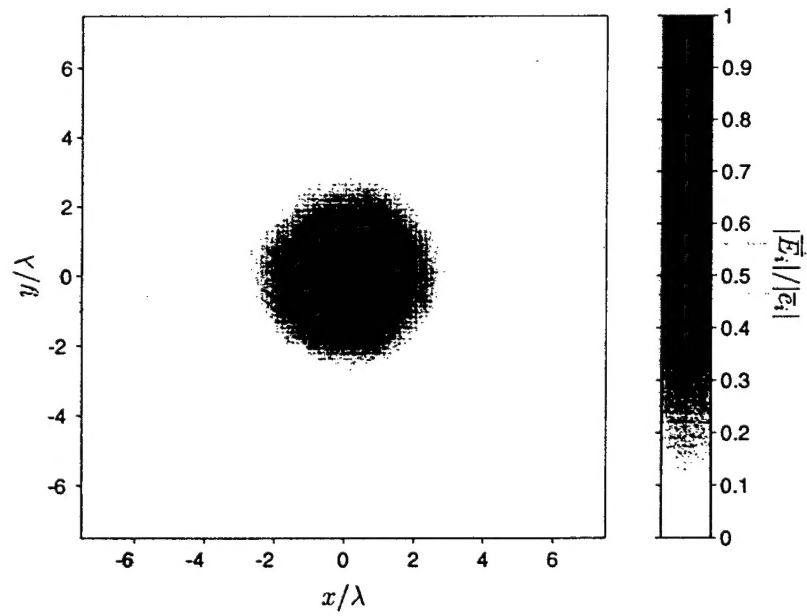
(b) Vertical polarization.

Fig. 5. Relative RMS error [dB] at $z = 0$ for the tapered wave introduced in this paper.

(a) Side view ($x = 0$).

(b) Footprint.

Fig. 6. Beam formation of the tapered wave at oblique incidence ($\theta_i = 40°$, $\phi_i = 90°$, $g = 2\,\lambda$, horizontal polarization).

(a) Side view ($x = 0$).

(b) Footprint.

Fig. 7.   Beam formation of the tapered wave at grazing incidence ($\theta_i = \phi_i = 90°$, $g = 2\,\lambda$, horizontal polarization).

ATTACHMENT NUMBER 1

REPORTS AND REPORT DISTRIBUTION

REPORT TYPES

(a)   Performance (Technical) Report(s) (Include letter report(s)) Frequency: Annual

(b)   Final Technical Report, issued at completion of Grant.
        NOTE: Technical Reports must have a SF-298 accompanying them.

(c)   Final Financial Status Report (SF 269)

(d)   Final Patent Report (DD 882)

REPORTS DISTRIBUTION		
ADDRESSEES	**REPORT TYPES**	**NUMBER OF COPIES**
Office of Naval Research Program Officer Ronald P. Radlinski ONR 334 Ballston Centre Tower One 800 North Quincy Street Arlington, VA 22217-5660	(a) & (b) w/(SF-298's)	3
Administrative Grants Officer OFFICE OF NAVAL RESEARCH REGIONAL OFFICE BOSTON * 495 SUMMER STREET ROOM 103 BOSTON, MA 02210-2109	(c), (d) & SF-298's only for (a) & (b)	1
Director, Naval Research Laboratory Attn: Code 2627 4555 Overlook Drive Washington, DC 20375-5326	(a) & (b) w/(SF-298's)	1
Defense Technical Information Center 8725 John J. Kingman Road STE 0944 Ft. Belvoir, VA 22060-6218	(a) & (b) w/(SF-298's)	2
Office of Naval Research Attn: ONR 00CC1 Ballston Centre Tower One 800 North Quincy Street Arlington, VA 22217-5660	(d)	1

If the Program Officer directs, the Grantee shall make additional distribution of technical reports in accordance with a supplemental distribution list provided by the Program Officer. The supplemental distribution list shall not exceed 250 addresses.

* For report types (a) and (b), send only a copy of the transmittal letter to the Administrative Contracting Officer; do not send actual reports to the Administrative Contracting Officer.

N00014-97-1-0172
(Rev. 4-96)